Cellular specialization of synaptic integration

in a mammalian sympathetic ganglion

By

Chen Li

B.S. Shanghai Jiao Tong University, 2000

Submitted to the Graduate Faculty of

the School of Medicine in partial fulfillment

of the requirements for the degree of

Doctor of Philosophy

University of Pittsburgh

2007

UNIVERSITY OF PITTSBURGH

SCHOOL OF MEDICINE

This dissertation was presented

by

Chen Li

It was defended on

December 7, 2007

and approved by

Committee Chair: Brian M. Davis, Associate Professor, Department of Neurobiology

Jonathan E. Rubin, Associate Professor, Department of Mathematics

Gonzalo E. Torres, Assistant Professor, Department of Neurobiology

Elias Aizenman, Professor, Department of Neurobiology

Daniel Weinreich, Professor, Department of Pharmacology & Experimental
Therapeutics, University of Maryland

Dissertation Advisor: John P. Horn, Professor, Department of Neurobiology

Cellular specialization of synaptic integration

in a mammalian sympathetic ganglion

Chen Li, PhD

University of Pittsburgh, 2007

Sympathetic ganglia are widely viewed as simply relays that are essential to convey neural activity from spinal preganglionic neurons to distinct peripheral targets. However, recent studies indicate that synaptic integration in sympathetic ganglia is more complex than that of a simple excitatory relay. It is proposed that synaptic organization of each functional subset of sympathetic ganglion cells is specialized to generate a unique synaptic gain function, thereby allowing for differential control of specific target modalities. This dissertation describes cellular specialization of some critical determinants of synaptic gain in rat superior cervical ganglion (SCG) neurons. The work was first focused on identifying presynaptic stimulus threshold and NPY immunoreactivity as neuronal classification criteria of secretomotor, pilomotor and vasoconstrictor cells. The results here show that these three functional phenotypes of neurons are indistinguishable in terms of synaptic convergence. Furthermore, norepinephrine (NE) causes different modulatory effects upon pre and postsynaptic α2-

adrenergic receptors in these cell types. Collectively, this work characterizes cellular specialization of synaptic convergence and NE neuromodulatory mechanism that are involved in synaptic integration in the rat SCG.

TABLE OF CONTENTS

LIST OF TABLES

CHAPTER 1

INTRODUCTION

1.1 OVERVIEW

This thesis examines the cellular specialization of synaptic integration in a mammalian sympathetic ganglion. Synaptic transmission in sympathetic ganglia is essential for conveying neural activity from spinal preganglionic neurons to postganglionic neurons that control peripheral targets consisting of smooth muscle, cardiac muscle and secretory epithelia. In this widely held view, sympathetic ganglia are seen as simple relays, in which the presynaptic release of acetylcholine produces nicotinic excitatory postsynaptic potentials (EPSPs) that trigger postsynaptic action potentials (Janig and Habler, 1999). These spikes then propagate to the peripheral ends of sympathetic axons where they initiate transmission at neuroeffector synapses on end-organs. In this way, sympathetic ganglia permit the expression of important autonomic behaviors such as control of blood pressure and flow, body temperature, and glandular secretion (Janig and Habler, 1999).

Several observations indicate that synaptic integration in sympathetic ganglia is more complex than that of a simple excitatory relay, like the vertebrate neuromuscular

junction, where a single axon produces strong suprathreshold nicotinic EPSPs that invariably cause action potentials in striated muscle fibers. First, postganglionic neurons receive convergent synaptic inputs from preganglionic neurons in the spinal cord (Purves and Hume, 1981; Purves and Lichtman, 1985). In paravertebral ganglia this pattern is characterized by the convergence of one strong suprathreshold input and several weak subthreshold inputs (Dodd and Horn, 1983a; Selyanko and Skok, 1992; Janig, 1995). This synaptic organization might allow postganglionic neurons to integrate presynaptic activity via the interaction between suprathreshold input and summation of subthreshold inputs (Karila and Horn, 2000). Second, it has been demonstrated that various phenotypes of ganglionic neurons are specialized to exclusively innervate and control distinct target types (McLachlan, 1995). Finally, studies of bullfrog ganglia have shown the cell-specific expression of muscarinic and other neuromodulatory responses. Muscarine, for example, triggers an excitatory response by inhibiting M-channels in secretomotor B neurons and an inhibitory response by activating G-protein-coupled inwardly rectifying potassium channels (GIRKs) in vasomotor C neurons in paravertebral sympathetic ganglia 9 and 10 (Horn, 1992).

Together these observations suggest the working hypothesis that functional subsets of sympathetic neurons are characterized by distinct and specialized synaptic organization. According to a theory developed by Karila and Horn (Karila and Horn, 2000), this might enable each phenotype of neurons to generate a unique input-output relation, thereby allowing for differential control of specific target modalities. Until now,

this idea has been best studied in bullfrog sympathetic ganglia. My thesis has three general goals. The first is to extend concepts from frog ganglia to a mammalian sympathetic preparation. For this purpose I developed criteria for identification of neuronal cell types in the isolated rat superior cervical sympathetic ganglion (Chapter 2). The second goal is to examine nicotinic convergence and compare it between functional subsets of neurons in the rat SCG (Chapter 3). My final goal is to analyze the neuromodulatory actions of catecholamines on identified rat sympathetic neurons (Chapters 4 and 5). The following sections of this chapter provide a more detailed review of ganglionic organization and specific gaps in understanding that the experiments in this thesis were designed to fill.

1.2. GENERAL ORGANIZATION OF THE SYMPATHETIC NERVOUS SYSTEM

Homeostatic regulatory processes are mediated by tight cooperation between the neuroendocrine system and the autonomic nervous system, which consists of sympathetic, parasympathetic and enteric subdivisions (McLachlan, 1995; Janig and Habler, 1999; Powley, 1999; Gibbins, 2004). By working together, these systems maintain a constant internal milieu in the face of varying external environmental conditions and behavioral states. Functionally, the sympathetic nervous system and parasympathetic nervous system usually exert opposite homeostatic control. They could produce these opposite effects by innervating the same peripheral structures such as the eyes, airways, heart and reproductive organs. In particular, parasympathetic

innervations are often considered "rest and digest" response such as decreasing blood pressure and heart rate. In contrast, the sympathetic activations are regarded as "fight or flight" response. The sympathetic nervous system, when stimulated, can increase blood pressure and heart rate, control hair erection and enlarge pupil size. These effects make it especially important for regulating "fight-or-flight" behaviors that allow animals to react to threats, preparing the animal for fighting a predator or fleeing.

Ganglia in the sympathetic nervous system serve as the final common pathway for relaying activity from spinal preganglionic neurons to various types of peripheral targets. The spinal preganglionic neurons are driven by neural circuits in the medulla and hypothalamus (Loewy and Spyer, 1990; McLachlan, 1995). Preganglionic sympathetic neurons are located in the intermediolateral cell column in lamina VII of spinal cord levels from T1 to L3. They form synapses with postganglionic neurons in paravertebral and prevertebral ganglia. Paravertebral ganglia are interconnected by a nerve trunk to form a chain on each side of the spinal cord. These paravertebral chains extend bilaterally from the first cervical segment to the last sacral segment. At the rostral end of the paravertebral chain lies the SCG, which projects to important targets in the head. The other paravertebral ganglia control the lungs, heart, skin and muscles in the limbs and trunk. Unlike the paravertebral ganglia, the prevertebral sympathetic ganglia lie close to major branches of the abdominal aorta. They include the celiac, superior mesenteric and inferior mesenteric ganglia that innervate the liver, spleen, kidneys, stomach, pancreas, intestine, bladder and reproductive organs.

An important feature of sympathetic ganglia is that subsets of postganglionic neurons exclusively innervate distinct target modalities including vasculature, piloerector and glands (McLachlan, 1995). This has been demonstrated in both amphibian and mammalian ganglia by retrograde tracing, immunocytochemistry and electrophysiology studies. Thus for example, in bullfrog and toad paravertebral ganglia, secretomotor B neurons are relatively large (around 50 µm in diameter) (Nishi et al., 1965; Dodd and Horn, 1983b; Morris et al., 1986), have axon conduction velocities of about 2.5 m/s, which places them in the B fiber range, (Nishi et al., 1965; Dodd and Horn, 1983b) and lack neuropeptide Y (NPY) (Horn et al., 1987; Morris et al., 1989). These neurons have been shown to project to glands by retrograde tracing with horseradish peroxidase (HRP) (Horn et al., 1988) and by functional observation of glandular secretion (Jobling and Horn, 1996). In contrast, vasomotor C neurons have small somata (typically less than 30 µm in diameter) (Nishi et al., 1965; Dodd and Horn, 1983b; Horn et al., 1987), relatively slow axon conduction velocity in the C fiber range (about 0.3 m/s) (Nishi et al., 1965; Dodd and Horn, 1983b; Horn et al., 1987) and contain NPY in *Rana catesbiana* (bullfrog) (Horn et al., 1987) and both NPY and galanin in *Bufo marinus* (toad) (Morris et al., 1986; Morris et al., 1989). The axons of C cells selectively project to blood vessels (Horn et al., 1988; Thorne et al., 1995) and can elicit vasocontraction (Thorne and Horn, 1997). Likewise, Gibbins and colleagues have found that subsets of postganglionic neurons in mammalian paravertebral ganglia can be divided into vasomotor, pilomotor and secretomotor neurons respectively according to their peripheral targets (Gibbins, 1991, , 1992). These various phenotypes of neurons can be distinguished by

neuropeptide content and soma size (Gibbins, 1991, , 1992). More detailed discussion

of this feature is provided in the context of the rat SCG in Chapter 1.3 and in Chapter 2.

Synaptic connections between spinal preganglionic and postganglionic neurons

are characterized by divergence and convergence. Significant divergence was first

revealed by the anatomical observation that the number of preganglionic fibers is much

smaller than that of postganglionic neurons. For example, in the rat there are ~25,000

neurons in the SCG (Gabella, 1976; Wright et al., 1983; Purves et al., 1986), while only

~5,000 preganglionic axons projecting to the SCG (Aguayo et al., 1973; Gabella, 1976).

The divergence is, therefore, 1:5. Subsequent studies directly counted the number of

preganglionic neurons by retrograde labeling with HRP application to preganglionic

fibers (Rando et al., 1981; Murata et al., 1982; Purves et al., 1986). This provided more

accurate estimates of divergence. For example, it has been shown that only ~1,000

spinal preganglionic cells project to the rat SCG (Rando et al., 1981; Purves et al.,

1986). Thus, the divergence determined by this method is 1: 25. These observations

suggest that a relatively small number of spinal preganglionic neurons send divergent

axons to a large number of postganglionic neurons (Purves et al., 1986; Janig, 1995;

Gibbins, 2004). This divergence may allow for the coordinated control of multiple

targets occupying a large area such as blood vessels in a large muscle or a limb.

The concept of ganglionic convergence was first suggested by early

morphological studies which have shown that more than one preganglionic fibers often

form synapses on the same neuron (Skok, 1973b).   Subsequent electrophysiological

studies revealed multiple steps in EPSP sizes evoked by stimulation of varying strength in postganglionic neurons. This indicated that several preganglionic axons with different thresholds terminate on a single neuron (Erulkar and Woodward, 1968; Mirgorodsky and Skok, 1970; Skok, 1973a). Furthermore, Purves and colleagues found that synaptic convergence scales up in proportion to animal sizes. In their studies, the number of axons innervating individual postganglionic neurons was counted by recording intracellularly and stimulating spinal ventral roots with gradually increasing stimulation intensity (Nja and Purves, 1977; Purves and Hume, 1981; Purves and Lichtman, 1985). All together, these findings indicate that each postganglionic neuron receives convergent inputs from several presynaptic neurons. Interestingly, these convergent inputs vary in synaptic strength (Janig, 1995). Purves and his colleagues also showed that the number of convergent inputs correlates with the dendritic complexity of sympathetic neurons (Purves et al., 1986). Although these studies have revealed principles of circuit organization between pre- and postganglionic neurons, the significance of these findings for synaptic integration in sympathetic ganglia remains unclear. McLachlan and colleagues have argued that preganglionic signals are transmitted through paravertebral ganglia with little modification (McLachlan, 2003), Janig and Horn, however, have argued for the alternative view that the integration of convergent inputs with different strength may lead to transformation of presynaptic activities in sympathetic ganglia (Janig, 1995; Karila and Horn, 2000). Nonetheless, from the available data it is not all clear whether the synaptic convergence varies between cellular phenotypes. The experiments in Chapter 3 are, therefore, designed to

compare convergence among functional subsets of neurons in the rat superior cervical ganglion (SCG).

Acetylcholine is the major neurotransmitter released by preganglionic neurons in sympathetic ganglia (Feldberg and Gaddum, 1934; Feldberg and Vartiainen, 1934; McLachlan, 1995). Nicotinic receptors mediate the fast excitatory postsynaptic potentials (EPSPs) that trigger action potentials (Skok, 1992, , 2002). In addition, muscarinic receptors have been shown to modulate neurotransmission by mediating a slow EPSP (Brown et al., 1980; Jones, 1985), a slow inhibitory postsynaptic potential (IPSP) (Dodd and Horn, 1983a) and presynaptic inhibition (Shen and Horn, 1996). Furthermore, preganglionic neurons also contain neuropeptides and other potential co-neurotransmitters. In amphibian ganglia, luteinizing hormone-releasing hormone (LHRH) is co-released with ACh from presynaptic C neurons (Jan et al., 1979; Jan and Jan, 1981). It is firmly established that LHRH mediates a non-cholinergic, late slow EPSP at the amphibian sympathetic ganglionic synapse (Jan and Jan, 1982). In mammalian ganglia, a variety of neuropeptides and substances such as pituitary adenylate cyclase-activating polypeptide (PACAP), vasoactive intestinal polypeptide (VIP) and substance P have been found in presynaptic nerve terminals in mammalian sympathetic ganglia (Gibbins, 1995; Beaudet et al., 1998; Beaudet et al., 2000). However, only recent studies have begun to provide evidence that such peptides released from preganglionic axon terminals might mediate synaptic transmission. Thus for example, PACAP has been shown to be released from nerve terminals via tetanic neural stimulation in pig intrinsic cardiac ganglia and contributes to slow EPSPs

(Tompkins et al., 2007). Likewise, substance P has been shown to be associated with axonal endings of preganglionic neurons in lumber sympathetic ganglia (Gibbins, 1992). The expression of substance P receptor (Jobling et al., 2001) as well as its physiological response via exogenous application of substance P (Zhao et al., 1995; Jobling et al., 2001) has also been demonstrated. However, the effects of endogenously released substance P upon synaptic transmission was only found by stimulating postganglionic axons in coeliac ganglion and these are thought to be sensory rather than preganglionic in origin (Zhao et al., 1996).

Sympathetic postganglionic neurons release norepinephrine (NE) as their principal neurotransmitter at neuroeffector synapses on target organs (McLachlan, 1995; Gibbins, 2004). In addition, various peptides and substances such as neuropeptide (NPY), adeonosine triphosphate (ATP) and VIP may function as postganglionic co-transmitters to regulate target organs (Lindh et al., 1989; Morris and Gibbins, 1992; Westfall et al., 2002). Because these putative co-transmitters are selectively produced in the somata of certain subsets of postganglionic neurons (Gibbins, 1995), they are often used as neurochemical markers to identify cellular phenotypes.

1.3 SPECIAL FEATURES OF MAMMALIAN SUPERIOR CERVICAL GANGLION (SCG)

9

1.3.1 Anatomical structure and functional phenotypes

Historically, major advances in the understanding of synaptic transmission have come from studies of peripheral autonomic ganglia, beginning with the first demonstration of a chemical neurotransmitter (Loewi, 1921; Dale et al., 1936). The superior cervical ganglion (SCG) was preferred in early anatomical studies that examined neuronal cytology and counted the total number of sympathetic ganglion cells (Gabella, 1976). Beginning with classical extracellular recording studies (Eccles, 1935) and then the first application of intracellular microelectrode recording in the rabbit SCG (Eccles, 1955), many subsequent physiological studies have focused on the mammalian SCG. Throughout this history, the SCG was favored over other paravertebral ganglia for three practical reasons. First, the SCG results from the fusion of the first four cervical segmental paravertebral ganglia, which makes it relatively large and simplifies its dissection. Second, by virtue of its location at the rostral end of cervical sympathetic trunk (CST), one can isolate preparations of the SCG with distinct input and output nerves. The ganglion receives preganglionic fibers through the cervical sympathetic trunk (CST), and the majority of postganglionic axons leave the ganglion through either the internal carotid nerve (ICN) or the external carotid nerve (ECN) (Bowers and Zigmond, 1979). Finally, the SCG is the only sympathetic ganglion that projects to a unique set of targets in the head. Neurons in the rostral half of the SCG project through the ICN to supply the cerebral vasculature, pineal gland, skin of forehead and the eye, while neurons in the caudal SCG project through the ECN to supply skin, muscles and piloerector hairs in the face and submandibular salivary and thyroid glands (Bowers et

10

al., 1984; Romeo et al., 1986; Edvinsson et al., 1989; Uddman et al., 1989; Flett and

Bell, 1991; Luebke and Wright, 1992)(see Fig. 1). For above-mentioned reasons, I

chose to study cellular identification and cellular specification of synaptic integration in

the rat SCG.

Based on soma size, neuropeptide expression and projection targets, most

neurons in the rat SCG belong to four major groups (Flett and Bell, 1991; Gibbins,

1995): ~50% are vasoconstrictors that are small in size (diameter range from 20 µm to

28 µm) and express neuropeptide Y (NPY) (Lundberg et al., 1982; Jarvi et al., 1986;

Gibbins, 1991; Headley et al., 2005); 20-25% are small NPY-negative pilomotor

neurons (Gibbins, 1991, , 1995; Grkovic and Anderson, 1997); ~15% are large

secretomotor neurons (diameter range from 30 µm to 40 µm) projecting to salivary

glands (NPY-negative, surrounded by terminals that are immunoreactive for calretinin

(Voyvodic, 1989; Grkovic and Anderson, 1995)); and 3-5% are pupilomotor neurons

projecting to the iris which are large NPY-positive cells surrounded by synaptic boutons

that contain immunoreactivity for calcitonin gene related peptide (CGRP) (Grkovic et al.,

1999). In addition to these four groups, the SCG contains smaller groups of

secretomotor cells that project to the pineal (Bowers et al., 1984; Reuss and Moore,

1989) and thyroid glands (Romeo et al., 1986; Grunditz et al., 1988) and vasodilator

neurons that project to the tongue (Flett and Bell, 1991). In this work I focused on the

largest groups of cells (secretomotor, pilomotor and vasoconstrictor neurons).
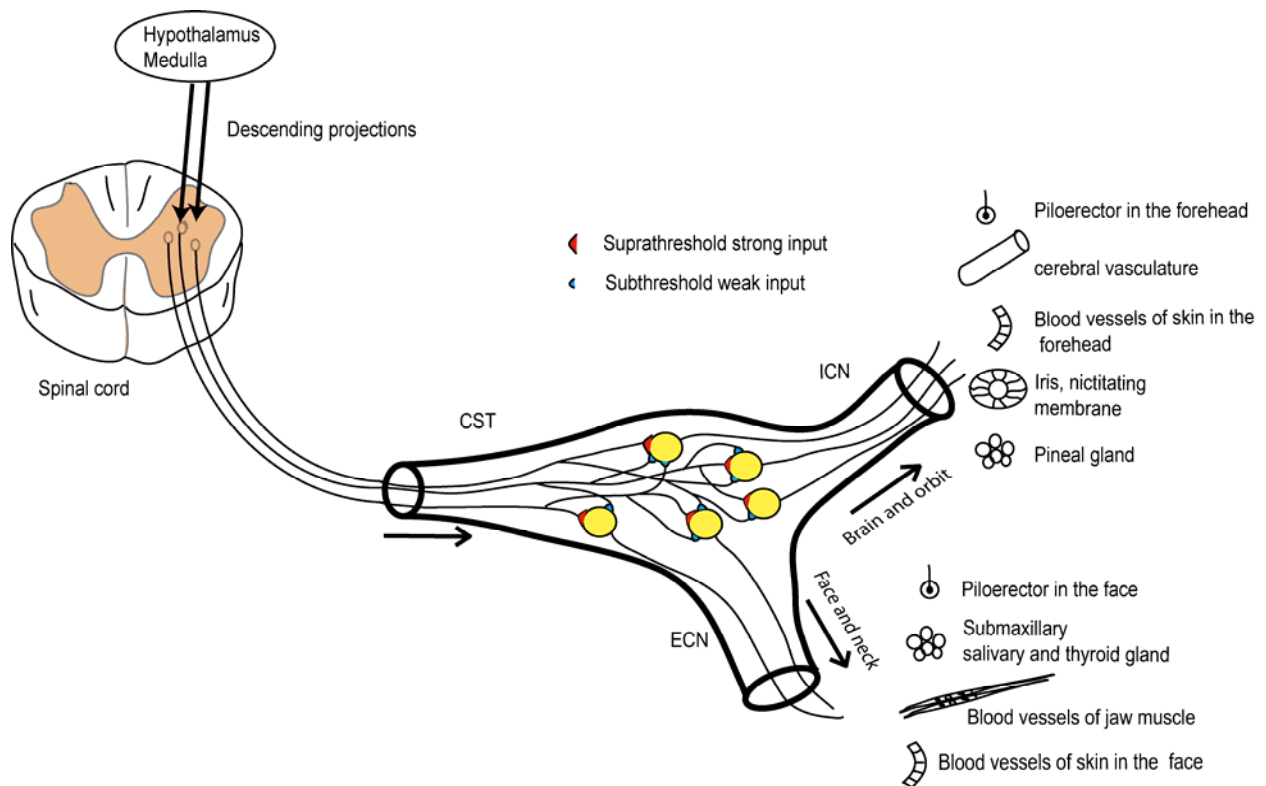
Figure 1. Circuit organization and sympathetic outflow of the rat superior cervical ganglion (SCG)
Spinal preganglionic neurons form nicotinic synapses on sympathetic neurons that project through either the ICN or the ECN. Subsets of sympathetic neurons selectively innervate blood vessels and other target modalities. Note the presynaptic divergence and postsynaptic convergence. Postganglionic neurons in the rat SCG typically receive one or sometimes two suprathreshold strong inputs and several subthreshold weak inputs from a relatively small number of preganglionic neurons in the spinal cord. Abbreviations: CST, cervical sympathetic trunk; ECN, external carotid nerve; ICN, internal carotid nerve.

1.3.2 Synaptic organization and microscopic structure of mammalian SCG neurons

Rat SCG neurons have round or ovoid cell bodies ranging from 15 μm to 45 μm in diameter. These cells are multipolar with 1 to 15 primary dendrites extending in the same plane as the major axis of the cell body (Purves and Lichtman, 1985; Li and Horn, 2006). Some of these processes are short (around 5-20 μm), while other long dendrites extend into neuropil for more than one hundred micrometers. Typically, postganglionic axons arise from soma or the proximal parts of a large dendrite and leave ganglia without collaterals. Presynaptic axon terminals form synapses on dendrites and soma (Gibbins and Morris, 2006). In the rat, the synaptic organization is characterized by a presynaptic divergence of 1:25 (Purves et al., 1986) and a postsynaptic convergence of 8.5:1 (Purves and Lichtman, 1985). In other mammalian SCGs, the convergence is 4.4:1 in the mouse, 11.3:1 in the guinea pig and 11.9:1 in the rabbit (Purves and Lichtman, 1985). Interestingly, the number of convergent preganglionic inputs correlates with the number of primary dendrites (Purves and Hume, 1981; Purves and Lichtman, 1985). Using this important finding, I studied synaptic convergence by counting the number of primary dendrites in electrophysiologically characterized neurons in the rat SCG and, for the first time, compared convergence between different cellular phenotypes in a sympathetic ganglion (Chapter 3).

1.3.3 Neurotransmission in the superior cervical ganglion

Synaptic neurotransmission in rat SCG neurons is mediated by acetylcholine (ACh)

released from preganglionic nerve terminals (McLachlan, 1995). Nicotinic receptors in

the rat SCG, like those in all other sympathetic ganglia, act as nonselective cation

channels by allowing mixed cation influx upon ACh binding and mediate fast EPSPs

(Selyanko et al., 1979; Selyanko and Skok, 1979). These fast EPSPs have short delay

of 1.5-2 ms, a fast onset phase (~2-5 ms) and a much slower (~50-100 ms) exponential

decay (Selyanko et al., 1979; Selyanko and Skok, 1979) and are responsible for spike

generation.

In addition, neuromodulatory mechanisms of synaptic transmission are

expressed in the rat SCG neurons (Tokimasa and Akasu, 1995; Janig and Habler,

1999). Activation of muscarinic, adrenergic and other G protein-coupled receptors

(GPCRs) either through synaptic release or the circulation can produce slow

electrophysiological events mediated by metabotropic signal transduction pathways.

These effects can alter cell excitability and therefore have consequences for synaptic

integration.

For example, muscarinic receptors have been found to mediate slow EPSPs,

slow IPSPs and presynaptic inhibition upon ACh binding (Hille, 1994; Tokimasa and

Akasu, 1995; Shen and Horn, 1996). Nearly all neurons in the rat SCG express multiple

muscarinic acetylcholine receptor (mAChR) subtypes consisting of M_1, M_2 and M_4

(Brown et al., 1980; Hulme et al., 1990; Shapiro et al., 2001). Because of this,

application of a nonspecific muscarinic agonist initiates multiple modulatory pathways

(Fig. 2). Adams, Brown and colleagues first found that muscarinic agonist depressed a novel K^+ current that they termed the M current (Adams et al., 1982). Subsequent studies have shown that this metabotropic event arises through the activation of M1 subtype of muscarinic receptor (Marrion et al., 1989). It causes the dissociation of heterotrimeric G proteins into the $G_{\alpha q/11}$-subunit and the $G_{\beta\gamma}$-complex. The dissociated $G_{\alpha q/11}$ (Bernheim et al., 1992; Caulfield et al., 1994) then results in the hydrolysis of phosphotidylinositol 4,5-bisphosphate (PIP_2) which normally maintain the activity of M type potassium channel under basal conditions. Thus, the depletion of PIP_2 causes the inhibition of M current (Zhang et al., 2003; Suh and Hille, 2005). In addition, the depletion of PIP_2 underlies an inhibition of calcium current through N-type (Mathie et al., 1992; Gamper et al., 2004; Liu et al., 2004) and L-type (Mathie et al., 1992; Liu et al., 2006) calcium channels that is slow, insensitive to PTX and membrane potential. However, activation of M_4 (Bernheim et al., 1992) mAChRs, which couple to $G_{i/o}$ G-proteins (Delmas et al., 1998b), produces a fast voltage dependent and PTX-sensitive calcium current inhibition via direct binding of dissociated $G_{\beta\gamma}$ with N-type calcium channels (Bernheim et al., 1992; Hille, 1994; Delmas et al., 1998b). Furthermore, endogenous M_2 (Fernandez-Fernandez et al., 1999) muscarinic receptors, which couple to G_i (Fernandez-Fernandez et al., 2001), can selectively activate G protein-gated inwardly rectifying K^+ (GIRK) channels in rat SCG neurons via direct binding of dissociated $G_{\beta\gamma}$ (Wang and McKinnon, 1996; Yamada et al., 1998; Fernandez-Fernandez et al., 1999; Fernandez-Fernandez et al., 2001).

In summary, muscarinic modulation involves synaptic release of ACh, activation of muscarinic receptors and altered channel activities via G-protein signaling pathways. Based on the synaptic gain model (see Chapter 1.4.3), recent simulation and dynamic clamp studies suggested that excitatory muscarinic modulation might enhance synaptic gain (Karila and Horn, 2000; Kullmann and Horn, 2006).
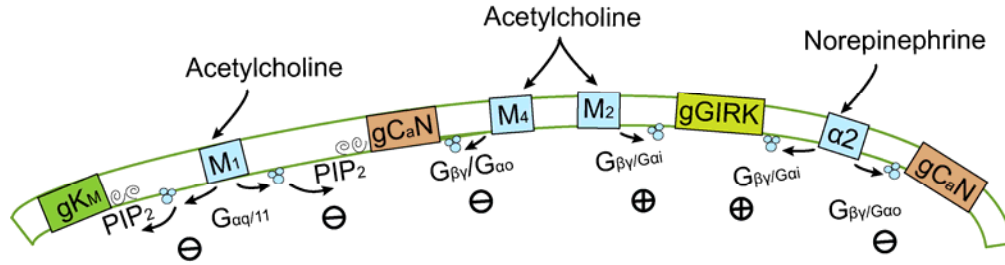
Figure 2. Muscarinic and adrenergic neuromodulatory pathways converging on three types of channels in neurons of rat SCG.

M1 muscarinic receptor proceeds via $G_{\alpha q/11}$ proteins to activate phospholipase C and hydrolyze PIP_2. This, in turn, inhibits N-type calcium channel and M-type potassium channel. M_2, M_4 muscarinic receptors and adrenoceptors, however, activate GIRK or inhibit N-type calcium channel via direct binding of $G_{\beta\gamma}$ subunits that are dissociated from $G_{i/o}$ family. Abbreviations: M_1, M_1 muscarinic receptor; M_2, M_2 muscarinic receptor; M_4, M_4 muscarinic receptor; α2, α2 adrenoceptor; gCaN, N-type calcium channel; gK_M, M-type potassium channel; gGIRK, G protein-gated inwardly rectifying potassium channel. $\ominus$, inhibition of channel activities; $\oplus$, activation of channel activities.

Catecholamines can act on both presynaptic α2-adrenergic and postsynaptic α2-adrenergic receptors in mammalian SCG. It has been demonstrated that endogenously released catecholamines by high frequency preganglionic stimulation inhibits ACh release from preganglionic nerve terminals (Bulbring, 1944; Araujo and Collier, 1986). This inhibition is mediated by presynaptic α2- adrenergic receptors in sympathetic ganglia (Vizi, 1979; Belluzzi et al., 1987; McCallum et al., 1998; Stephens and Mochida, 2005). In terms of postsynaptic effects induced by catecholamines, early studies have shown that application of exogenous catecholamines can hyperpolarize neurons in sympathetic ganglia (De Groat and Volle, 1966; Brown and Caulfield, 1979). Subsequent molecular studies demonstrated that α2-adrenergic receptor is the major type of adrenoceptors expressed in rat SCG (Pieribone et al., 1994; Gold et al., 1997; Vidovic and Hill, 1997). Recent evidence showed that exogenously applied NE both activates GIRK channels via direct binding of βγ dimers that are dissociated from G_i/G_o (Ruiz-Velasco and Ikeda, 1998; Fernandez-Fernandez et al., 2001) and inhibits Ca^{2+} channels (Horn and McAfee, 1980; Galvan and Adams, 1982) via βγ dimers dissociated from $G_{\alpha o}$ (Caulfield et al., 1994; Delmas et al., 1998a; Delmas et al., 1999) (Fig. 2). However, the source of NE remains elusive. NE might be a neurotransmitter released in ganglia as suggested by studies using tetanic nerve stimulation. The adrenergic receptor might also serve as circulation targets by NE released from the adrenal gland during strong sympathetic activation (Izzo and Black, 2003). In this study, I focus on NE modulation of synaptic transmission and further discuss its source in Chapter 4.5.2.

18

1.4. A GENERAL MODEL OF SYNAPTIC INTEGRATION IN SYMPATHETIC GANGLIA

1.4.1 Cellular properties involved in synaptic integration, including synaptic convergence/strength and norepinephrine modulatory mechanism

Rat SCG neurons, like other postganglionic neurons, receive presynaptic convergent inputs with different strength. Interestingly, postganglionic neurons in paravertebral sympathetic ganglia seem to obey an "n+1" rule, in which each cell receives one very strong nicotinic synapse, called the primary (strong), and a variable number, n, of weak nicotinic synapses, called secondary (weak, see Fig. 1) (Janig and Habler, 1999). Primary synapses produce fast EPSPs that are suprathreshold in strength while secondary synapses produce fast EPSPs that are subthreshold in strength (McLachlan, 1995; Karila and Horn, 2000; Wheeler et al., 2004). Postsynaptic firing can be driven by individual EPSPs triggered by strong input and summation between pairs of weak secondary inputs. This summation, in turn, could be boosted by spontaneous fluctuations of EPSP amplitude, two-pulse facilitation, coactivation with other secondary synapses and coactivation with slow neuromodulatory EPSPs (Karila and Horn, 2000). Synaptic integration in sympathetic ganglia, therefore, is thought to be due to the interaction between suprathreshold strong input and subthreshold weak inputs onto neurons (Janig and McLachlan, 1992; McLachlan et al., 1997; McLachlan et al., 1998; Karila and Horn, 2000). Karila and Horn (Karila and Horn, 2000) proposed that this synaptic organization leads to activity-dependent amplification of presynaptic activity.

Neuromodulation may regulate synaptic integration by altering the strength of secondary nicotinic synapses. Although this modification of secondary nicotinic synapses doesn't change the probability of coincidences among secondary inputs, it can allow EPSPs generated by the combination of multiple secondary inputs to reach firing threshold more easily. For example, NE, the main neurotransmitter at neuroeffector synapse, was found to be able to modulate synaptic transmission in postganglionic neurons by hyperpolarizing the resting membrane potential via α2-adrenoceptors (Brown and Caulfield, 1979; Ivanov and Skok, 1980). In addition, a voltage-sensitive Ca^{2+} channel is inhibited after NE binding on α2-adrenoceptors (Horn and McAfee, 1980; Galvan and Adams, 1982; Caulfield et al., 1994). These effects can change cell excitability. In this thesis, I focus on exploring the physiological role of norepinephrine modulation of synaptic integration in rat SCG neurons.

1.4.2 Synaptic integration in functional subsets of neurons

Synaptic transmission study in bullfrog SCG neurons revealed some phenotypic difference between secretomotor B neurons (projecting to glands) and vasomotor C neurons (projecting to blood vessels). Thus for example, the neuromodulatory responses in B and C neurons are different. Muscarine triggers an excitatory response in B neurons but an inhibitory response in C neurons (Horn, 1992). One might envision that the difference in neuromodulatory mechanism and other cellular properties between B and C neurons contribute to differential synaptic integration. Different levels of input-

20

output relationship, in turn, are probably required for SCG neurons controlling different peripheral targets. For instance, it is conceivable that tight spatial and temporal control over blood pressure is more important than similar tight control over piloerection. It is, however, not at all clear whether these differences exist in subsets of neurons in rat SCG and how they affect synaptic integration. The following section (Chapter 1.4.3) proposes a possible model that explains the functional consequence of synaptic integration and how it allows differential control over various phenotypic targets.

1.4.3 Synaptic gain model

Sympathetic ganglia process information by decoding and integrating spike trains leaving the spinal cord. How then, do the connectivity and strength of nicotinic synapses combine with the expression of neuromodulatory mechanisms to shape ganglionic integration?

By focusing first on nicotinic synapses, Karila and Horn (Karila and Horn, 2000) used experimental data to develop a model that shows how convergence can produce gain (Fig. 3). The term gain had its root in the field of engineering and the meaning of it is generalized as the output to input ratio of any system or chain of system (Sagawa, 1978). In sympathetic ganglia, Karila and Horn (Karila and Horn, 2000) defined synaptic gain as the ratio of the average postsynaptic firing frequency to presynaptic firing frequency. The postsynaptic firing is driven by single primary EPSPs and by temporal coincidences between pairs of secondary EPSPs. From this simple example

(Fig. 3), it can be seen that having each presynaptic neuron in the preganglionic pool firing an average of 4 times can lead to generation of 7 postsynaptic spikes. In other words, the synaptic organization of nicotinic synapses enables the postsynaptic cells to fire faster than the presynaptic cells, which means the synaptic gain (7/4) is greater than 1.
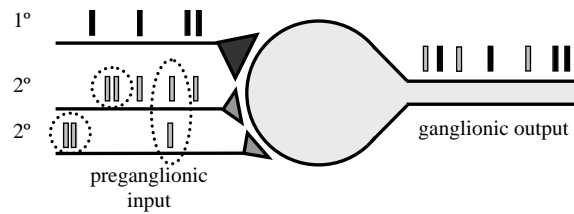
Figure 3. N + 1 convergence yields synaptic gain

In this model, it is assumed that ganglionic neurons do not form synapse upon one another and that presynaptic activity is noisy. As a consequence of these assumptions, behavior of an entire cell population can be represented by a single cell. Adapted from (Wheeler et al., 2004). In this simple scheme of n+1 synaptic convergence (n=2), each presynaptic input fires an average of 4 times, and the postsynaptic cell responds by firing 7 times, 4 driven by primary (1°) EPSPs (black bars) and 3 driven by temporal summation between secondary (2°) EPSPs (grey bars). The organization of nicotinic synapse, therefore, results in a gain of 1.75.

In this model, presynaptic divergence does not alter gain, but simply scales up the number of postsynaptic cells being controlled. The model also predicts that neuromodulatory mechanisms can regulate synaptic gain by altering the strength of secondary nicotinic synapses. If, for example, synapses are strengthened, then the temporal window for suprathreshold coincidences is lengthened and the probability of such events goes up, leading to an increase in gain (Schobesberger et al., 2000; Wheeler et al., 2004).

If one accepts the premise that ganglionic convergence and neuromodulatory mechanism can produce gain, then the next question relates to its significance for autonomic behavior. Baroreceptor mediated control of blood pressure is an example of a negative-feedback loop that uses sensory information to control the descending drive to spinal preganglionic neurons that drive vasoconstrictors (Levison et al., 1966; Persson and Kirchheim, 1991). When blood pressure goes down, preganglionic activity goes up and when blood pressure goes up, preganglionic activity is inhibited. For such control systems to work properly, they must have gain or amplification associated with them. It can be shown mathematically that the speed and accuracy of control is proportional to G/G+1, where G is the open-loop gain (Persson and Kirchheim, 1991). As gain increases, blood pressure will therefore approach its physiological set point. However, the neural origin of its gain remains unclear. Earlier studies focused on synapses in the nucleus tractus solitarius and the rostral ventral lateral medulla (Dampney, 1994; Sun, 1995). Recently, Horn and Karila's theory, together with more

recent simulations, suggested that much of this gain may arise in sympathetic ganglia (Karila and Horn, 2000; Wheeler et al., 2004).

1.5 WORKING HYPOTHESIS

It is, therefore, hypothesized that the synaptic organization of each phenotype of rat SCG neurons is specialized to generate a unique input-output relation, thereby allowing for differential control of specific target modalities.

Many of the key experimental observations for the theory of ganglionic gain have come from work on bullfrog sympathetic ganglia (Karila and Horn, 2000; Wheeler et al., 2004). This is an important model system in which clear criteria exist for studying identified vasomotor and secretomotor neurons (Dodd and Horn, 1983b; Horn et al., 1987; Jobling and Horn, 1996; Thorne and Horn, 1997). The goal of my thesis work is to test these ideas more directly in the mammalian sympathetic system. The problem, however, is a lack of established criteria for identifying sympathetic cell types in isolated ganglionic preparations that are suitable for cellular electrophysiology.

I , therefore, developed a new scheme for neuronal identification in the rat SCG in the first step. It opened the possibility of studying mechanisms of ganglionic integration that are specialized for different sympathetic modalities. Afterwards, as an initial stage of testing the "gain hypothesis", I analyzed factors that can affect synaptic

gain in identified vasoconstrictor neurons and compared the results with properties of

other neuronal subpopulations. The concepts developed through this research may

influence how we think about sympathetic control of distinct target modalities and may

also be relevant to other parts of nervous system that employ analogous relay circuitry.

CHAPTER 2

FUNCTIONAL CLASSIFICATION OF SYMPATHETIC NEURONS IN THE RAT SUPERIOR CERVICAL GANGLION

2.1 ABSTRACT

A new scheme is presented for identifying 3 sympathetic phenotypes in the rat SCG using electrophysiology and neuropeptide Y expression. Postganglionic compound action potentials recorded from the external and internal carotid nerves each contained two peaks, 1 and 2, with distinct preganglionic stimulus thresholds. Peak 2 in the external carotid response contained subpeaks 2a and 2b having a similar stimulus threshold. Neurons corresponding to peaks 1, 2a and 2b were identified intracellularly by antidromic stimulation, graded preganglionic stimulation, injection with neurobiotin and immunostaining. Seventeen of 53 neurons studied this way had a low threshold for preganglionic stimulation of firing that corresponded to activation of extracellular peak 1. All low threshold neurons were NPY-negative. The other 36 neurons had a high presynaptic stimulus threshold that corresponded to activation of extracellular peak 2, and 12 of these cells contained NPY. Together with other known features of ganglionic organization, the results indicate that low threshold, NPY-negative neurons are secretomotor cells projecting to salivary glands, that high threshold NPY-negative

neurons are pilomotor cells responsible for extracellular peak 2a, and that high threshold, NPY-positive neurons are vasoconstrictor cells responsible for peak 2b.   Secretomotor, pilomotor and vasomotor neurons identified in this way had distinct axonal conduction velocities (0.52, 0.20 and 0.10 m/s) and diameters (33, 29 and 25 μm), but were indistinguishable in terms of preganglionic conduction velocities (0.30 – 0.34 m/s). The cell classification scheme presented here will allow future comparison of ganglionic integration in different sympathetic modalities.

2.2 INTRODUCTION

Subsets of neurons in the rat superior cervical ganglia control a diverse set of peripheral targets (Chapter 1.3.1). In addition to target specificity, other physiological properties and anatomical features can serve to distinguish between different sympathetic phenotypes. These properties may play important functional roles and also be useful experimentally as markers for cellular identification. Thus, for example, NPY is selectively expressed by a large population of vasoconstrictor neurons in the SCG (Jarvi et al., 1986; Gibbins, 1991) and by smaller populations of cells projecting to the iris (Bjorklund et al., 1985; Grkovic et al., 1999) and pineal gland (Reuss and Moore, 1989). Studies of sympathetic ganglia other than the SCG indicate that functional subsets of neurons may also have distinct axonal conduction velocities. This criterion forms the basis for identification of secretomotor B type neurons and vasoconstrictor C type neurons in bullfrog paravertebral ganglia (Dodd and Horn, 1983b) and similarly has

been shown to correlate with functional cell types in lumbar paravertebral ganglia of the cat (Janig and Szulczyk, 1981; Janig and McLachlan, 1992). The aim of the present study was to determine whether axonal electrophysiology and NPY expression could be used to identify functional subclasses of neurons in the rat SCG. Our approach combined extracellular and intracellular recordings together with cellular dye labeling, reconstruction of dendritic morphlogy and immunocytochemistry. It thus became possible to identify individual cells in the caudal SCG as belonging to three discrete neuronal populations.

2.3 MATERIALS AND METHODS

2.3.1 Preparation of ganglia

Young adult male rats (Sprague-Dawley 180 - 250g) were euthanized by CO_2 inhalation using procedures approved by the Institutional Animal Care and Use Committee at the University of Pittsburgh. Under a dissecting microscope, the SCG was removed together with a closely adhering 2 cm segment of the carotid artery. After pinning out the tissue in a 60 mm Petri dish, the ganglion and associated nerves were carefully dissected away from the artery. The ganglion along with the cervical sympathetic trunk (CST) and the internal and external carotid nerves (ICN, ECN) was then transferred to a recording chamber made from a 35 mm Petri dish whose bottom had been replaced with a round glass coverslip (31 mm, #1) and a thin 0.9 mm layer of Sylgard. The

connective tissue capsule that surrounds the ganglion was then split open along its longitudinal axis and used to stretch and pin the preparation with a combination of cut down Minutien pins (100 – 150 µm diameter, Austerlitz) and short lengths of 50 µm diameter stainless steel wire (hard temper AISI 302, Goodfellow Cambridge Ltd., Berwyn, PA). Careful stretching and pinning of the final preparation served to improve subsequent microscopy by flattening the ganglion and was essential for penetration of microelectrodes through the remaining connective tissue that surrounds all ganglionic neurons. Tight fitting suction electrodes were then applied to the ganglionic nerves for extracellular stimulation and recording (Fig. 4), and the recording chamber was transferred to the stage of an upright fixed-stage Zeiss Axioskop microscope with 40x Nomarski immersion optics.

2.3.2 Physiological saline and superfusion

Throughout dissection and recording, the SCG was bathed in oxygenated mammalian Ringer's solution with a modified composition of (in mM): 146 NaCl, 4.7 KCl, 2.5 $CaCl_2$, 0.6 $MgSO_4$, 1.6 $NaHCO_3$, 0.13 NaH_2PO_4, 20 HEPES acid and 7.8 glucose (pH 7.3). During recording, the preparation was superfused at 1 – 2 ml/min with a peristaltic pump (bath volume ~ 1 ml). Most recordings were made at room temperature (23 ºC). For one series of extracellular recordings (Fig. 5), the bath was temporarily raised to 35 ºC using an SC-20 inline heater and CL-100 power supply (Warner Instruments, Hamden, CT).

2.3.3 Extracellular recording

The suction electrode used to stimulate preganglionically through the CST was fabricated from Pt wire and polyethylene tubing. Electrodes made from chlorided Ag wire and plastic tubing were used to record extracellular postganglionic responses from the ECN and ICN (Fig. 3A) and also to stimulate antidromic action potentials (Fig. 3B). For nerve stimulation, we employed brief (0.1 ms) electrically isolated pulses (A300/360, WPI, Sarasota, FL) with polarity adjusted for minimum response latency. Extracellular compound action potentials (CAP) were recorded by connecting the ICN and ECN electrodes to two AC coupled differential amplifiers (Grass P15, West Warwick, RI) and then to a Digidata 1200 computer interface (Molecular devices, Union City, CA). In addition, the extracellular amplifiers were connected to a bath ground consisting of a Ag-AgCl pellet.
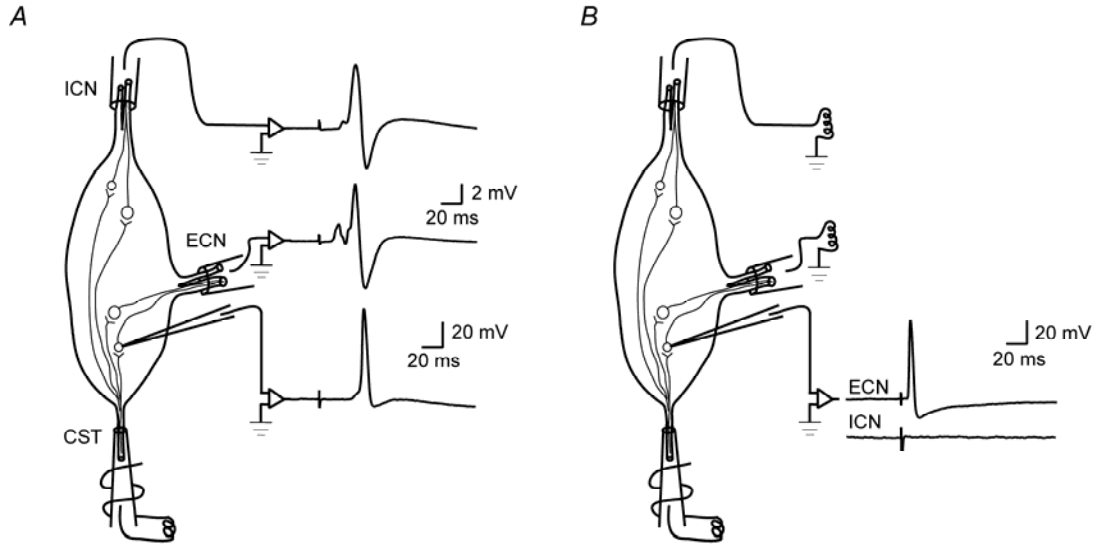
Figure 4. Experimental arrangement for recording postsynaptic responses to orthodromic stimulation and antidromic stimulation

The left panel, *A*, illustrates orthodromic responses to presynaptic stimulation of the CST through a suction electrode. Suction electrodes on the ECN and ICN record postganglionic compound action potentials and an intracellular microelectrode records EPSPs that can initiate action potentials. The right panel, *B*, illustrates the antidromic intracellular action potential evoked by postsynaptic stimulation of axons in the ECN and ICN. In this example, stimulation of the ECN, but not the ICN elicits a response, thereby demonstrating that this neuron projects to the ECN. During experiments, suction electrodes on the ECN and ICN were switched as needed between the stimulating and recording configurations.

2.3.4 Intracellular recording

Microelectrodes for intracellular recording were pulled from 1.2 mm fiber-capillary tubing, filled with 0.5M KCl and 0.5% neurobiotin (Vector Labs, Burlingame, CA) and had resistances of 60 – 130 MΩ. All intracellular recordings were made under visual guidance from neurons on the surface of the ganglion. The data were monitored on an oscilloscope and digitized at 10 kHz using a Digidata 1200 computer interface and pClamp 7 software (Molecular Devices, Union City, CA). The intracellular recording amplifier (Axoclamp 2B, Molecular Devices, Union City, CA) were connected to a common bath ground together with the extracellular amplifiers.

Resting membrane potential (V_{rest}) was measured as the difference between the potentials immediately before and after withdrawal of the microelectrode from a cell. Only cells with $V_{rest} < -40$ mV and an overshooting action potential >60 mV in amplitude were included in the analysis. To calculate conduction velocities, conduction distances were divided by the latencies of orthodromic and antidromic responses. The distances were measured by photographing each preparation at low power at the end of the recording session and measuring the shortest distances through the ganglion between extracellular suction electrodes (CST and ICN, CST and ECN) and between extracellular electrodes and sites of intracellular recording (Fig. 4).

2.3.5 Neuronal fills and morphometry of filled cells

After successful electrophysiological study, neurons were injected with neurobiotin by passing 400 – 500 pA, 150 ms depolarizing current pulses at 1Hz for 2 – 3 minutes. Generally, 2 – 3 neurons were filled in each experiment during 4 – 6 hours of recording and their positions carefully noted. The SCG was then immersed for one hour at room temperature in fixative containing 2% paraformaldehyde and 0.2% picric acid in 0.1M phosphate buffer (pH 7.3) and stored overnight in phosphate buffered saline (PBS) at 4 ºC. The next day, the tissue was given three 10 minute washes in 80% ethanol, followed by three 10 minute washes in dimethyl sulfoxide and three 10 minutes washes in PBS. The wholemount was then incubated for 2 hours at room temperature in streptavidin conjugated to CY3 (Jackson ImmunoResearch Laboratories, West Grove, PA) diluted 1:200 in PBS. After six 2 minute washes in PBS, the ganglion was wholemounted in 1:1 glycerol:PBS on a glass slide and coverslipped.

To reconstruct neurobiotin-filled neurons, SCG wholemounts were photographed with an Olympus Fluoview FV1000 laser scanning confocal microscope. The resulting Z-stacks of images were then transferred to a workstation and reconstructed using Imaris 4.0 software (Bitplane, Saint Paul, MN). To measure the size of filled cell bodies, planar projections of reconstructed cells were imported into Zeiss Axiovision and traced. Somatic area (A) was converted to an equivalent diameter (d) by the relation $d = 2(A/\pi)^{0.5}$.

2.3.6. Immunocytochemistry

After imaging filled neurons, ganglia were embedded, sectioned and immunostained for neuropeptide Y (NPY). Each ganglion was rinsed 3 times in PBS, then dehydrated through graded ethanols and infiltrated with polyethylene glycol (PEG 1000) for 30 min under vacuum at 47 ºC. It was then embedded in molten PEG (MW 1450) and hardened at -20 ºC for 15 min. After embedding, the ganglion was cut into serial 10 µm sections on a Leica RM 2165 microtome. For immunocytochemistry, floating sections were rinsed in PBS, blocked for 2 hours at room temperature in PBS containing 1.5% donkey serum (Jackson ImmunoResearch Laboratories) and 0.3% triton-X100 (Sigma) and incubated overnight at 4 ºC in rabbit anti-NPY (Peninsula, San Carlos, CA), diluted 1:2000 in blocking buffer. The sections were then rinsed in PBS and incubated in 1:200 donkey anti-rabbit CY2 (Jackson ImmunoResearch Laboratories) for 2 hours at room temperature. After final rinsing in PBS, sections were mounted on glass slides, dried overnight, dehydrated through graded ethanols, cleared in xylenes, and coverslipped with Krystalon. Neurobiotin-filled neurons were then scored for NPY-immunofluorescence under a Zeiss Axioskop 2 microscope and photographed (Axiocam HrC, Axiovision 4.2).

NPY-immunoreactivity appeared as an intense ring of perinuclear staining, which in some, but not all cells filled the cytoplasm. This pattern of staining replicates previous descriptions of NPY-immunoreactivity in rat and mouse sympathetic ganglia (see fig. 1 in(Jarvi et al., 1986)), figs. 1B,2A in (Jobling and Gibbins, 1999) and in fig 1 in (Headley et al., 2005). In addition to this characteristic subcellular distribution, there was a sparkly quality to NPY-immunoreactivity that was easily distinguished from non-

specific background. All immunoreactivity was eliminated by omission of the primary

antibody and by preabsorbtion of the primary antibody with 10 µM porcine NPY

(Peninsula) for 18 hours at 4 ºC.

2.3.7. Analysis and Statistics

Grouped data are presented as the mean $\pm$ standard deviation (S.D.). Statistical

differences between groups describing presynaptic conduction velocities, postsynaptic

conduction velocities, cellular diameters and numbers of primary dendrites were

examined using a one-way ANOVA, followed by Tukey's test for multiple comparisons

(Prism 4.0, GraphPad, San Diego, CA) and $P < 0.05$ as the criterion for significance.

Figures were prepared using Igor 5.0 (Wavemetrics, Lake Oswego, OR), Adobe

Photoshop CS and Adobe Illustrator CS.

2.4 RESULTS

2.4.1 Postganglionic compound action potentials contain two major components

The extracellular CAPs that were recorded from the external and internal carotid nerves each contained two major peaks with distinct conduction velocities (Fig. 5, Table 1). Graded stimulation of the preganglionic cervical sympathetic trunk (CST) demonstrated that the faster peak 1 had a lower stimulus threshold than the slower peak 2. Although the exact form of the two peaks varied from one ganglion to another, in 50 preparations peak 1 was consistently smaller than peak 2 in both nerves. In addition, peak 1 was generally smaller in the ICN than in the ECN. Raising the temperature from 23 ºC (Fig. 5, A and B) to 35 ºC (Fig. 5, C and D) caused an approximate doubling of all conduction velocities (Table 1), but did not alter the basic appearance of peaks 1 and 2 or their relative stimulus thresholds. In many preparations, a notch divided peak 2 into subpeaks 2a and 2b (Fig. 5A), but these components had the same presynaptic stimulus threshold. The entire CAP was postsynaptic in origin because in separate control experiments it was reversibly blocked by 100 μM Cd^{2+}, an antagonist of voltage-dependent Ca^{2+} channels or by 10 μM dihydro-β-erythroidine, a nicotinic receptor antagonist.

These results suggest that the SCG contains at least two subpopulations of neurons whose nicotinic synapses have distinct presynaptic stimulus thresholds. To test this possibility, we recorded intracellularly from neurons in the caudal ganglion that

37

project to the ECN (Bowers and Zigmond, 1979), which were identified by antidromic

stimulation (Fig. 4B). We focused on ECN projecting neurons because peak 1 is larger

in the ECN than ICN (Fig. 5). This suggests that neurons giving rise to the first peak

would be most abundant in the caudal ganglion and therefore easier to find than low

threshold ICN projecting neurons, which are localized in the rostral ganglion.
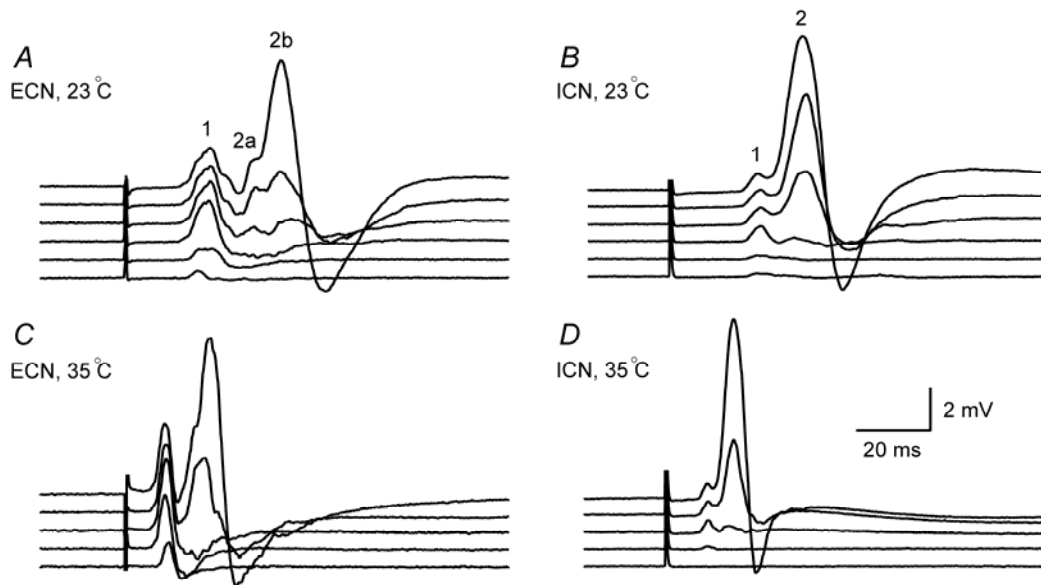
Figure 5. Components of the postganglionic compound action potential and their temperature dependence

Each panel illustrates a family of extracellular CAPs elicited by graded preganglionic stimulation of increasing intensity from bottom trace to top trace. On the left, panels *A* and *C* show responses recorded from the ECN at room temperature and 35 ^{o}C. On the right, panels *B* and *D* illustrate responses recorded from the ICN at these two temperatures. In all four panels, graded stimulation first recruits an early response defined as peak 1 and then a larger later response defined as peak 2. In the ECN recordings, peak 2 was often subdivided into subpeaks, labeled as 2a and 2b in panel *A*. These subpeaks had overlapping stimulus thresholds and were considered together as belonging to the high threshold peak. Elevating the temperature to a physiological level, *C* and *D*, had the effect of speeding conduction but did not alter the basic appearance of peaks 1 and 2 or their relative stimulus thresholds.

Table 1- Extracellular conduction velocities and their temperature dependence

Postganglionic nerve	CAP peak	Conduction velocity (m/s) 23 °C	Conduction velocity (m/s) 35 °C
ECN	1	0.40 ± 0.09	0.87 ± 0.11
	2a	0.28 ± 0.05	0.57 ± 0.09
	2b	0.21 ± 0.04	0.43 ± 0.06
ICN	1	0.34 ± 0.04	0.67 ± 0.10
	2	0.23 ± 0.03	0.42 ± 0.06

Conduction velocities were calculated using the latencies of peaks in the compound action potentials recorded from the ECN and ICN in response to supramaximal preganglionic stimulation of the cervical sympathetic trunk (n= 50). The scheme for numbering different peaks in extracellular records is illustrated in Figure 5. Raising the temperature from 23 °C to 35 °C caused a doubling in the conduction velocities of all action potential components.

2.4.2 Low and high threshold neurons

On average, sympathetic neurons in the rat SCG receive nicotinic synaptic input from 8.7 preganglionic neurons (Purves and Lichtman, 1985). By carefully adjusting the strength of graded presynaptic nerve stimuli applied to the CST, we fractionated these converging preganglionic inputs into subthreshold and suprathreshold EPSPs (Fig. 6, A and C) and observed how this corresponded to recruitment of peaks in the extracellular compound action potential (Fig. 6, B and D). Consistent with previous studies (Skok and Ivanov, 1983; Hirst and McLachlan, 1986; McLachlan et al., 1997; McLachlan et al., 1998; Jobling and Gibbins, 1999), we found that one or occasionally two of the nicotinic inputs were suprathreshold in strength. In some neurons the presynaptic stimulus threshold for firing corresponded to peak 1 of the extracellular CAP (Fig. 6, A and B) and in other cells to peak 2 (Fig. 6, C and D). Using this correspondence, we classified neurons as being low threshold or high threshold cells based on the minimal presynaptic stimulus required to trigger firing of a postsynaptic action potential. In cases where all of the inputs to a cell were examined, it was evident that some neurons received a combination of low threshold and high threshold inputs. For example, Figure 6A illustrates a low threshold cell with a weak high threshold input and Figure 6C illustrates a high threshold cell with a weak low threshold input.
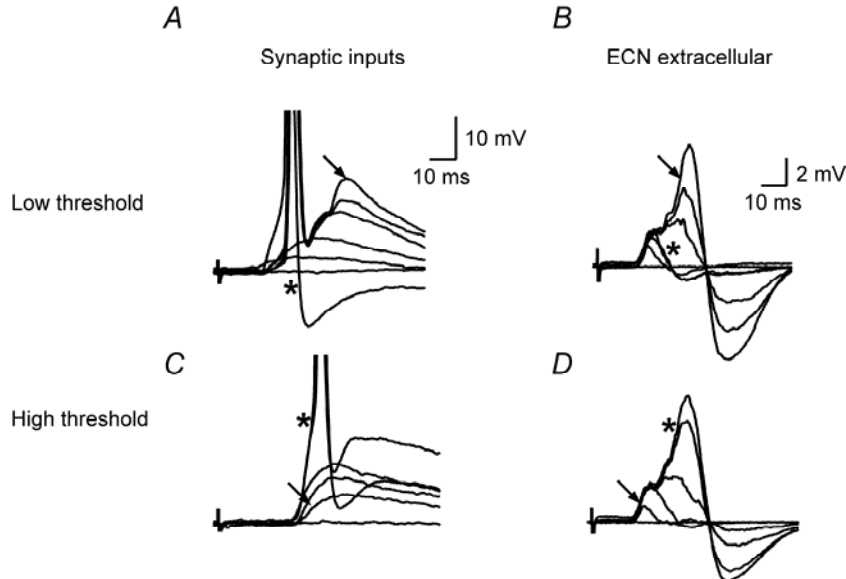
Figure 6. Intracellular identification of low threshold and high threshold neurons

Simultaneous intracellular and extracellular recordings at room temperature were used to determine how the stimulus thresholds for EPSP components corresponded to peaks in the CAPs recorded from the ECN. In panels *A* and *C*, an asterisk marks recruitment of a suprathreshold EPSP by graded presynaptic stimulation and in panels *B* and *D*, one can see the corresponding extracellular responses. The low threshold cell in panel *A* fired upon activation of peak 1 in the extracellular recording in panel *B*. This contrasted with the high threshold cell in panel *C*, which fired when peak 2 was recruited, *D*. These records also show that sympathetic neurons can receive combined low and high threshold synaptic input. Arrows in the top row mark a high threshold EPSP in the low threshold neuron and in the bottom row they denote a low threshold EPSP in the high threshold cell.

2.4.3. NPY expression is restricted to a subset of high threshold neurons

To determine whether the classification of neurons as low or high threshold correlated with other cellular properties that could help to establish functional identity, we broadened the study to include additional physiological and anatomical characteristics. We focused first upon NPY, a postganglionic co-transmitter that is expressed primarily by vasoconstrictor neurons (Lundberg et al., 1982; Lundberg et al., 1984), a group that constitutes about half of all ganglion cells (Jarvi et al., 1986). When 53 ECN-projecting neurons were classified using presynaptic stimulus threshold and NPY-immunoreactivity, only three of the four possible combinations were found (Fig. 7). None of the 17 low threshold neurons contained NPY. This contrasted with the 36 high threshold cells, which included a group of 12 NPY-positive neurons. With additional data from these neurons, we then compared the three cell types in terms of their axonal conduction velocities and soma sizes (Figs. 8 and 9, Table 2).
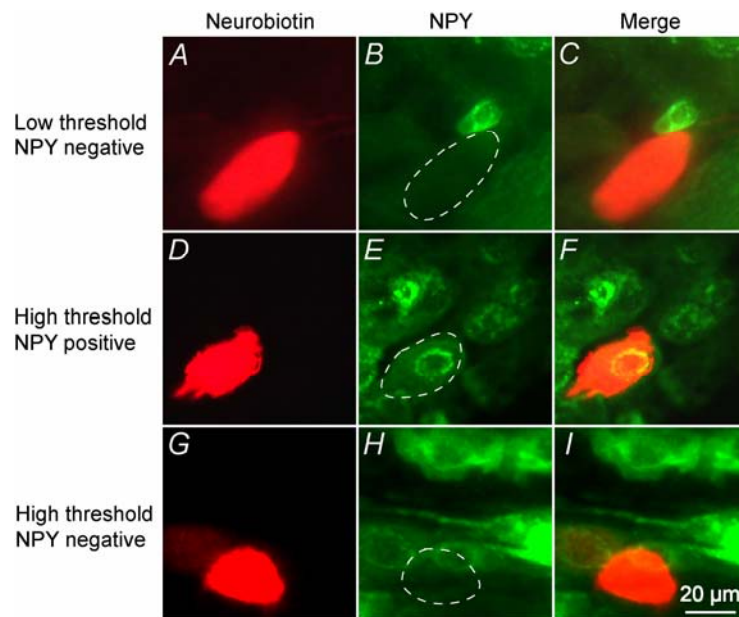
Figure 7. NPY is selectively expressed by a subpopulation of high threshold neurons

ECN projecting neurons were identified by antidromic stimulation and classified by their presynaptic

stimulus threshold for firing an action potential. They were then injected with neurobiotin and processed

for NPY-immunoreactivity. This approACh led to the identification of three cell types, each illustrated as a

row in this figure. In the left column, panels *A,D* and *G*, show neurobiotin filled cells. In the middle

column, panels *B,E* and *H* illustrate NPY-immunoreactivity, with white dashed lines highlighting the

neurobiotin filled cells. Panels *C*, *F* and *I* in the right column contain merged images of the two labels.

2.4.4 Electrophysiological profiles of three neuronal types

The range of conduction velocities associated with peaks 1 and 2 in the extracellular CAP (Fig. 5) could arise from presynaptic or postsynaptic differences in axonal conduction velocities or from differences that were both pre- and postsynaptic. To address this issue, axonal conduction velocities were calculated by measuring intracellular conduction latencies for each of the three cell types (Fig. 8) along with conduction distances between stimulating and recording electrodes. This revealed that the slower conduction velocity of peak 2 in the CAP was mainly postganglionic in origin.

Due to the inverse relation that normally exists between extracellular stimulus thresholds and axonal conduction velocities (Keynes, 1991), one would expect low threshold neurons to have faster preganglionic conduction rates than high threshold neurons. Although this trend was evident in our data (Figs. 6A and C, 8, 9A, Table 2), the differences were small and not statistically significant. This contrasted with postganglionic conduction velocities, which differed significantly between all three groups (Figs. 8, 9B, Table 2). Postganglionic axons of low threshold neurons had the fastest rates while high threshold, NPY-positive cells had the slowest conducting axons. Resting potentials of the three cell types were indistinguishable (-50.1 ± 5.8 mV for low threshold neurons, -50.9 ± 5.4 mV for high threshold, NPY-positive neurons, -51.7 ±7.4 mV for high threshold, NPY-negative neurons).

By combining the intracellular pre- and postsynaptic conduction latencies and conduction distances, it was possible to calculate overall conduction velocities for the three cell groups (Table 2) and then compare them with the extracellular conduction data from ECN recordings (Table 1). This comparison confirmed that low threshold neurons produce peak 1 in the CAP. It also revealed that high threshold, NPY-negative neurons correspond to peak 2a and that high threshold, NPY-positive neurons correspond to peak 2b.
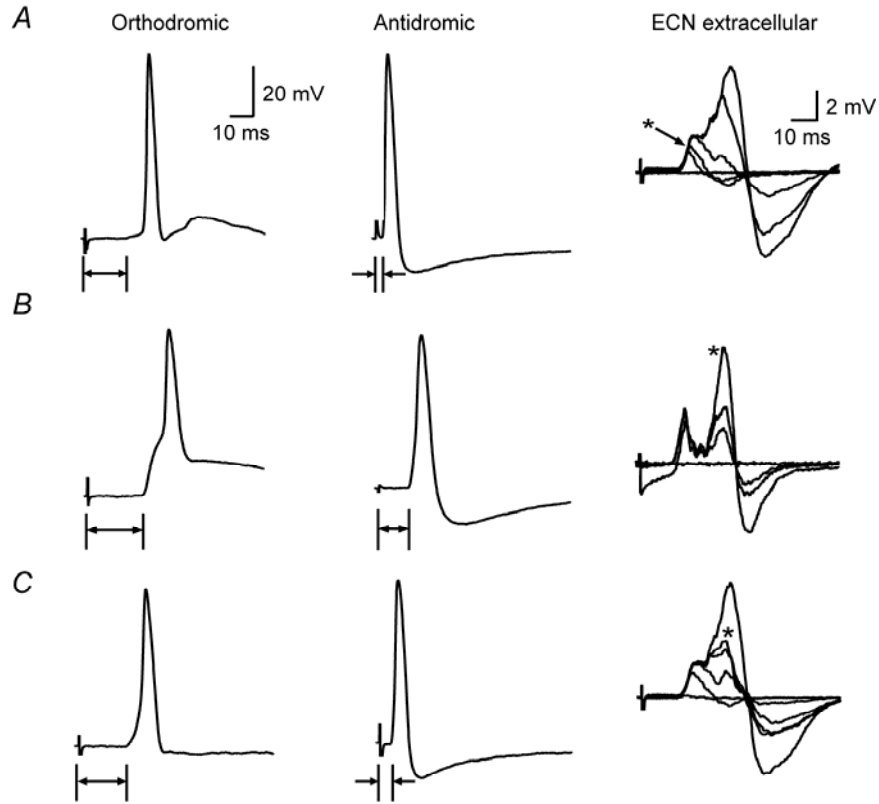
Figure 8. Electrophysiological profiles of three neuronal types that project to the ECN

Each row in this figure illustrates the intracellular orthodromic and antidromic responses for a cell type, together with extracellular recordings that were used to classify it as low or high threshold. Row *A* illustrates a low threshold, NPY-negative cell, row *B* shows a high threshold, NPY-positive cell and row *C* shows a high threshold, NPY-negative cell. Arrows drawn below the intracellular recordings denote conduction delays. Asterisks in the CAP denote the response used to classify the cell as being low or high threshold.
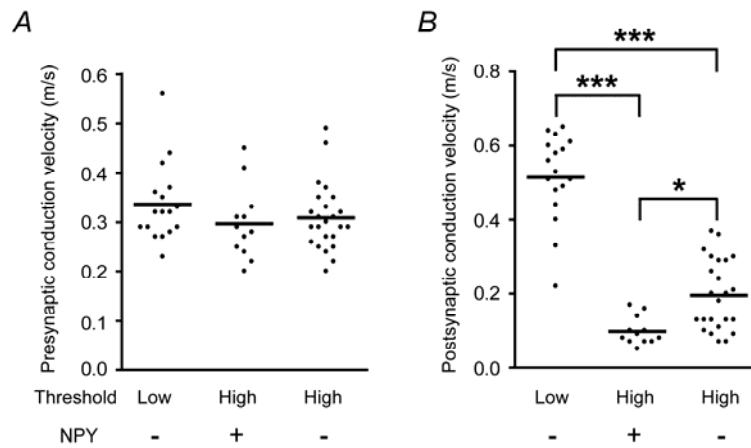
Figure 9. Comparison of axonal conduction velocities in the three cell types

Scatter plots compare the distribution in each neuronal type of presynaptic conduction velocities, *A*,

postsynaptic conduction velocities, *B*. For each property, every cell is represented as a single point and

horizontal bars denote the population mean. For the purpose of visual clarity, the data points for each

group are also spread horizontally. The only statistically significant differences between cell types were in

postsynaptic conduction velocities; *** indicates P<0.001 and * indicates P<0.05. Means and standard

deviations for these data are in Table 2.

2.4.5. The three cell types differ in size

In sympathetic ganglia of the bullfrog, mouse and guinea pig, cell body size can correlate with phenotypic identity (Dodd and Horn, 1983b; Gibbins, 1991; Gibbins et al., 1996). The possibility that a similar relation exists in the rat SCG is suggested by the observation that NPY-negative neurons in the caudal ganglion are about 6 μm larger in diameter than NPY-positive neurons [30.2 μm compared to 24.3 μm, (Headley et al., 2005)]. When we compared ECN projecting neurons that had been classified using presynaptic stimulus threshold and NPY expression, it revealed significant size differences between all three cell types (Table 2). Low threshold, NPY-negative neurons were the largest cells with a mean diameter of 33.40 ± 3.47 μm, high threshold, NPY-negative neurons were intermediate in size with a mean diameter of 25.40 ± 2.88 μm, and high threshold, NPY-positive neurons were the smallest cells with a mean diameter of 29.34 ± 6.03 μm.

Table 2- Properties of neurons projecting to the ECN

Cell type	Presynaptic conduction velocity (m/s)	Postsynaptic conduction velocity (m/s)	Overall conduction velocity (m/s)	Cell body diameter (µm)	Number of primary dendrites
Low threshold/NPY- (n=17)	0.34 ± 0.08	0.52 ± 0.12	0.36 ± 0.07	33.40 ± 3.47	8.4 ± 3.3
High threshold/NPY+ (n=12)	0.30 ± 0.07	0.10 ± 0.04	0.22 ± 0.05	25.40 ± 2.88	8.6 ± 3.3
High threshold/NPY- (n=24)	0.31 ± 0.10	0.20 ± 0.10	0.27 ± 0.06	29.34 ± 6.03	8.4 ± 4.2

Presynaptic and postsynaptic conduction velocities were calculated from intracellular latency measurements at room temperature, as illustrated in Fig. 8. Overall conduction velocities were calculated for each cell by combining the pre- and postsynaptic conduction distances and dividing it by the combined latency. The cell type specific differences in postsynaptic conduction velocity, overall conduction velocity and diameter were statistically significant. Differences in presynaptic conduction velocity and number of primary dendrites were not significant.

2.5 DISCUSSION

This work shows for the first time that three types of sympathetic neuron can be identified in the rat SCG using the combined criteria of antidromic activation, presynaptic stimulus threshold and NPY expression. The analysis has focused on neurons in the caudal portion of the ganglion that project to targets in the jaw and neighboring regions of the head by way of the external carotid nerve. In light of other knowledge describing the cellular organization of the SCG, it is proposed that low threshold, NPY-negative cells are secretomotor neurons that supply salivary glands, that high threshold, NPY-positive cells are vasoconstrictor neurons, and that high threshold, NPY-negative cells are pilomotor neurons. Development of this scheme for neuronal identification in the isolated SCG opens the possibility of studying mechanisms of ganglionic integration that are specialized for different sympathetic modalities.

2.5.1 Origin of a new scheme for cellular identification

Our approach to neuronal identification in the rat SCG draws on previous studies of other ganglia. In the early 1960's it was discovered that neurons in amphibian paravertebral ganglia can be classified as B and C cells by their axonal conduction velocities (Nishi et al., 1965). This provided a starting point for comparing cell types that led to many discoveries. B cells are larger than C cells (Nishi et al., 1965; Jan and Jan, 1982; Dodd and Horn, 1983b). B and C cells innervate different end-organs (Jobling

and Horn, 1996; Thorne and Horn, 1997) and they express different muscarinic synaptic mechanisms (Brown et al., 1980; Dodd and Horn, 1983a; Smith, 1994; Shen and Horn, 1996) and different neuropeptides (Jan and Jan, 1982; Horn et al., 1987; Horn and Stofer, 1989). Importantly, some of these features have parallels in the mammalian sympathetic system.

In the cat, lumbar paravertebral ganglia contain functional subsystems of sympathetic neurons that control different end organs (Janig and Szulczyk, 1981; Janig and McLachlan, 1992). These phenotypes are activated through different reflexes in the intact animal and they are characterized by distinct pre- and postganglionic axonal conduction velocities. Feline preganglionic axons are generally B fibers that conduct at 1 – 10 m/s and most postganglionic axons are C fibers that conduct at < 1 m/s. As in frogs and toads, vasoconstrictors in the cat have the slowest pre- and postganglionic conduction velocities.

We found that almost all postganglionic axons in the rat SCG were C fibers, even at physiological temperatures. Warming the ganglion from room temperature to 35 ºC caused a doubling of the slowest and fastest components of the compound action potential from 0.21 and 0.40 m/s to 0.42 and 0.87 m/s (Table 1). Using this result and the single cell data, one can see that about half of the postganglionic fibers belonging to low threshold neurons were borderline B fibers – doubling the intracellular estimates of their conduction velocities at room temperature indicates that at physiological temperature they would conduct at 1 – 1.4 m/s (Table 2, Fig 9. A, B). This differed from

preganglionic fibers, which all behaved as C fibers, and was in marked contrast to the B fibers commonly observed in preganglionic sympathetic axons of the cat (Janig and Szulczyk, 1981). This distinction is probably due to the fact that B fibers of preganglionic sympathetic axons of the cat are myelinated while almost all preganglionic axons projecting to rat SCG are unmyelinated (Bray and Aguayo, 1974; Gabella, 1976).

In our experiments, stimulus threshold proved to be a more sensitive criterion than conduction velocity for distinguishing between subpopulations of preganglionic axons. One possible explanation for the inability to distinguish between the presynaptic conduction velocities of low and high threshold neurons is that high threshold neurons can also have low threshold inputs. Although these synapses are too weak to drive action potentials, they could in some cases have led to underestimates of the conduction latencies for high threshold fibers.

In addition to making it more difficult to measure presynaptic latencies, the finding that some cells receive combined low and high threshold input raises an important physiological question. Does this observation indicate that different functional classes of preganglionic fibers converge on individual ganglion cells or might it simply reflect the technical limitations of isolating subtle differences between populations of preganglionic fibers whose stimulus thresholds overlap? At this time, we can not rule out the possibility of preganglionic "cross-talk" between sympathetic modalities. If it exists, then this would represent a clear departure from the case of B and C cells in

amphibian paravertebral ganglia, which receive separate preganglionic inputs (Skok, 1973c; Dodd and Horn, 1983b; Horn and Stofer, 1988; Smith, 1994).

2.5.2 Relation to secretomotor, pilomotor, and vasoconstrictor neurons

Support for the proposed functional identification of low and high threshold neurons in the caudal SCG comes from previous work that combined retrograde axonal tracing with cell counts and immunocytochemistry. From retrograde tracing it is clear that neurons in the caudal SCG project selectively into the ECN and that neurons in the rostral SCG project selectively into the ICN (Bowers and Zigmond, 1979). For purposes of intracellular neuronal identification, the present study focused on neurons whose ECN projection was confirmed by antidromic stimulation (Figs 4, 8). The largest groups of ECN projecting neurons consist of vasoconstrictors, piloerectors and secretomotor neurons that control salivary glands. We propose that low threshold neurons are secretomotor salivary neurons because they had the largest cell bodies, the fastest antidromic conduction velocities and were NPY-negative (Figs. 7, 8, 9, Table 2). Retrograde tracing from the salivary glands labels about 16% of rat SCG neurons (Voyvodic, 1989). Cells labeled this way are amongst the largest and 95% of them are NPY-negative (Andrews et al., 1996; Grkovic and Anderson, 1997). This contrasts with NPY-positive sympathetic neurons, which for the most part are vasoconstrictors (Lundberg et al., 1982; Lundberg et al., 1984; Jarvi et al., 1986). Three exceptions to this generalization are neurons that innervate the iris, pineal gland and thyroid gland (Bowers et al., 1984; Bjorklund et al., 1985; Grunditz et al., 1988; Reuss and Moore,

1989; Sundler et al., 1989; Flett and Bell, 1991; Grkovic et al., 1999). However, each of these phenotypes constitutes only 1-2 % of SCG neurons and those supplying the iris and pineal leave the SCG through the ICN. For these reasons it seems most likely that the high threshold, NPY-positive neurons projecting to the ECN were primarily vasoconstrictors. Other properties of these neurons also match the known features of vasoconstrictors. As in the mouse, cat and bullfrog (Janig and Szulczyk, 1981; Dodd and Horn, 1983b; Gibbins, 1991), NPY-positive rat neurons had the smallest cell bodies and the slowest postganglionic axonal conduction velocities (Table 2, Fig. 9B). Finally, it seems most likely that high threshold, NPY-negative cells are pilomotor in function, based on their similarity to sympathetic neurons in the mouse and cat. Piloerectors in the mouse SCG, are NPY-negative, intermediate in size and relatively abundant, probably constituting 20% of all cells (Gibbins, 1991).   Feline piloerector neurons have faster postganglionic conduction velocities than vasoconstrictors (Janig and Szulczyk, 1981; Janig and McLachlan, 1992).

In our study, the number of neurons representing each of the three cell types did not reflect their relative abundance in the intact ganglion. Thus for example, 32% of the cells in Table 2 are putative secretomotor neurons, but this group only represents about 16% of SCG neurons (Voyvodic, 1989) and 23% of the cells are putative vasoconstrictors, but this group represents about half of SCG neurons (Jarvi et al., 1986). These disparities arise largely from the fact that it is more difficult to record from small cells than large cells. Low threshold, NPY-negative neurons proved to be the largest cells, probably accounting for why they are over-represented in our sample.

High threshold, NPY-positive neurons were the smallest cells, which contributed to their under-representation. In addition, we cannot rule out the possibility that the process of filling cells damaged them and caused some false negative results in the immunocytochemistry. However, we do not think this can explain the fact that 17 of 17 low threshold cells were NPY-negative. Similarly, impalement damage may have confounded the high threshold data to some degree, but not enough to obscure significant differences between NPY-positive and negative neurons in terms of their sizes and axonal conduction velocities (Table 2). The above discussions support the solidity of my interpretation that low threshold, NPY negative cells are secretomotor neurons, high threshold, NPY negative cells are pilomotor neurons and high threshold, NPY positive cells are vasoconstrictor neurons.

CHAPTER 3

SYNAPTIC CONVERGENCE IN FUNCTIONAL SUBSETS OF RAT SCG NEURONS

3.1 ABSTRACT

According to the gain hypothesis, synaptic convergence is one of the mechanisms that could affect synaptic integration and produce gain (Karila and Horn, 2000; Wheeler et al., 2004). It is, however, not at all clear that synaptic convergence varies in different functional subsets of sympathetic neurons. In Chapter 2, we have established a new scheme for classifying secretomotor, pilomotor and vasoconstrictor neurons in the rat SCG. In this chapter, the convergence of nicotinic synapses in these different cell groups is examined in identified neurons by counting the numbers of primary dendrites. Our results showed that the average number of primary dendrites in these three types of neurons was 8.4, 8.4 and 8.6 respectively (no significant difference). It suggested that nicotinic convergence does not contribute to variations in the synaptic amplification of preganglionic activity.

3.2 METHODS

After successful electrophysiological study, neurons studied in Chapter 2 were injected with neurobiotin by passing 400 – 500 pA, 150ms depolarizing current pulses at 1Hz for 2 -3 minutes. The whole procedure of neuronal fills has been described in details in Chapter 2.3.5.

To reconstruct neurobiotin-filled neurons, SCG wholemounts were photographed with an Olympus Fluoview FV1000 laser scanning confocal microscope. After reconstruction of Z-stacks of images using Imaris 4.0 software (Bitplane, Saint Paul, MN), the axon of each filled neuron was identified based on its length, which in some cells could be traced for several hundred microns, and by the relative lack of branching. Rotating the 3-D reconstructions facilitated identification and counting of primary dendrites, using established criteria (Purves and Hume, 1981). Dendrites were defined as non-axonal processes that extended from the soma by more than 5 μm. In some neurons with complex shapes (Figure 6), processes sometimes arborize very close to the soma. These were counted as a single dendrite when the branch point was <5 μm from the soma(Purves and Hume, 1981).

3.3 RESULTS: USE OF DENDRITE BRANCHING AS AN INDEX OF SYNAPTIC CONVERGENCE

It was of interest to compare nicotinic convergence in the three cell types because convergence is an important determinant of synaptic amplification in autonomic neurons and could, in principle, differ between subclasses of neurons that serve different physiological roles (Karila and Horn, 2000; Wheeler et al., 2004). To test this idea, neurons that had been electrophysiologically classified were filled with neurobiotin and the number of primary dendrites on each cell was counted from confocal images (Fig. 10). The rationale for this approach relied on previous studies of the SCG from several mammalian species, which demonstrate a systematic correlation between nicotinic convergence and the number of primary dendrites (Purves and Lichtman, 1985).   We observed that the number of dendrites ranged from 3 to 17, with an overall average of 8.4 ± 3.7 (n = 53), which agrees with the earlier assessment of the rat SCG (Purves and Lichtman, 1985). There were, however, no differences between the three cell groups classified on the basis of stimulus threshold and NPY expression. The cells in each group had a similar range and average number of primary dendrites (Figs. 10, 11, Table 2 in Chapter 2).
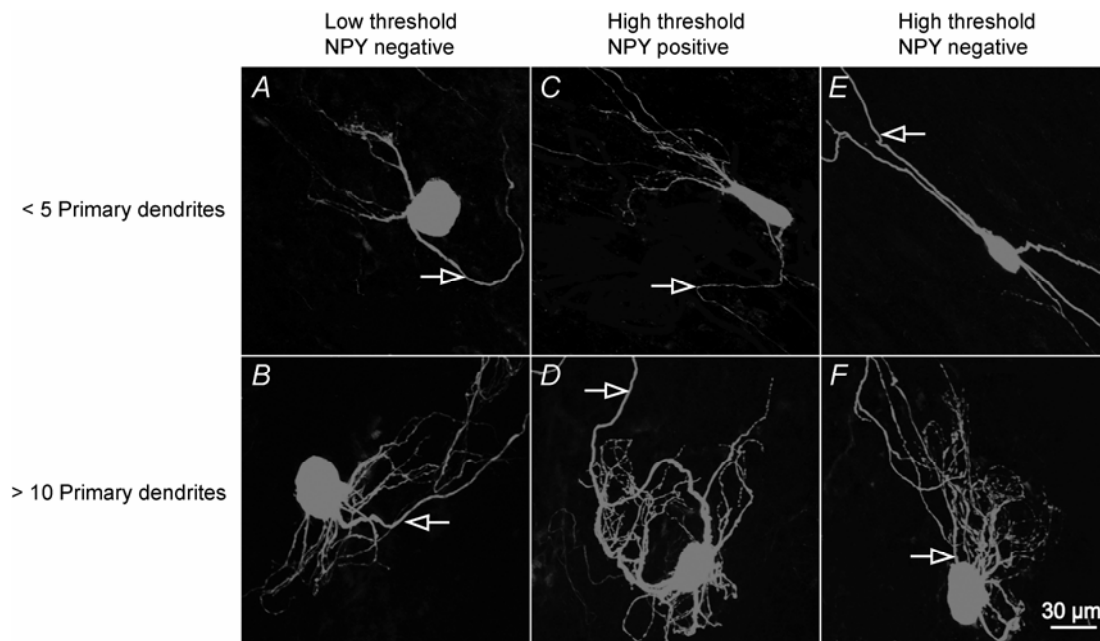
Figure 10. Variations in dendritic complexity do not distinguish the three neuronal types

Confocal reconstructions of neurobiotin filled ECN projecting neurons that were classified as low threshold, NPY-negative (*A,B*), high threshold, NPY-positive (*C,D*) or high threshold, NPY-negative cells (*E,F*). For each cell type, there were some neurons with fewer than five primary dendrites, *A,C,E* and others with more than ten primary dendrites, *B,D,F*. Arrows point to the axon of each neuron.
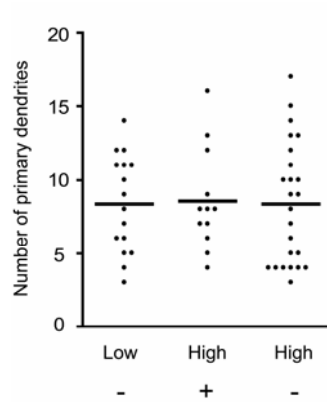
Figure 11. Comparison of dendrite number in the three cell types

Scatter plots compare the distribution in each neuronal type of the number of primary dendrites. Every

cell is represented as a single point and horizontal bars denote the population mean. For the purpose of

visual clarity, the data points for each group are also spread horizontally. Means and standard deviations

for these data are in Table 2.

3.4 DISCUSSION: IMPLICATIONS FOR GANGLIONIC INTEGRATION

A key goal of the present experiments was to compare nicotinic convergence in different

sympathetic phenotypes. Although previous work has examined systematically the

variations in convergence that occur in different mammalian species (Purves and Hume,

1981; Purves and Lichtman, 1985), the physiological role of this diversity remains

enigmatic. In a recently developed theory of ganglionic integration, it has been

proposed that nicotinic convergence enables sympathetic ganglia to function as

synaptic amplifiers of preganglionic activity (Karila and Horn, 2000; Wheeler et al.,

2004). If one were to observe cell-specific differences in convergence, then it would

suggest that gain varies in different sympathetic modalities. When this hypothesis was

tested by comparing the number of primary dendrites in putative secretomotor,

vasoconstrictor and pilomotor neurons (Figs 10, 11, Table 2), the results showed clearly

that all three cell types were similar. This finding supports the results from two other

studies using somewhat different approaches. In the first, guinea pig lumbar

sympathetic vasoconstrictor and pilomotor neurons were filled with neurobiotin and

classified on the basis of NPY expression (Gibbins and Matthew, 1996). In the second,

rat SCG neurons projecting to the middle cerebral artery, submandibular gland and iris

were back labeled and then injected in fixed tissue (Andrews et al., 1996). Although all

of these studies indicate that the number of primary dendrites is unrelated to the

phenotypic identity, it is important to note that other mechanisms could generate

phenotypic specialization of nicotinic integration. This diversity could arise, for example,

through selective developmental regulation of synaptic strength and also through

mechanisms of short-term plasticity such as facilitation, depression and metabotropic

modulation (Karila and Horn, 2000; Wheeler et al., 2004). Pursuit of these possibilities

is now feasible using the scheme for neuronal identification presented in this paper.

CHAPTER 4

CELLULAR SPECIALIZATION OF POSTSYNAPTIC ALPHA-ADRENERGIC MODULATION IN THE RAT SUPERIOR CERVICAL GANGLIA

4.1 ABSTRACT

In sympathetic neurons of the rat superior cervical ganglion (SCG), postsynaptic $\alpha2$-adrenergic receptors inhibit N-type calcium currents. Consequently, norepinephrine (NE) inhibits the shoulder on the repolarization phase of the action potential (AP) and the Ca^{2+}-dependent spike afterhyperpolarization (AHP). We now report that these responses are expressed in only two of the three functional subsets of sympathetic neurons that can be identified in isolated preparations of the rat SCG. Using intracellular and extracellular recording followed by cell marking and immunocytochemistry, we identified secretomotor, pilomotor and vasoconstrictor neurons and then tested the responses of these cell types to bath-applied 10 µM NE. In 16 of 16 secretomotor neurons and 14 of 15 pilomotor neurons, NE reversibly decreased AP half-width, lowered peak AHP amplitude and shortened AHP half-width. This contrasted with vasoconstrictor neurons, where NE produced no effect on AP shape in any of the 14 cells tested. These cell-type-specific effects of NE remained when tetraethylammonium chloride (TEA, 10 mM) was applied to cells in order to accentuate the AP shoulder and

AHP. However, addition of 100 µM CdCl$_2$ reduced AP shoulder and AHP. In addition, the cell-specific effects of NE were not associated with differences in resting membrane potential, input resistance or AP amplitude. These results suggest that postsynaptic noradrenergic modulation through adrenergic receptors might play a role in modulation of sympathetic neurons that control glands and pilomotor glands but not blood vessels. In addition, the data establish that insensitivity to NE can serve as a practical experimental criterion for functional identification of vasomotor neurons in future physiological studies of the SCG.

4.2 INTRODUCTION

Synaptic neurotransmission in the rat SCG neurons is mediated by acetylcholine (ACh) released from preganglionic nerve terminals (McLachlan, 1995; Gibbins, 2004). Nicotinic receptors act as nonselective cation channels by allowing mixed cation influx upon ACh binding and mediate fast EPSPs (Selyanko et al., 1979; Selyanko and Skok, 1979). In addition, neuromodulatory mechanisms of synaptic transmission are expressed in the rat SCG neurons (Tokimasa and Akasu, 1995; Janig and Habler, 1999). Activation of G-protein coupled receptors (GPCRs) such as muscarinic (Brown et al., 1980; Hille, 1994; Tokimasa and Akasu, 1995; Shen and Horn, 1996; Shapiro et al., 2001), Angiotensin II AT1 receptors (Lewis and Reit, 1965; Shapiro et al., 1994; Zaika et al., 2006) and adrenergic receptors (Brown and Caulfield, 1979; Horn and McAfee, 1980; Caulfield et al., 1994) all produce slow electrophysiological events

mediated by metabotropic signal transduction pathways. They can alter SCG neuronal excitability and thus have consequences for synaptic integration.

Postganglionic neurons in the rat SCG exclusively innervate distinct target modalities including vascular beds in the brain, muscle and skin as well as piloerector and glands throughout the head (McLachlan, 1995; Gibbins, 2004). These neuronal phenotypes have different anatomical and physiological features in soma size, NPY expression and axonal conduction velocity (Gibbins, 1995; Li and Horn, 2006). It is not clear, however, whether neuromodulatory mechanisms are different in distinct functional subsets of neurons. Thus for example, early functional studies have shown that application of exogenous catecholamines can hyperpolarize neurons in sympathetic ganglia (De Groat and Volle, 1966; Brown and Caulfield, 1979). Pharmacological analysis of the extracellularly recorded hyperpolarizing response (Brown and Caulfield, 1979) and of receptor ligand binding (Kafka and Thoa, 1979) indicated the presence of post-synaptic α–adrenergic receptor. Subsequent molecular studies demonstrated that the α2-adrenergic receptor is the major type of adrenoceptors expressed in rat SCG (Pieribone et al., 1994; Gold et al., 1997; Vidovic and Hill, 1997). Recent evidence showed that exogenously applied NE both activated GIRK channels via direct binding of βγ dimers that are dissociated from G_i/G_o (Ruiz-Velasco and Ikeda, 1998; Fernandez-Fernandez et al., 2001) and inhibited N-type Ca^{2+} channels (Horn and McAfee, 1980; Galvan and Adams, 1982) via βγ dimers dissociated from $G_{\alpha o}$ (Caulfield et al., 1994; Delmas et al., 1998a; Delmas et al., 1999). Nonetheless, none of these previous studies examined adrenergic effects in the context of functional cell groups. The aim of

this study is to examine cellular specialization of α2-adrenergic modulation of post-synaptic responses in the rat SCG neurons. To do this, we took advantage of the observation that bath applied 10 µM NE produces robust and reversible reduction of the shoulder on the repolarization phase of AP and the Ca^{2+}-dependent spike AHP via the inhibition of N-type calcium channels (Horn and McAfee, 1980; Galvan and Adams, 1982) and used these effects to assay the cell-specific expression of α2-adrenergic receptors.

4.3 MATERIALS AND METHODS

4.3.1 Preparation of ganglia

Young adult male rats (Sprague-Dawley 180 - 250g) were euthanized by CO_2 inhalation using procedures approved by the Institutional Animal Care and Use Committee at the University of Pittsburgh. The preparation procedures were as described previously in Chapter 2.3.1. Briefly, the SCG together with the CST and the ICN and ECN was dissected and then transferred to a recording chamber. The connective tissue capsule that surrounds the ganglion was then split open and used to stretch and pin the preparation with cut-down Minutien pins (100 – 150 µm diameter, Austerlitz). Tight fitting suction electrodes were applied to the ganglionic nerves for extracellular stimulation and recording, and the recording chamber was transferred to the stage of an upright fixed-stage Zeiss Axioskop microscope with 40x Nomarski immersion optics.

4.3.2 Solutions

Throughout dissection and recording, the SCG was bathed in oxygenated mammalian Ringer's solution with a modified composition of (in mM): 146 NaCl, 4.7 KCl, 2.5 $CaCl_2$, 0.6 $MgSO_4$, 1.6 $NaHCO_3$, 0.13 NaH_2PO_4, 20 HEPES acid and 7.8 glucose (pH 7.3) at room temperature (23ºC). During recording, the preparation was superfused at 1 – 2 ml/min with a peristaltic pump (bath volume ~ 1 ml).

4.3.3 Extracellular recording and intracellular recording

The procedures of nerve stimulation, extracellular and intracellular recordings were described in Chapters 2.3.3 and 2.3.4. For drug application, 10 µM NE (Sigma), 10 mM TEA chloride (Eastman Kodak) and 100 µM $CdCl_2$ (Fisher Scientific) were bath-applied in a Ringer solution.

Resting membrane potential (V_{rest}) was measured as the difference between the potentials immediately before and after withdrawal of the microelectrode from a cell. Only cells with $V_{rest} < – 45$ mV and total spike size >80 mV in amplitude were included in the analysis. AP amplitude was measured between resting membrane potential and peak value of AP. AP half width was measured at half the difference between resting membrane potential and the peak of each AP. Peak AHP amplitude was measured as

the maximum negative voltage deflection relative to resting membrane potential. Half

amplitude duration (AHP half width) was defined as width at half amplitude.

4.3.4 Neuronal fills and immunocytochemistry

The procedures of neuronal fills with neurobiotin and immunostaining against NPY

primary antibody were described in Chapters 2.3.5 and 2.3.6.

4.3.5 Analysis and statistics

Grouped data were presented as the mean $\pm$ standard error (S.E.). NE effect upon

resting membrane potential, AP amplitude, AP half-width, peak AHP and AHP half-width

between control and 10 µM NE groups were compared using student's t-test. Statistical

differences between the three functional cell groups describing input resistance, resting

membrane potential and AP amplitude were examined using a one-way ANOVA,

followed by Tukey's test for multiple comparisons (Prism 4.0, GraphPad, San Diego,

CA) and $P < 0.05$ as the criterion for significance. Figures were prepared using Igor 5.0

(Wavemetrics, Lake Oswego, OR), Adobe Photoshop CS and Adobe Illustrator CS.

4.4 RESULTS

4.4.1 NE alters action potential shape in secretomotor and pilomotor neurons

Secretomotor neurons innervating salivary glands were identified as ECN projecting, low threshold and NPY negative cells according to our classification criteria [Fig. 12, B and C; (Li and Horn, 2006)]. In 16 of 16 secretomotor neurons, bath-applied NE (10 µM) decreased AP half-width from 3.21 ± 0.15 ms to 3.01 ± 0.11 ms (P<0.05), lowered peak AHP amplitude from 12.1 ± 0.5 mV to 7.8 ± 0.6 mV (P<0.001) and shortened AHP half-width from 103.5 ± 6.2 ms to 39.8 ± 5.1 ms (P<0.001) (Fig. 12, A, Table 3). These NE effects did not desensitize during 10 minutes of exposure, and the AP shoulder and AHP of these cells recovered within 15 minutes of washing in drug-free Ringer solution. In addition, NE produced no significant effects upon AP amplitude (90.1 ± 1.7 mV in control compared with 88.6 ± 2.2 mV in NE), input resistance (125.6 ± 8.8 M Ω in control compared with 113.7 ± 11.3 MΩ in NE) and membrane potential (-54.0 ± 1.5 mV to -55.4 ± 1.8 mV) (Table 4). The effects upon AP shape were not due to the hyperpolarizing action of NE. They were seen in cells which did not exhibit a hyperpolarizing response and in cells when resting membrane potential was re-established by depolarizing current injection during hyperpolarizing responses (data not shown).

Pilomotor neurons were identified as high threshold, NPY negative cells according to our classification criteria [(Fig. 13, B and C; (Li and Horn, 2006)]. NE produced similar effects in 14 out of 15 pilomotor neurons as in secretomotor neurons (Fig. 13, A; Table 3), where it reversibly reduced AP half-width from 3.32 ± 0.10 ms to 3.01 ± 0.09 ms (P<0.01), peak AHP from 13.0 ± 0.9 mV to 7.9 ± 0.8 mV (P<0.001) and

AHP half-width from 71.4 ± 10.3 ms to 26.2 ± 4.4 ms (P<0.001). Likewise, these effects

occurred in less than six minutes of exposure to NE, did not desensitize over repeated

application, and were reversed with 15 minutes of washing. In control Ringer, the

average resting membrane potential was -54.7 ± 1.6 mV, AP amplitude was 92.0 ± 1.4

mV and input resistance was 130.7 MΩ. Bath-applied NE (10 µM) did not produce any

significant effects upon membrane potential, AP amplitude and input resistance (Table

4). Similarly, the effects of AP shape were seen in cells whose membrane potentials

were insensitive to bath-applied NE and in cells when resting membrane potentials were

depolarized to control value by passing current during hyperpolarizing responses (not

shown)
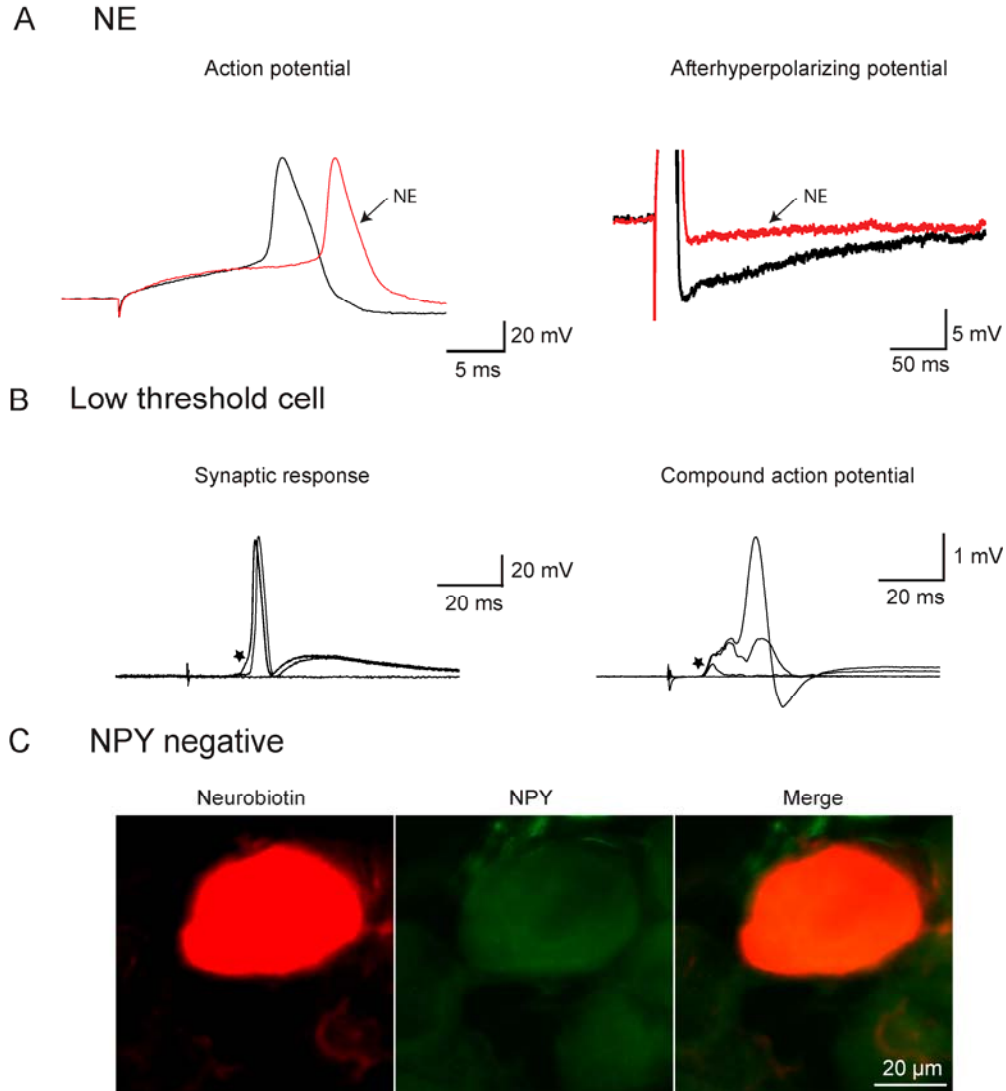
Figure 12. NE alters AP shape in secretomotor neurons.

A: Intracellular records of postsynaptic discharge elicited by current pulses delivered directly through the recording microelectrode (300 pA, 10 ms). Traces dictate control response (black) and 10 µM NE response after 10 minutes' bath-application (red). Left, the action potential is displayed with a fast-time base. Right, the AHP is displayed with a slow-time base. B: Intracellular identification of low threshold neurons. Simultaneous intracellular and extracellular recordings at room temperature were used to determine how the stimulus thresholds for excitatory postsynaptic potential (EPSP) components

corresponded to peaks in the compound action potentials (CAPs) recorded from the ECN. Left *, recruitment of a suprathreshold EPSP by graded presynaptic stimulation. Right *, corresponding extracellular response. Note: the cell fired on activation of peak 1 in the extracellular recordings. C: ECN projecting neurons were identified by antidromic stimulation and classified by their presynaptic stimulus threshold for firing an action potential. They were then injected with neurobiotin and processed for NPY immunoreactivity. Left, neurobiotin-filled cell; Middle, NPY immunoreactivity; Right, merged images of the 2 labels. These approaches led to the identification of low threshold, NPY negative cells.

Figure 13. Pilomotor neurons are sensitive to NE

A: cell discharges were elicited by depolarizing current (300 pA, 9 ms) through recording microelectrode.

Traces dictate control response (black) and 10 μM NE response after 10 minutes bath-application (red).

Left, the action potential is displayed with a fast-time base. Right, the AHP is displayed with a slow-time

base. B: Intracellular identification of high threshold neurons. Simultaneous intracellular and extracellular

recordings at room temperature were used to determine how the stimulus thresholds for excitatory

postsynaptic potential (EPSP) components corresponded to peaks in the compound action potentials

(CAPs) recorded from the ECN. Left, recruitment of a suprathreshold EPSP by graded presynaptic

stimulation. Right, corresponding extracellular response. * represents that the cell fired on activation of

peak 2 in the extracellular recordings. C: NPY was not expressed in this type of neuron. After identified

as high threshold cells, they were then injected with neurobiotin and processed for NPY immunoreactivity. Left, neurobiotin-filled cell; Middle, NPY immunoreactivity; Right, merged images of the 2 labels. These approaches led to the identification of high threshold, NPY negative cells.

Table 3. NE effects upon AP shape of secretomotor, pilomotor and vasoconstrictor neurons.

Cell types		AP half-width (ms)	Peak AHP (mV)	AHP half-width (ms)
Low threshold/NPY-	Control	3.21 ± 0.15	12.1 ± 0.5	103.5 ± 6.2
(n=16)	NE	3.01 ± 0.11*	7.8 ± 0.6***	39.8 ± 5.1***
	P value	<0.05	<0.001	<0.001
High	Control	3.32 ± 0.10	13.0 ± 0.9	71.4 ± 10.3
threshold/NPY- **(n=15)**	NE	3.01 ± 0.09**	7.9 ± 0.8***	26.2 ± 4.4***
	P value	<0.01	<0.001	<0.001
High	Control	3.28 ± 0.13	12.1 ± 0.7	47.7 ± 2.9
threshold/NPY+	NE	3.22 ± 0.13	12.0 ± 0.5	46.1 ± 2.1
(n=14)	P value	0.14	0.79	0.67

AP half-width, Peak AHP and AHP half-width were measured at room temperature as described in methods. The cell-specific differences of AP half-width, Peak AHP and AHP half-width in secretomotor and pilomotor neurons were statistically significant. In contrast, the differences of these three parameters in vasoconstrictor neurons were not significant. *, P <0.05; **, P<0.01; ***, P<0.001

Table 4. NE effects upon membrane properties of three functional cell subclasses.

Cell types		RMP (mV)	AP amplitude (mV)	Input Resistance (meg Ω)
Low threshold/NPY- (n=16)	Control	-54.0 ± 1.5	90.1 ± 1.7	125.6 ± 8.8
	NE	-55.4 ± 1.8	88.6 ± 2.2	113.7 ± 11.3
	P value	0.17	0.31	0.41
High threshold/NPY- (n=15)	Control	-54.7 ± 1.6	92.0 ± 1.4	130.7 ± 15.1
	NE	-56.7 ± 1.4	91.5 ± 1.4	127.5 ± 23.2
	P value	0.16	0.62	0.91
High threshold/NPY+ (n=14)	Control	-55.2 ± 0.9	92.7 ± 1.9	143.1 ± 8.7
	NE	-55.7 ± 1.0	91.3 ± 1.8	130.3 ± 3.9
	P value	0.99	0.21	0.32

Resting membrane potential (RMP), action potential (AP) amplitude and input resistance were measured at room temperature. No significant differences of these three parameters were found in the three subclasses of SCG neurons.

4.4.2 Vasoconstrictor neurons are insensitive to NE

Vasoconstrictor neurons were identified as high threshold, NPY positive cells [Fig. 14, B and C; (Li and Horn, 2006)]. Interestingly, NE produced no effect on AP shape in any of the 14 cells (Fig. 14, A; table 1) − AP half-width was 3.28 ± 0.13 ms in control saline and 3.22 ± 0.13 ms in NE (P = 0.14); peak AHP amplitude was 12.1± 0.7 mV in controls and 12.0 ± 0.5 mV in NE (P = 0.79); AHP half-width was 47.7 ± 2.9 ms in controls compared with 46.1 ± 2.1 ms in NE (P = 0.67). Similar to experiments of NE response in secretomotor and pilomotor neurons, these effects were examined after six minutes of exposure to NE, 15 minutes of washing in drug-free Ringer and tested for repeated application. In control Ringer, the average resting membrane potential, AP amplitude and input resistance of these neurons were -55.2 ± 0.9 mV, 92.7 ± 1.9 mV and 143.1 MΩ, respectively. Bath-applied NE (10 µM) did not cause significant effects upon membrane potential, AP amplitude and input resistance (Table 4).

One-way ANOVA analysis was performed in the context of AP half-width, peak AHP amplitude, AHP half-width, resting membrane potential, input resistance and AP amplitude in secretomotor, pilomotor and vasoconstrictor cell groups. Our results showed that no significant difference of these parameters was found except that the AHP half-width of these phenotypes in control Ringer solution was significantly different (P<0.01, Table 4). Subsequent Turkey's multiple comparison tests indicated that significant difference of AHP half-width was only found between secretomotor and vasoconstrictor neurons (P<0.01). This resembles the difference between bullfrog B

and C neurons (unpublished results in our lab). In addition, cells that were

hyperpolarized in response to NE were selected to compare their input resistance. No

significant difference was found.

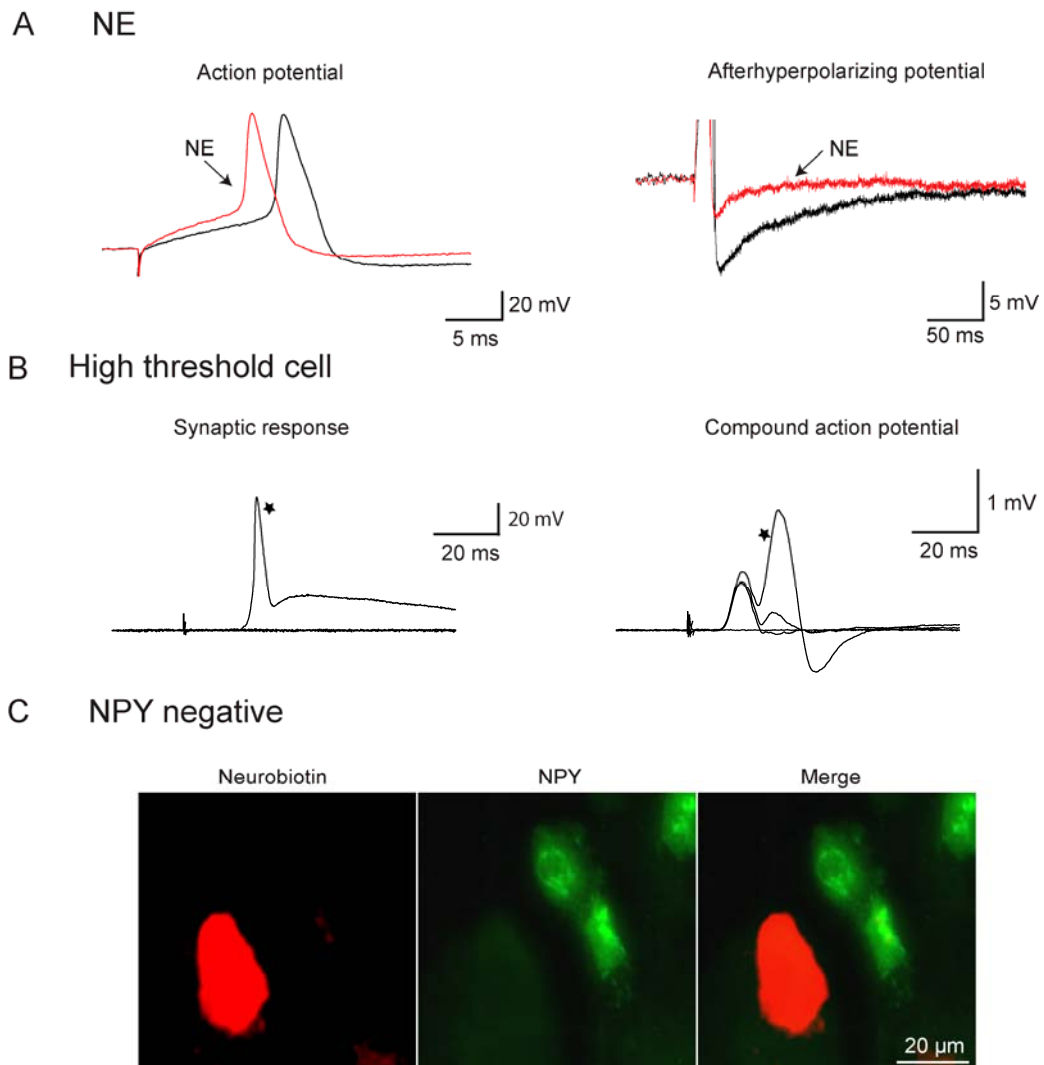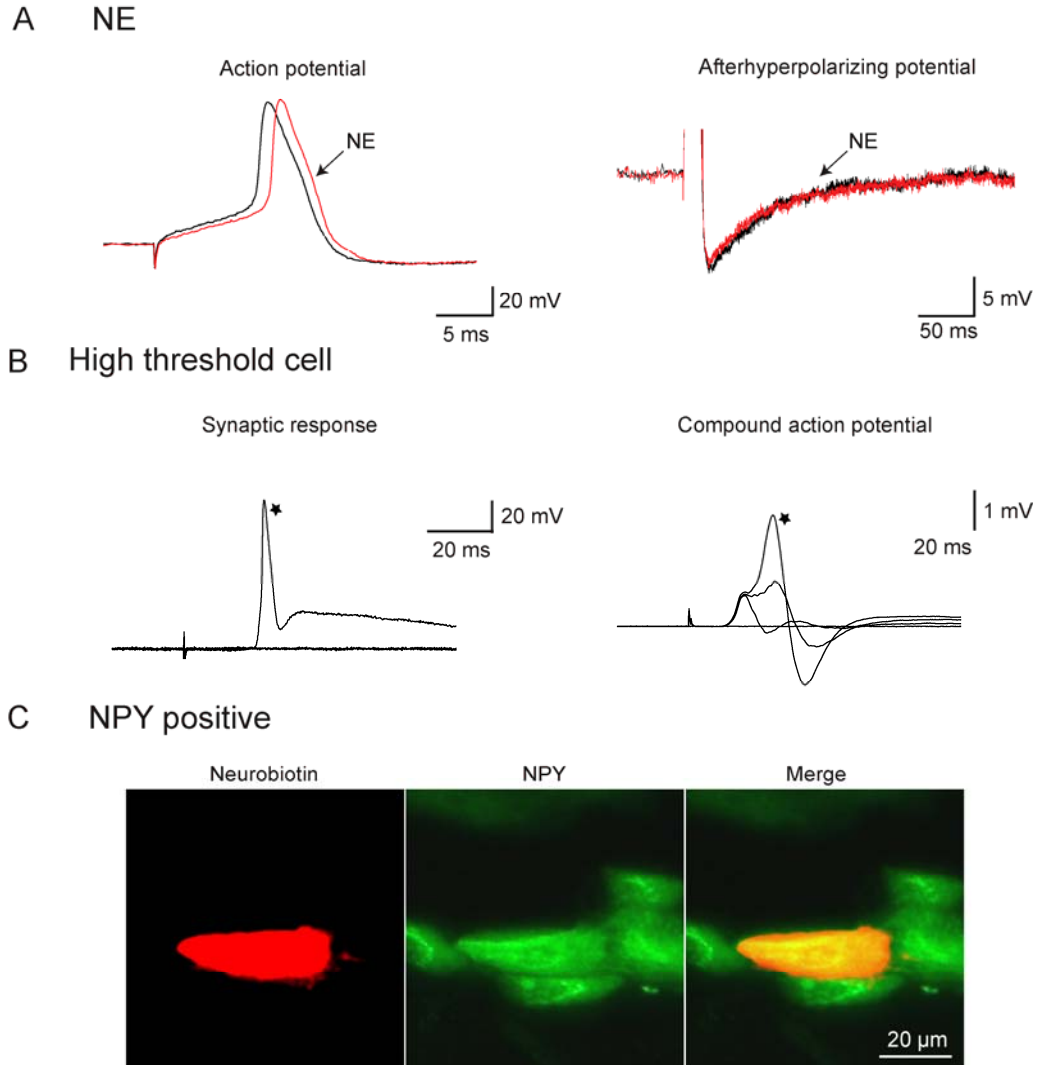Figure 14. Vasoconstrictor neurons are insensitive to NE

A: postsynaptic discharges were elicited by depolarizing current (300 pA, 10 ms) through recording

microelectrode. Traces dictate control response (black) and 10 µM NE response after 10 minutes of

bath-application (red). Left, the action potential is displayed with a fast-time base. Right, the AHP is

displayed with a slow-time base. Note: there are no differences of AP shoulder and AHP between control

and in NE. B: Intracellular identification of high threshold neurons. These neurons were classified by

their presynaptic stimulus threshold for firing an action potential. Left, recruitment of a suprathreshold

EPSP by graded presynaptic stimulation. Right, corresponding extracellular response. * represents that

the cell fired on activation of peak 2 in the extracellular recordings. C: NPY was selectively expressed in

this type of neurons. After recording, they were injected with neurobiotin and processed for NPY immunoreactivity. Left, neurobiotin-filled cell; Middle, NPY immunoreactivity; Right, merged images of the 2 labels. These approaches led to the identification of high threshold, NPY positive cells.

4.4.3 Vasoconstrictor neurons in Ringer with TEA are insensitive to NE

To test whether the NE insensitivity of vasoconstrictor neurons was caused by cell damage, another series of experiments was performed. Each neuron was first classified as low or high threshold and tested for NE responsiveness in normal Ringer solution. TEA+ was then applied to accentuate AP shoulder and AHP and the NE effects upon AP shape were re-examined. Finally, the cell was injected with neurobiotin and processed for NPY-immunoreactivity to complete the cell identification process. In secretomotor neurons (n=6) with bath-applied TEA$^+$ (10 mM), NE (10 μM) reversibly reduced AP half-width from 24.28 ± 3.21 ms to 16.32 ± 2.14 ms (P < 0.01), peak AHP from 13.2 ± 1.5 mV to 8.0 ± 1.3 mV (P < 0.01) and AHP half-width from 173.3 ± 31.3 ms to 71.8 ± 15.4 ms (P < 0.01) (Fig. 15, Table 5). In addition, NE did not cause significant differences upon RMP (from -55.3 ± 1.5 mV to -56.2 ± 1.4 mV, P > 0.05) and AP amplitude (86.1 ± 2.2 mV in control compared with 86.8 ± 2.5 mV in NE, P > 0.05, Table 5). Similarly, in seven pilomotor neurons, NE (10 μM) reversibly narrowed AP half-width from 21.90 ± 2.01ms to 15.50 ± 2.11 ms (P < 0.01), decreased peak AHP from 12.7 ± 1.1 mV to 9.1 ± 1.3 mV (P < 0.01) and shortened AHP half-width from 108.7 ± 24.8 ms to 62.2 ± 17.1 ms (P < 0.05) in Ringer solution containing 10 mM TEA$^+$ (Fig. 16, Table 5). NE did not cause significant effects upon RMP (-56.9 ± 1.7 mV to -57.9 ± 1.9 mV P > 0.05, Table 5). AP amplitude remained the same (85.8 ± 1.6 mV in control and 84.3 ± 1.7 mV in NE) (P > 0.05). In contrast, NE (10 μM), as in normal Ringer, did not cause any significant change of AP shape in vasoconstrictor neurons (n=5) with bath-applied TEA (10 mM). AP half-width was 27.06 ± 5.68 ms in control and 28.22 ±

5.33 ms in NE (P > 0.05); peak AHP amplitude was 11.7 ± 1.1 mV in controls and 11.2

± 1.3 mV in NE (P > 0.05); AHP half-width was 114.2 ± 28.1 ms in controls compared

with 120.5 ± 33.9 ms in NE (P > 0.05) (Fig. 17, Table 5). In addition, NE did not

produce any effect upon RMP of vasoconstrictor neurons (from -52.6 ± 2.1mV in Ringer

solution to -53.8 ± 2.5 mV in NE, P > 0.05) and AP amplitude (85.7 ± 3.3 mV in control

compared with 83.8 ± 4.0 mV in NE, P > 0.05). To test whether the insensitivity to NE

of vasoconstrictor neurons is caused by lack of expression of calcium channels, we

added 100 μM $CdCl_2$ to compete with Ca^{2+}. Our data showed that addition of Cd^{2+}

narrowed AP shoulder, reduced peak AHP and shortened AHP half-width (Fig. 18).

This indicated that AP shape of vasoconstrictor neurons, like secretomotor and

pilomotor neurons, is also controlled by Ca^{2+} and Ca^{2+}-dependent conductance.

Secretomotor neuron
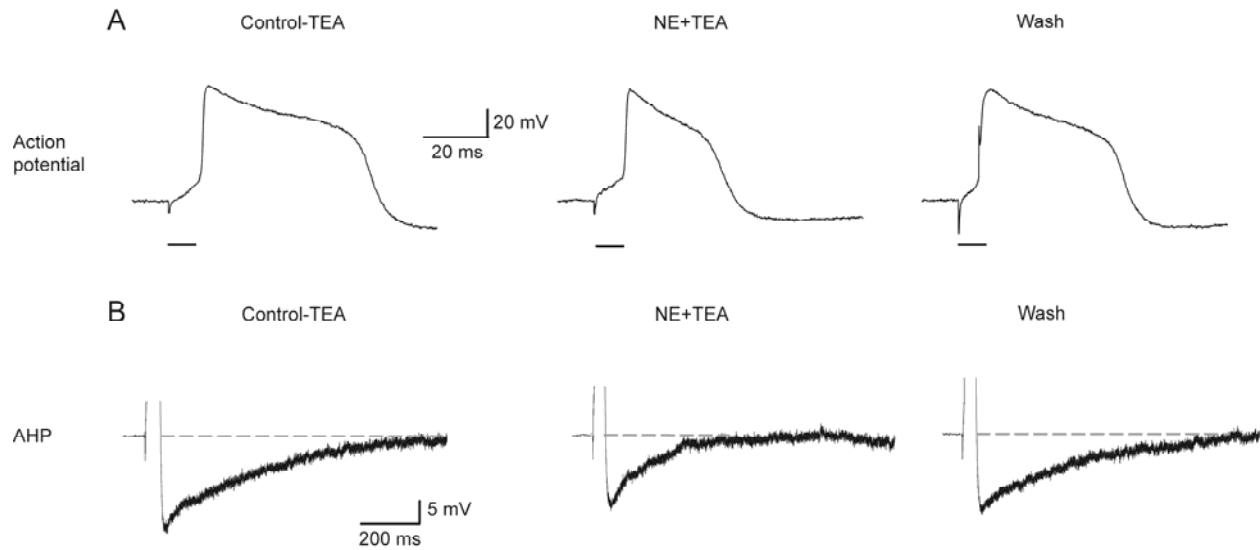
Figure 15. The effects of NE on discharge of secretomotor neurons in a Ringer solution containing 10 mM TEA$^+$

Cell discharges were elicited by depolarizing current (300 pA, 8 ms) through recording microelectrode.

The records are presented in chronological order: Left column: control in TEA$^+$; Middle column: after 10 minutes in 10 μM NE; Right column: after 15 minutes in NE-free TEA+ Ringer. A: the action potential is displayed with a fast-time base. B: the AHP is displayed with a slow-time base.

Pilomotor neuron
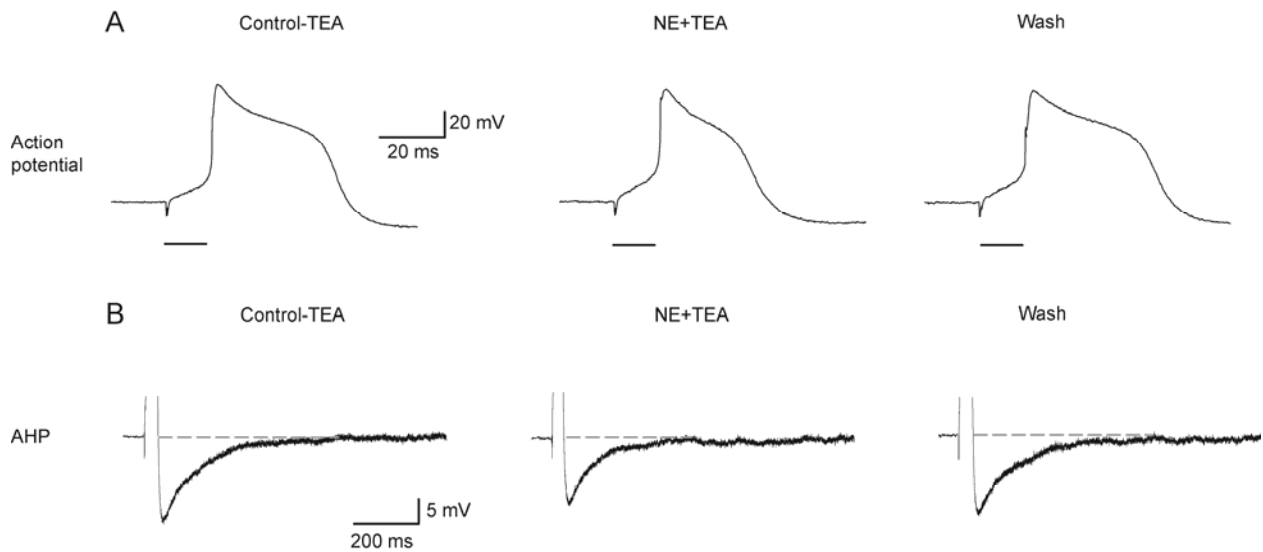
Figure 16. The effects of NE on discharge of pilomotor neurons in a Ringer solution containing 10 mM

TEA^+

Intracellular records of postsynaptic discharges were elicited by depolarizing current (300 pA, 12 ms)

through recording microelectrode. The records appear in chronological order from left to right: control,

after 10 minutes in 10 μM NE and after 15 minutes in NE-free TEA+ Ringer. A: the action potential is

displayed with a fast-time base. B: the AHP is displayed with a slow-time base.

Vasoconstrictor neuron
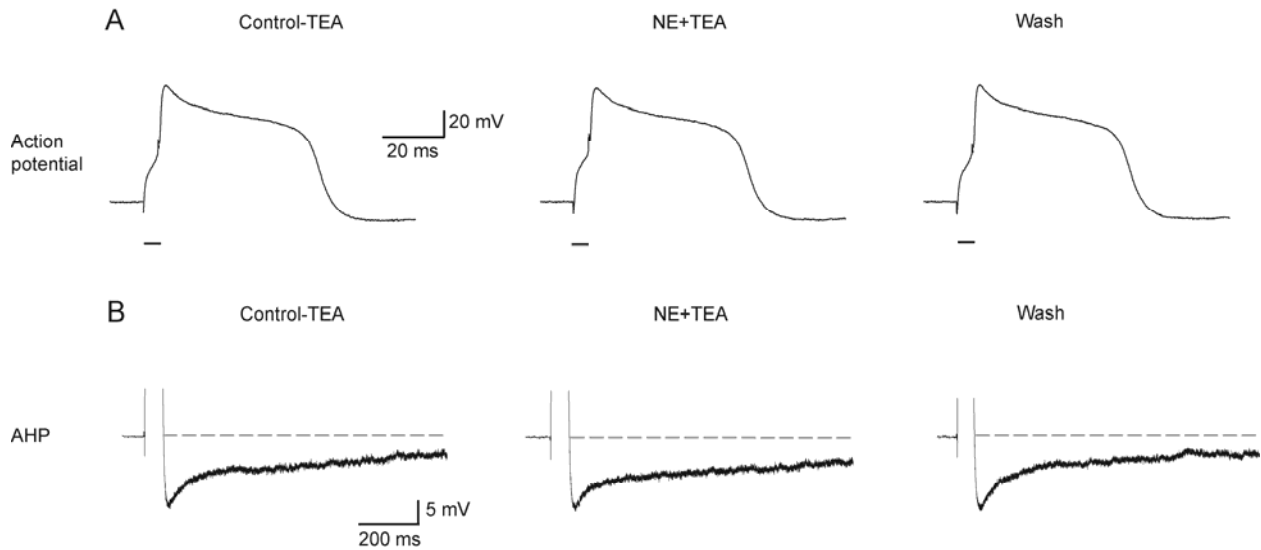
Figure 17. The effects of NE on discharge of vasoconstrictor neurons in a Ringer solution containing 10 mM TEA$^+$

Postsynaptic discharges were evoked by current (300 pA, 5 ms) injected through recording microelectrode. The records are presented in chronological order: Left column: control; Middle column: after 10 minutes in 10 μM NE; Right column: after 15 minutes in NE-free TEA+ Ringer. A: the action potential is displayed with a fast-time base. B: the AHP is displayed with a slow-time base. Note: neurons are still insensitive to NE.

Vasoconstrictor neuron
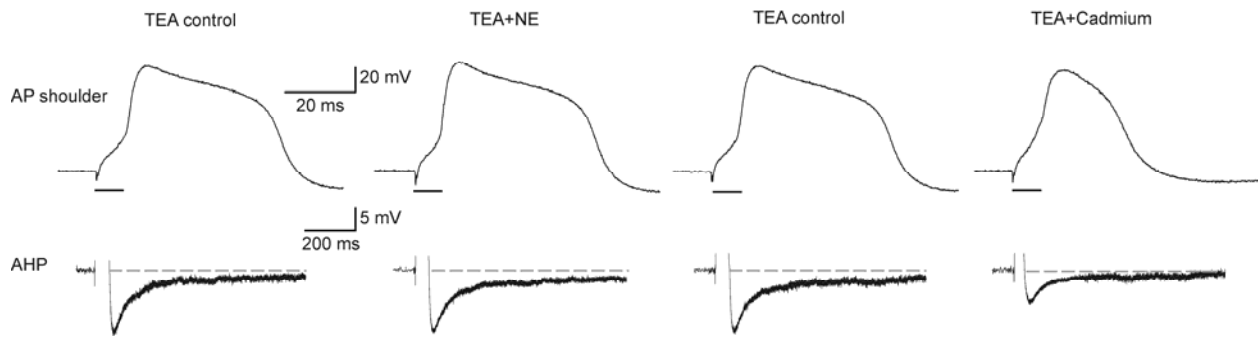
Figure 18. The effects of NE (10 µM) compared with the effects of cadmium (100 µM) on cellular

discharge of a vasoconstrictor neuron in Ringer containing TEA$^+$.

The records are presented in chronological order: control in Ringer containing 10 mM TEA$^+$; after 10

minutes in 10 µM NE; after 12 minutes in NE-free TEA$^+$ Ringer (wash); and after 10minutes in 100 µM

CdCl$_2$. The vasoconstrictor neuron was first identified as high threshold and insensitive to NE, as

illustrated in the first three columns. Note: addition of 100 µM CdCl$_2$ reduced AP shoulder and AHP.

Table 5. The effects of NE upon three types of neurons superfused with 10 mM TEA$^+$

		RMP (mV)	AP amplitude (mV)	AP half-width (ms)	Peak AHP (mV)	AHP half-width (ms)
Low threshold/NPY- (n=6)	Control	-55.3 ± 1.5	86.1 ± 2.2	24.28 ± 3.21	13.2 ± 1.5	173.3 ± 31.2
	NE	-56.2 ± 1.4	86.8 ± 2.5	16.32 ± 2.14**	8.0 ± 1.3**	71.8 ± 15.4**
	P value	0.11	0.61	<0.01	<0.01	<0.01
High threshold/NPY- (n=7)	Control	-56.9 ± 1.7	85.8 ± 1.6	21.90 ± 2.01	12.7 ± 1.1	108.7 ± 24.8
	NE	-57.9 ± 1.9	84.3 ± 1.7	15.50 ± 2.11**	9.1 ± 1.3**	62.2 ± 13.1*
	P value	0.16	0.23	<0.01	<0.01	<0.05
High threshold/NPY+ (n=5)	Control	-52.6 ± 2.1	85.7 ± 3.3	27.06 ± 5.68	11.7 ± 1.1	114.2 ± 28.1
	NE	-53.8 ± 2.5	83.8 ± 4.0	28.22 ± 5.33	11.2 ± 1.3	120.5 ± 33.9
	P value	0.14	0.27	0.21	0.22	0.31

Resting membrane potential (RMP), Action potential (AP) amplitudes, AP half-width, Peak AHP and AHP half-width were measured at room temperature, as described in methods. The cell-specific differences of AP half-width, Peak AHP and AHP half-width in secretomotor and pilomotor neurons were statistically significant. In contrast, similar effects were not observed in vasoconstrictor neurons. *, P <0.05; **, P<0.01; ***, P<0.001.

4.5 DISCUSSION

This Chapter shows that secretomotor, pilomotor and vasoconstrictor sympathetic neurons differ in their postsynaptic responses to NE. The analysis focused on neurons in the caudal portion of the rat SCG that project to targets in the jaw and neighboring regions of the head by way of the external carotid nerve. Our results demonstrated that secretomotor and pilomotor neurons responded to NE while vasoconstrictor neurons did not.

4.5.1 Ca^{2+} conductance and Ca^{2+}-dependent potential changes

It has already been established that α-adrenoceptor activation antagonizes Ca^{2+} conductance and consequent Ca^{2+}-dependent potassium potential changes in the rat SCG neurons (Horn and McAfee, 1980; Galvan and Adams, 1982). Similar effects of adrenergic inhibition of calcium channels were also found in bullfrog sympathetic ganglion neurons (Minota and Koketsu, 1977) and cultured chick dorsal root ganglion (Dunlap and Fischbach, 1978). This Ca^{2+} conductance is large enough to affect the magnitude of the shoulder during AP repolarization period. This shoulder can also be augmented by agents that inhibit outward K^+ currents (TEA^+), and antagonized by Co^{2+}, a Ca^{2+} antagonist (Horn and McAfee, 1980). In addition, the shoulder is relatively insensitive to resting membrane potential. Therefore, the AP shoulder is a direct manifestation of this inward Ca^{2+} current. The consequent Ca^{2+}-dependent processes include Ca^{2+}-sensitive K^+ conductance (Horn and McAfee, 1980) and other subsequent

signal transduction pathways. Horn and McAfee (Horn and McAfee, 1980) have demonstrated that the amplitude and duration of AHP is predominantly controlled by Ca^{2+} rather than by voltage. In addition, AHP is primarily composed of relatively long Ca^{2+}-sensitive K^+ conductance. As a result, we chose AHP as a direct measurement of consequent Ca^{2+}-sensitive process. The mechanism by which adrenergic receptor agonist modulate this Ca^{2+} conductance and Ca^{2+}-dependent potential changes has also been demonstrated as inhibition of N-type Ca^{2+} channels (Horn and McAfee, 1980; Galvan and Adams, 1982). This inhibition occurs via direct binding of $\beta\gamma$ dimers of $G\alpha_0$ protein (Caulfield et al., 1994; Delmas et al., 1998a; Delmas et al., 1999). Our findings suggested that in secretomotor and pilomotor neurons the binding of adrenergic receptor agonist caused change of AP shape due to direct inhibition of N-type Ca^{2+} currents. However, in vasoconstrictor neurons the binding of adrenergic receptor agonist did not produce any effect upon AP shape. Addition of 100 µM $CdCl_2$ reduced AP shoulder and the amplitude and length of AHP. These data indicated that AP shapes of vasoconstrictor neurons are also controlled by Ca^{2+} and Ca^{2+} dependent conductance.

We propose three possible reasons of NE insensitivity of vasoconstrictor neurons here. First, much less α-adrenergic receptors are expressed in vasoconstrictor neurons. However, there is a wealth of evidence that indicates that α2-adrenergic receptors are expressed in the axonal terminal of postganglionic neurons, which are involved in an autoinhibitory feedback mechanism by reducing NE release in neuroeffector end organs (Langer, 1980; Limberger et al., 1992; Starke, 2001). In fact,

anatomical studies including *in situ* hybridization and immunocytochemistry demonstrated that α2-adrenergic receptors are expressed in the cell body of most rat SCG neurons (Pieribone et al., 1994; Gold et al., 1997; Vidovic and Hill, 1997). These suggested that α2-adrenergic receptors are most likely expressed in somata unless by some unknown mechanism that α2-adrenergic receptors synthesized in the cell body are only transported to axonal terminal. Second, the G-protein system in vasoconstrictor neurons might couple α-adrenergic receptors to other types of calcium channels. Previous studies showed that ω-agatoxin IVA sensitive P/Q-type currents are not observed in SCG neurons (Mintz et al., 1992; Zhu and Ikeda, 1993). Indeed, these sympathetic neurons have substantial N-type and L-type Ca^{2+} currents in their cell bodies, in which 80-90% of the Ca^{2+} is carried by N-type Ca^{2+} channels (Plummer et al., 1989; Regan et al., 1991). In addition, evidence showed that adrenergic receptors only couple to N-type Ca^{2+} channels (Caulfield et al., 1994; Delmas et al., 1998a; Delmas et al., 1999) while M_1 muscarinic receptors couple to N-type and L-type Ca^{2+} channels (Mathie et al., 1992; Liu et al., 2006). Therefore, it seems unlikely that this possibility account for the insensitivity to NE of vasoconstrictor neurons. Third, α-adrenergic receptors might be unable to modulate N-type calcium channels in vasoconstrictor neurons. This third possibility will be discussed in detail in Chapter 6.3.2. The insensitivity to NE of vasoconstrictor neurons could results in distinct pattern of synaptic integration between preganglionic terminal and vasoconstrictor neurons or less gene expression due to less calcium influx (see Chapter 6.2 for detailed discussion). However, the biological relevance of this insensitivity requires further study.

4.5.2 Origin of norepinephrine

α-adrenergic receptor antagonists such as yohimbine and phentolamine can increase evoked ACh release during preganglionic 20 Hz stimulation of the cat SCG (Araujo and Collier, 1986). This suggests that endogenous catecholamines released by high frequency preganglionic stimulation inhibits ACh release from preganglionic nerve terminals (Christ and Nishi, 1971; Araujo and Collier, 1986). Subsequent studies demonstrated that this inhibition is mediated by presynaptic α2- adrenergic receptors in sympathetic ganglia (Vizi, 1979; Unnerstall et al., 1984; McCallum et al., 1998; Stephens and Mochida, 2005). Concerning postsynaptic α-adrenergic receptors, previous studies have demonstrated that activation of α2-adrenergic receptors both activate GIRK (Ruiz-Velasco and Ikeda, 1998; Fernandez-Fernandez et al., 2001) and inhibit N-type Ca^{2+} channels (Horn and McAfee, 1980; Galvan and Adams, 1982). Three hypotheses have been proposed to explain possible sources from which NE might come *in vivo*. First, ganglionic α-adrenergic receptors might be activated by NE released from preganglionic fibers (Goldberg and Dacosta, 1960; Noon et al., 1975). However, Reinert argued against this hypothesis and claimed that ganglionic noradrenaline originates almost exclusively from the somata of the postganglionic adrenergic neurons (Reinert, 1963). He showed that denervation did not affect the noradrenaline concentration and antidromic stimulation releases noradrenaline in normal and denervated ganglia. Second, electromicroscopy has revealed a surprisingly high prevalence of interconnectivity between ganglionic neurons (Kondo et al., 1980;

Kiraly et al., 1989; Kawai et al., 1993). These contacts are both dendrodendritic and dendrosomatic. Commonly, no synaptic specialized structures were found within these dendrodendritic or dendrosomatic appositions, although features like numerous small vesicles packed in the dendrites and their collaterals indicated the possibility of dendritic release at sites of apposition (Kondo et al., 1980; Kawai et al., 1993). These anatomical evidences suggested that NE might be released from dendrodendritic contacts. If this possibility exists, it could alter synaptic integration and modulate synaptic gain function. However, no convincing physiological evidence has been provided to demonstrate the functional dendrodendritic interaction. This suggests that dendrodendritic interaction might be rare in rat SCG neurons. It could only affect synaptic integration to a small extent and would not affect the assumption of gain model. Third, catecholamines can be released into the circulation by the adrenal gland during strong sympathetic activation (Izzo and Black, 2003). This might also be another possible source of NE in sympathetic ganglia. In fact, the concentration of NE in the circulation might reach the level that affects synaptic transmission during stress (Buhler et al., 1978).

CHAPTER 5

CELLULAR SPECIALIZATION OF PRESYNAPTIC ALPHA-ADRENERGIC MODULATION IN THE RAT SUPERIOR CERVICAL GANGLIA

5.1 ABSTRACT

Presynaptic α2-adrenergic activation inhibits the release of acetylcholine (ACh) in the mammalian sympathetic ganglia. It is, however, not clear how this inhibition affects synaptic transmission and whether differences exist among the three functional subclasses of SCG neurons. Using simultaneous intracellular and extracellular recording, we identified secretomotor, pilomotor and vasoconstrictor neurons based on their synaptic stimulus threshold and postsynaptic sensitivity to NE (Chapter 4) and then tested the modulatory effects of NE upon synaptic transmission. In 23 of 23 secretomotor neurons, NE reversibly augmented action potential (AP) success ratio of firing from 76 ± 4 % to 99 ± 1 % and reduced cumulative EPSPs from 17.5 ± 1.4 mV to 7.6 ± 0.9 mV during a spike train. Interestingly, NE also increased AP size ratio (normalizing the average size of spikes in a train to that of the first spike) from 56 ± 2 % to 91 ± 1 %. Likewise, in 20 of 20 pilomotor neurons, NE raised AP success ratio of firing from 41 ± 3 % to 88 ± 4 % and AP size ratio from 65 ± 3 % to 77 ± 2 %. NE lowered cumulative EPSPs from 20.5 ± 1.2 mV to 13.2 ± 1.2 mV. Similarly, in 13 of 13

vasoconstrictor neurons, NE raised AP success ratio from 35 ± 5 % to 89 ± 4 % and AP size ratio from 64 ± 5 % to 74 ± 3 %. In addition, NE lowered cumulative EPSPs from 19.3 ± 1.7 mV to 9.9 ± 1.3 mV. These results suggest that presynaptic modulation through α2-receptors occurs in all functional subsets of neurons and affects synaptic transmission during high frequency neuronal activities. However, these modulatory effects appear stronger in pilomotor and vasoconstrictor neurons.

5.2 INTRODUCTION

The blocking action of catecholamines on ganglionic transmission was first reported in the cat superior cervical ganglion (Marrazzi, 1939). Subsequently, Bulbring demonstrated that an epinephrine-like substance can be released in activated ganglia upon preganglionic stimulation (Bulbring, 1944). The inhibitory effects of adrenergic blocking drugs upon ganglionic potentials following preganglionic stimulation suggested that endogenous NE influences ganglionic transmission (Eccles and Libet, 1961). In both cat and rabbit SCG, bath-applied catecholamines have been demonstrated to hyperpolarize membrane potential, which provides a post-synaptic inhibitory mechanism (De Groat and Volle, 1966; Kobayashi and Libet, 1970; Libet, 1970). Moreover, exogenous catecholamines and endogenous NE have been found to exert potent inhibitory effect on the release of acetylcholine (ACh) in the SCG of the rabbit (Christ and Nishi, 1971), the SCG of the guinea pig (Dun and Karczmar, 1977) and the SCG of the cat (Martinez and Adler-Graschinsky, 1980). The NE-induced inhibition of ACh

release can decrease the EPSPs in the mammalian SCG (Christ and Nishi, 1971; Dun and Karczmar, 1977; Vizi, 1979; Belluzzi et al., 1987; McCallum et al., 1998; Stephens and Mochida, 2005).

Although numerous studies have established both the presynaptic and postsynaptic inhibitory effects of NE, it is not clear how this inhibitory mechanism modulates ganglionic transmission. In this chapter, the modulatory effects of NE upon short term depression of synaptic transmission at high frequency (15 Hz) presynaptic stimulation were examined. The modulatory effects of NE upon this depression were studied for two reasons. First, the NE effects upon synaptic transmission were more prominent at 15 Hz stimulation. Second, *in vivo* studies show that discharge rates of sympathetic neurons in the cat and rat can occasionally exceed 10 Hz (Janig, 1985, , 1988; Janig, 1995). It suggested that adrenergic modulation of synaptic transmission might be physiologically expressed under certain conditions.

5.3 MATERIALS AND METHODS

5.3.1 Preparation of ganglia

Young adult male rats (Sprague-Dawley 180 - 250g) were euthanized by CO_2 inhalation using procedures approved by the Institutional Animal Care and Use Committee at the

University of Pittsburgh. The preparation procedures were as described preciously in Chapter 2.3.1.

5.3.2 Extracellular and intracellular recording

The procedures of nerve stimulation, extracellular and intracellular recordings have been described in Chapter 2.3.3 and Chapter 2.3.4. For drug application, L-(−)-Noradrenaline (+)-bitartrate salt monohydrate (NE), atropine sulfate salt, pyridoxal phosphate-6-azophenyl-2,4-disulfonic acid (PPADS), propranolol hydrochloride, prazosin hydrochloride and yohimbine hydrochloride (all purchased from Sigma-Aldrich) were bath-applied in Ringer solution.

Spike trains were elicited by 10 or 15 supramaximal presynaptic stimuli at 15 Hz applied to the CST. Resting membrane potential (V_{rest}) was measured as the difference between the potentials immediately before and after withdrawal of the microelectrode from a cell. Only cells with $V_{rest} < - 45$ mV and a total spike size >80 mV in amplitude were included in the analysis. AP amplitude was measured between resting membrane potential and peak value of AP. AP size ratio was calculated to reflect AP attenuation by normalizing the average size of spikes in a train to that of the first spike. Success ratio of firing was calculated to reflect failure of post-synaptic firing by counting the percentage of successful spikes in a spike train. Cumulative EPSPs were measured by comparing the membrane potential at the end of spike trains and the resting membrane potential in each cell.

5.3.3 Analysis and Statistics

Grouped data were presented as the mean $\pm$ standard error (S.E.). NE effect upon AP attenuation (AP size ratio), AP failure (AP success ratio of firing) and cumulative EPSPs between control and 10 µM NE groups were compared using student's t-test. Statistical differences between the three functional cell groups describing AP size ratio, success ratio of cell firing and cumulative EPSPs were examined using a one-way ANOVA, followed by Tukey's test for multiple comparisons (Prism 4.0, GraphPad, San Diego, CA) and $P < 0.05$ as the criterion for significance. Figures were prepared using Igor 5.0 (Wavemetrics, Lake Oswego, OR), Adobe Photoshop CS and Adobe Illustrator CS.

5.4 RESULTS

5.4.1 The depression of postganglionic CAPs at 15 Hz presynaptic stimulation is antagonized by NE

Based on our findings in Chapter 2, ECN projecting neurons can be subdivided into secretomotor, pilomotor and vasoconstrictor neurons. Therefore, by recording compound action potentials (CAPs) at ECN, it is possible to access population responses of these functional subtypes of sympathetic neurons. Our results showed that the amplitudes of extracellular CAPs recorded from ECN at room temperature

depressed during 15Hz presynaptic stimulation (Fig. 19, n = 23). The tenth response of

peak 1 (corresponding to secretomotor neurons) was reduced to about 40% of the first

response and peak 2 (corresponding to pilomotor and vasoconstrictor neurons) to 20%

of its initial response. Bath application of 10 µM NE had no effect upon the first spike in

the train but antagonized the effect on CAP amplitude depression. It attenuated the

depression of both peak 1 and peak 2 in a CAP train in six minutes, making the tenth

response reduced to only 70% and 50% of the first response in peak 1 and peak 2,

respectively (Fig. 19). In addition, at presynaptic stimulus frequencies below 15 Hz (2-

10 Hz), there was only a small degree of use-dependent facilitation or depression

evident in CAPs. However, this was not altered by NE (Fig. 20, n = 11).

These extracellular recording experiments showed that both low threshold cells

(peak 1) and high threshold cells (peak 2) can be affected by NE. They also showed

that NE had less effect upon peak 1 than peak 2. It is, however, difficult to determine

whether peak 2a and peak 2b are similarly affected because they were not always well

separated in 15Hz spike trains. To reveal the cellular mechanism of this modulation

and examine the possibility of difference between functional classes of neurons, we

recorded intracellularly from neurons in the caudal ganglion that project to ECN. We

focused on ECN projecting neurons because we have already set up a set of criteria for

identifying functional phenotypes including secretomotor, pilomotor and vasoconstrictor

neurons in this region (Chapters 2 and 4).
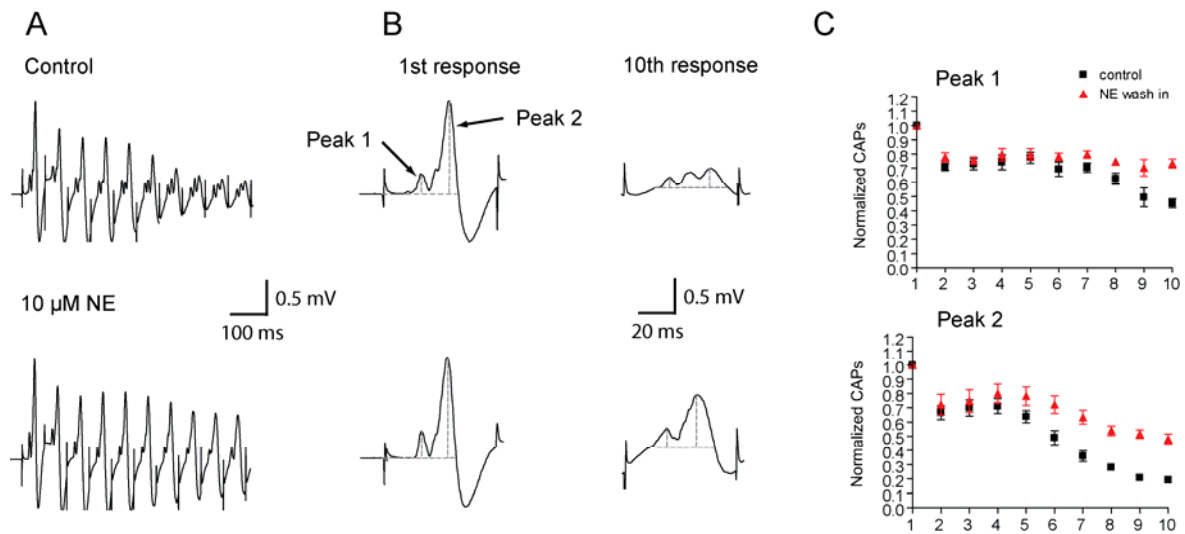
Figure 19. Extracellular recordings of compound action potentials (CAPs) at room temperature from the external carotid nerve during 15 Hz repetitive preganglionic stimulation of the rat SCG. A, Comparison of CAPs recorded in control Ringer (upper trace) and 10 µM NE (lower trace). B, Expanded time scale display of the first and last CAPs from trains in panel A. Grey dotted lines indicates how amplitudes of the low and high threshold peaks were measured. C, Normalized grouped data from 23 experiments showed that NE produced a similar effect in the low threshold (secretomotor) and high threshold (vasomotor & pilomotor) populations. The ratio between peak 1 and peak 2 in control is 0.24 of the first response and 0.56 of the tenth response. In addition, the ratio between peak 1 and peak 2 in 10 µM NE is 0.25 in the first response and 0.35 in the tenth response. The results indicated that depression was greater in the second peak and NE effects were more apparent in the second peak.
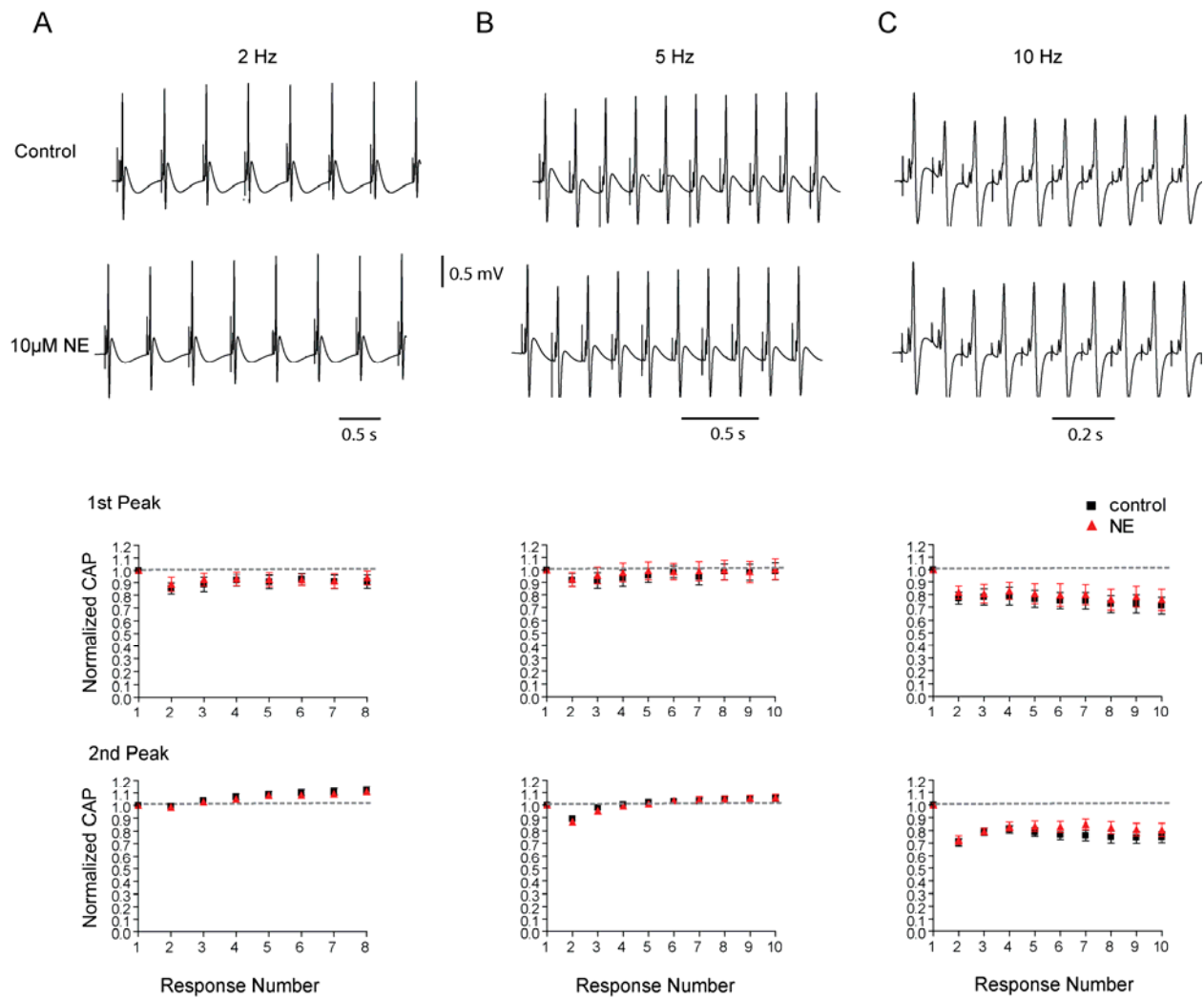
Figure 20. CAP amplitude was insensitive to NE during preganglionic stimulation at lower frequencies.

A, B and C, Trains of CAPs recorded at room temperature were evoked by repetitive preganglionic

stimulation at 2, 5 and 10 Hz respectively.

Top row, recordings in normal Ringer; Second row, recordings in 10 µM NE; Graphs, Grouped data from

11 experiments. All CAP amplitudes were normalized to the peak amplitude of the first response in each

train.

5.4.2 NE effects upon short-term depression in secretomotor, pilomotor and vasoconstrictor neurons.

Secretomotor, pilomotor and vasoconstrictor neurons were first identified based on presynaptic stimulus threshold and postsynaptic sensitivity to NE as described in Chapter 4. The modulatory effects of NE upon synaptic transmission were studied in the three functional cell groups. The depression of CAPs may be explained by the failure of cell firing during a spike train at 15 Hz presynaptic stimulation. Fewer cells having response to a train of stimulation can lead to decreased population response as measured by CAPs. Indeed, we found that failure of spike generation occurred in secretomotor (Fig. 21, A, n = 23), pilomotor (Fig. 22, A, n = 20) and vasoconstrictor neurons (Fig. 23, A, n = 13). Interestingly, our results also showed that the amplitude of spikes became smaller in a spike train at 15 Hz stimulation in all the three functional subsets of neurons (Fig. 21, A; Fig. 22, A; and Fig. 23, A). This suggested that action potentials generated might not be robust enough to propagate through axons and reach downstream targets. It could also contribute to the depression of CAPs that we observed. Bath application of 10 µM NE antagonized spike attenuation and failure produced by 15 Hz presynaptic stimulation in secretomotor (Fig. 21, B), pilomotor (Fig. 22, B) and vasoconstrictor cells (Fig. 23, B). These effects occurred in less than 6 minutes of exposure to NE, did not desensitize over repeated application, and were reversed with 10 minutes of washing (Fig. 21, C; Fig. 22, C and Fig. 23, C). In addition, NE inhibited the slow cumulative depolarization produced by synaptic stimulation. In

control experiments this depolarization was not blocked by muscarinic receptor antagonist, atropine (1 μM; n = 4; 15.6 ± 1.9 mV in control compared with 15.3 ± 1.7 mV in NE; P>0.05) and noncompetitive P2X receptor antagonist, PPADS (10 μM; n = 8; 16.5 ± 2.1 mV in control compared with 16.01 ± 1.9 mV in NE; P>0.05). Furthermore, these reversible effects of NE on single cells corresponded quite well with simultaneously recorded extracellular CAPs (bottom rows in Fig. 21, Fig. 22 and Fig 23).
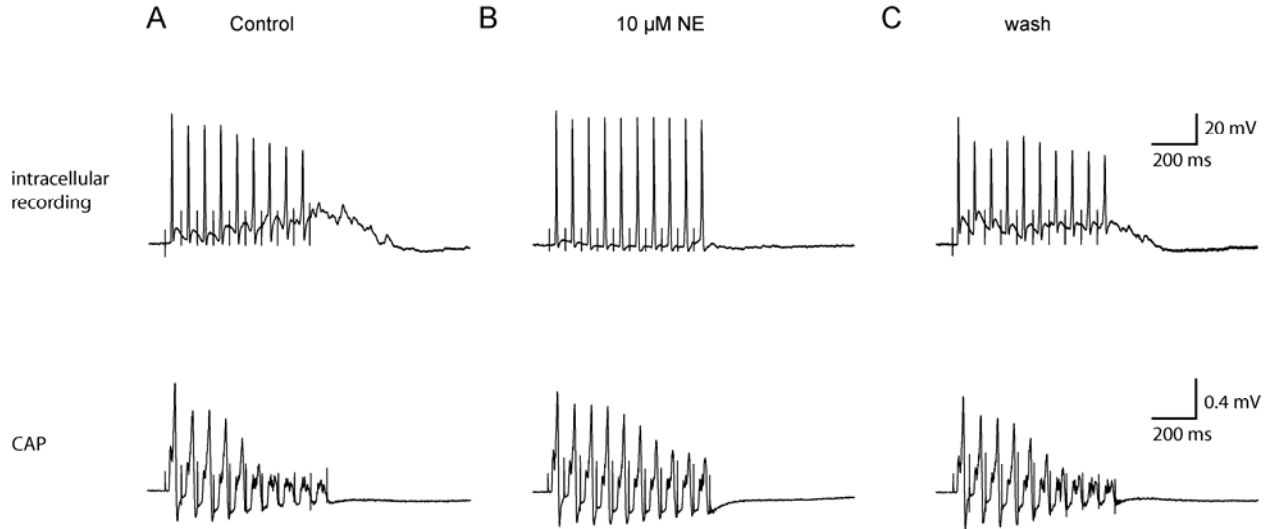
Figure 21. NE effects upon 15 Hz spike train in a secretomotor cell.

Secretomotor neurons were classified as low threshold and having postsynaptic NE response. Top row

shows postsynaptic discharge of a secretomotor neuron evoked at presynaptic 15 Hz stimulation. Bottom

row illustrates simultaneous extracellular recording of CAPs from the output nerve ECN. A, B and C,

Comparison of single cell response and CAPs recorded during control (A), 10 μM NE application (B) and

washing (C). Note that NE prevented the reduction of spike amplitude at 15 Hz presynaptic stimulation. In

addition, it increased successful firing and inhibited the cumulative EPSPs.
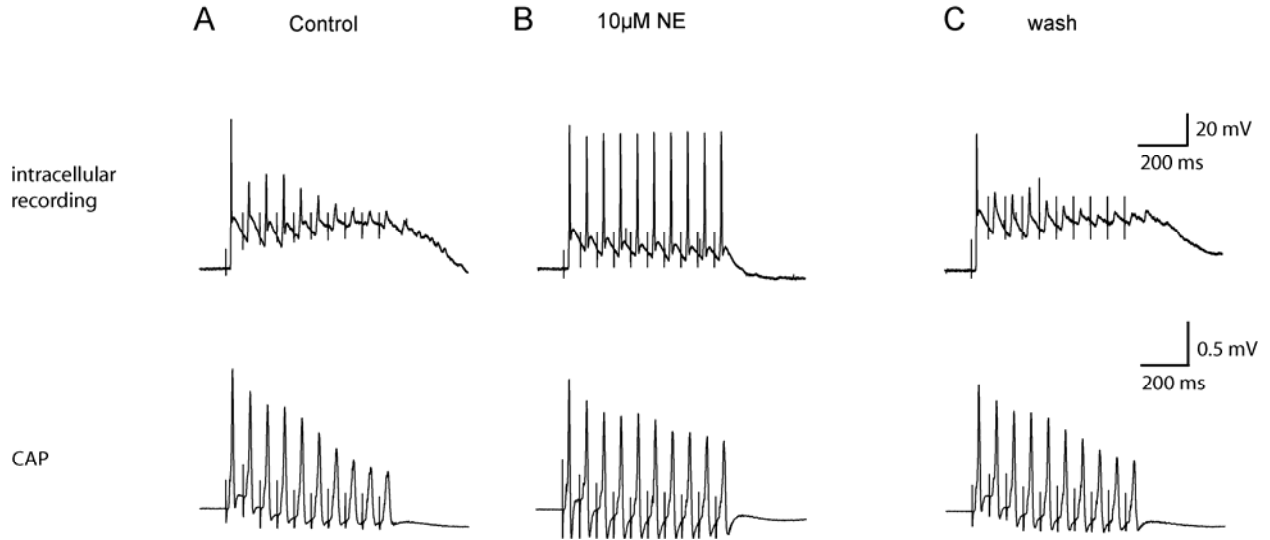
Figure 22. NE effects upon 15 Hz spike train in a pilomotor cell.

Pilomotor neurons were classified as high threshold and having postsynaptic NE response. Top row shows postsynaptic discharge of a pilomotor neuron evoked at presynaptic 15 Hz stimulation. Bottom row illustrates simultaneous extracellular recording from the ECN. A, B and C, Comparison of single cell response and CAPs recorded during control (A), 10 μM NE application (B) and washing (C). Note that NE prevented the reduction of spike amplitude at 15 Hz presynaptic stimulation. In addition, it increased success ratio of firing and inhibited the cumulative EPSPs.
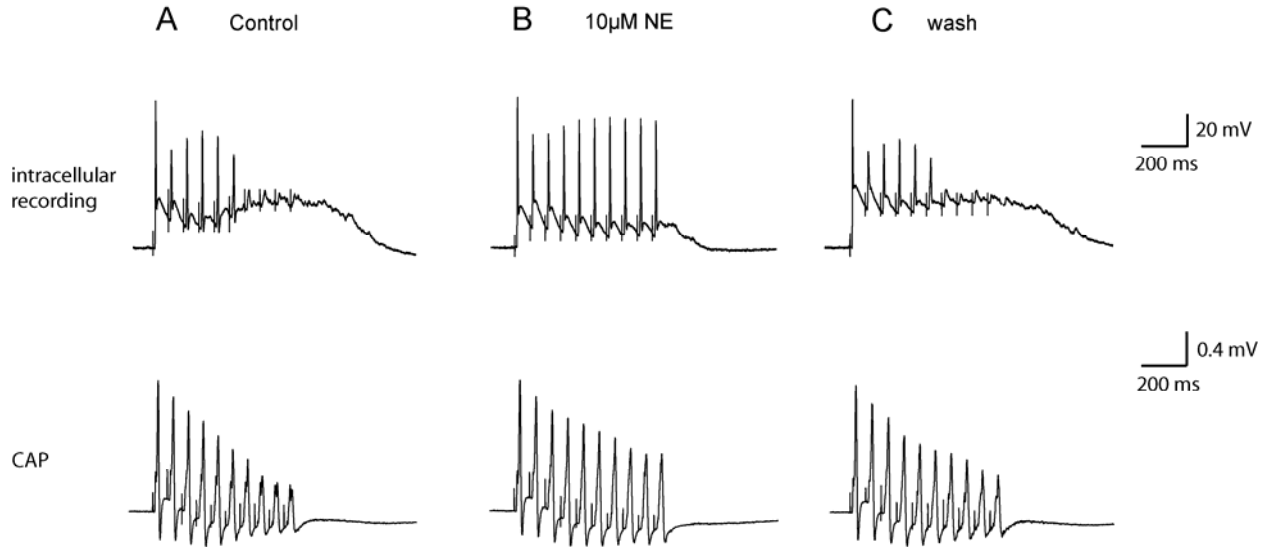
Figure 23. NE effects upon 15 Hz spike train in a vasoconstrictor cell.

Vasoconstrictor neurons were classified as high threshold and not having postsynaptic NE response.

Top row shows postsynaptic discharge of a vasoconstrictor neuron evoked at presynaptic 15 Hz

stimulation. Bottom row illustrates simultaneous extracellular recording from the ECN. A, B and C,

Comparison of single cell response and CAPs recorded during control (A), 10 µM NE application (B) and

washing (C). Note that NE prevented the reduction of spike amplitude at 15 Hz presynaptic stimulation. In

addition, it increased success ratio of firing and inhibited the cumulative EPSPs.

5.4.3. Electrophysiological profiles of three functional subsets of neurons

Interestingly, both secretomotor and pilomotor cells can be subdivided into two groups based on the types of response at 15 Hz presynaptic stimulation (Fig. 24). One type of cells (type 1) fired action potentials with reduced amplitude together with failure of firing, while the second type of cells (type 2) only fired smaller APs in a spike train. 15 out of 23 secretomotor cells were type 1 (Fig 24. A, top tow), while the other eight cells were type 2 (Fig 24. A, bottom row). In pilomotor cells, 16 out of 20 cells were type 1 neurons (Fig 24. B, top tow) and 4 cells were type 2 neurons (Fig 24. B, bottom tow). In contrast, all of vasoconstrictor neurons belong to type 1 neurons (Fig. 24, C).

Presynaptic stimulation at 15 Hz produced three effects: reduced spike amplitude, failure of cell firing and a cumulative EPSP. To further quantify the modulatory effects of NE and compare these effects on different cell types, we defined AP size ratio to quantify spike (AP) attenuation and success ratio of firing to quantify spike (AP) failure (Fig. 25, 26, see methods for calculation details). Our results revealed a significant difference of AP size ratio in secretomotor neurons (0.75 ± 0.02 in control Ringer compared with 0.92 ± 0.01 in 10 µM NE, $P<0.001$, Fig. 25A). In pilomotor cells, AP size ratio was 0.65 ± 0.03 in control Ringer compared with 0.77 ± 0.02 in 10 µM NE ($P<0.001$, Fig. 25B). Vasoconstrictor neurons had an average AP size ratio of 0.64 ± 0.05 in control Ringer compared with 0.74 ± 0.03 in 10 µM NE ($P<0.001$, Fig. 25C). In addition, success ratio of secretomotor neurons in control Ringer was 0.76 ± 0.04 and 0.99 ± 0.01 in 10 µM NE ($P<0.001$, Fig. 25A). Pilomotor neurons had a

success ratio of 0.41 $\pm$ 0.03 in control Ringer compared with 0.88 $\pm$ 0.04 in 10 µM NE

(P<0.001, Fig. 25B). Success ratio of vasoconstrictor neurons in control Ringer was

0.35 $\pm$ 0.05 and 0.89 $\pm$ 0.04 in 10 µM NE (P<0.001, Fig. 25C). Furthermore, NE effects

upon cumulative EPSPs of these three functional phenotypes were also examined (Fig.

25). The secretomotor cells expressed 17.5 $\pm$ 1.4 mV cumulative EPSPs in control

Ringer compared with 7.6 $\pm$ 0.9 mV in 10 µM NE (P<0.001). The pilomotor cells had

20.5 $\pm$ 1.2 mV cumulative EPSPs in control Ringer compared with 11.8 $\pm$ 0.9 mV in 10

µM NE (P<0.001). Cumulative EPSPs of vasoconstrictor neurons in control Ringer was

19.3 $\pm$ 1.7 and 9.9 $\pm$ 1.3 in 10 µM NE (P<0.001).

Moreover, we also performed one-way ANOVA followed by Turkey's test for

multiple comparisons among these three functional subsets of neurons. The data

showed that AP size ratio of each cell groups in control Ringer had no significant

difference (Fig. 26, A). This contrasted with AP size ratio of each cell groups in NE,

which differed significantly among all three cell groups (Fig. 26, B). It suggested that

spike attenuation can be recovered more in secretomotor neurons. In contrast, success

ratio of firing differed significantly between all three subsets of neurons in control Ringer

but had nearly no difference among secretomotor, pilomotor and vasoconstrictor

neurons in NE (Fig. 26, A and B). These data showed that spike failure is less

prominent in secretomotor neurons during a spike train. It also suggested that NE can

increase successful firing of all three cell groups to a maximum value and have more

apparent effects in pilomotor and vasoconstrictor neurons. The comparison of spike

attenuation and spike failure between secretomotor cells (low threshold) and pilomotor

and vasoconstrictor cells (high threshold) corresponded quite well with results obtained in extracellular recordings (Fig. 19). In addition, cumulative EPSPs had no significant difference in control among three cell types and only small difference in NE between secretomotor and pilomotor neurons (Fig. 26, A and B).
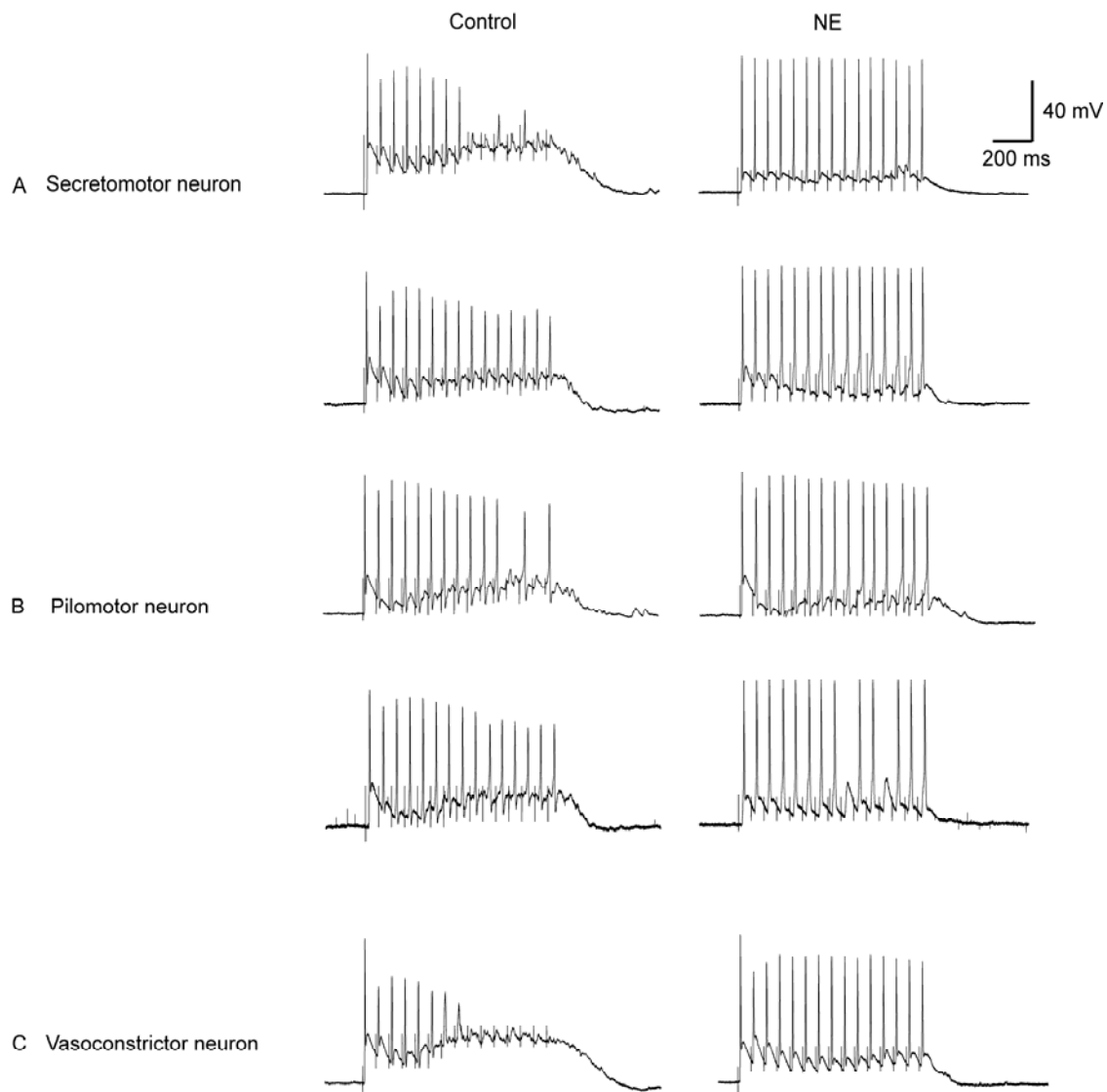
Figure 24. Representative traces of two types of responses at 15 Hz presynaptic stimulation in secretomotor, pilomotor and vasoconstrictor neurons.

Cell responses were evoked by 15 Hz presynaptic stimulation. Some cells in control Ringer had both failure of cell firing and smaller AP size (first row in A, B and C), while other cells fired small APs without failure (second row in A and B). Note there are still two firing failures during application of 10 μM NE in B.
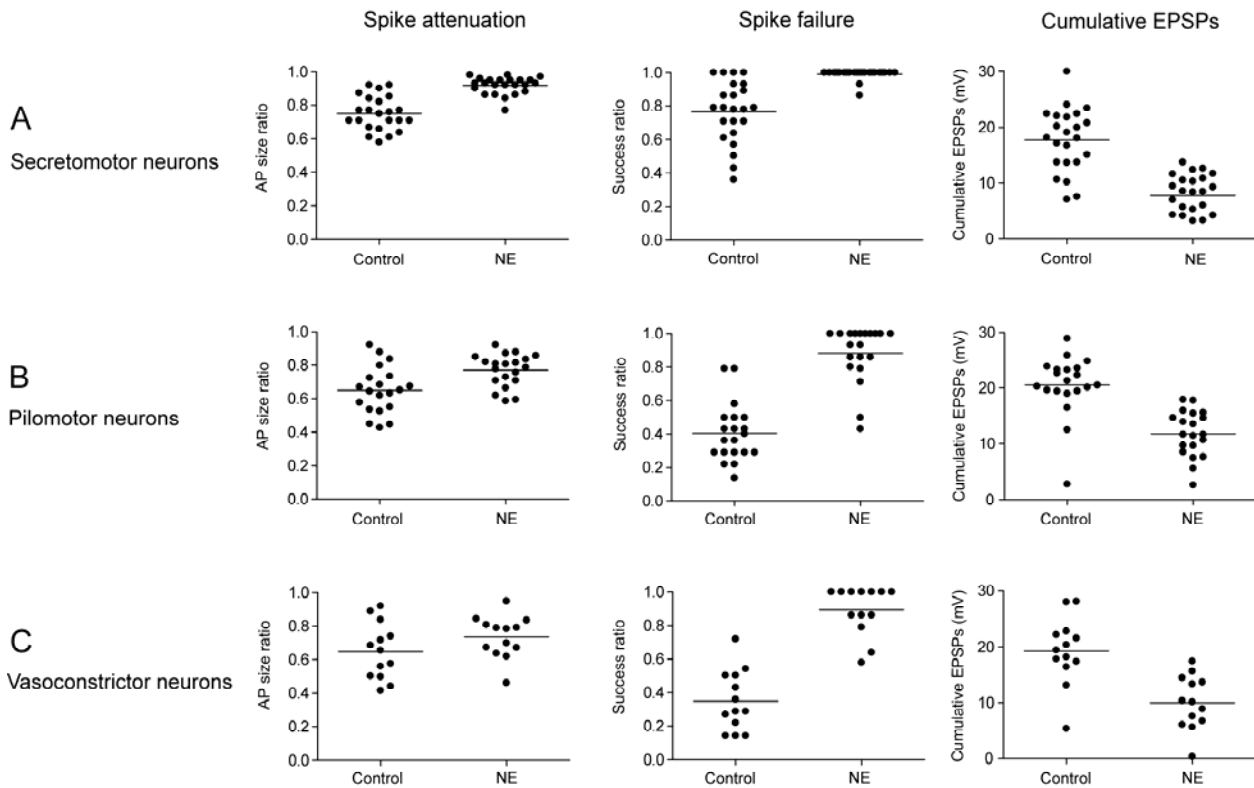
Figure 25. Effects of NE on spike attenuation, spike failure and cumulative EPSPs in each functional

phenotype.

Scatter plots compare the distribution in each neuronal type of normalized AP size ratio (*A*); success ratio

of firing (*B*); the amplitude of cumulative EPSPs (*C*). For each property, every cell is represented as a

single point and horizontal bars denoted the population mean. For the purpose of visual clarity, the data

points for each group are also spread horizontally. Note: all these NE effects in each subtype of neurons

have significant difference.
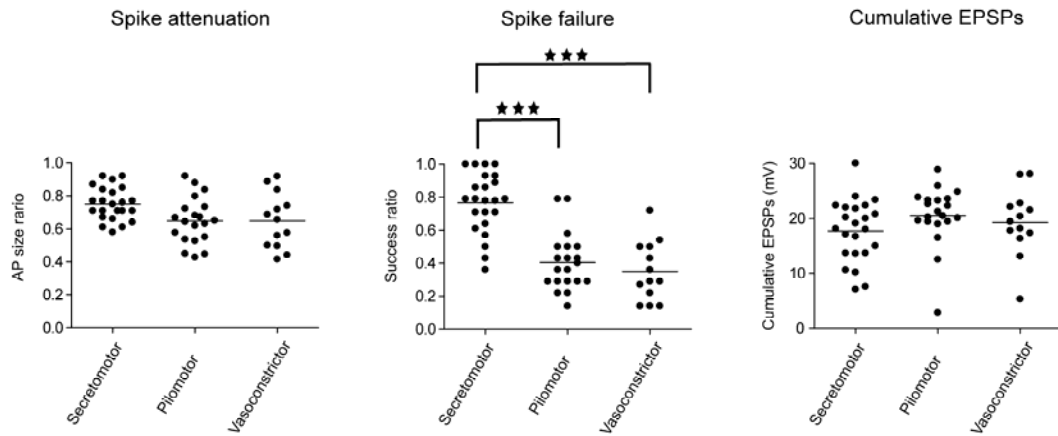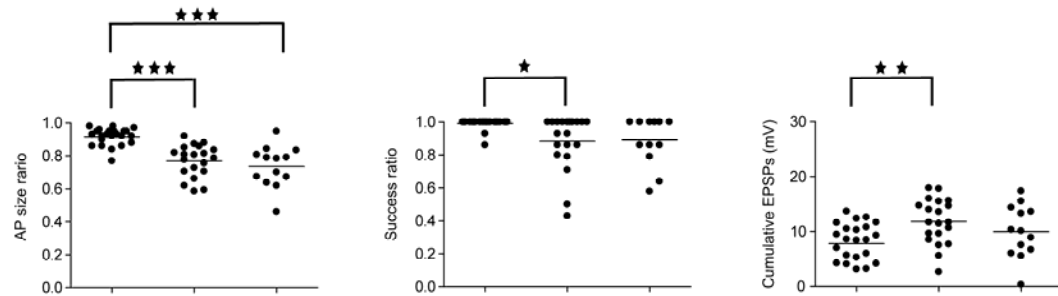
Figure 26. Comparison of three cell types in the context of spike attenuation, spike failure and cumulative EPSPs.

Scatter plots compare the distribution in each neuronal type of normalized AP size ratio (*A*); Success ratio of firing (*B*); and the amplitude of cumulative EPSPs (*C*). For each property, every cell is represented as a single point and horizontal bars denotes the population mean. For better visual clarity, the data points for each group are also spread horizontally. ***, P<0.001; **, P<0.01; *, P<0.05.

5.4.4 Cellular mechanism of norepinephrine modulation of synaptic transmission.

Spike failure could arise, in principle, from depolarization induced inactivation of Na^+ channels or from a non-specific shunting of the membrane conductance during the accumulated EPSPs. To distinguish these possibilities, we first examined whether neurons were capable of firing at 15 Hz non-synaptic stimulation. We then determined whether membrane hyperpolarization, which should relieve inactivation of Na^+ channels, could reverse spike attenuation. Our results showed that both low and high threshold neurons were able to fire normal size action potentials at 15 Hz, when directly stimulated by injected 10 ms, 300 pA pulses (Fig. 27, 2nd row). Both cell groups could also fire full amplitude spikes in response to antidromic stimulation (Fig. 27, 3rd row). In addition, hyperpolarization of the resting potential to -100 mV did not fully relieve the attenuation of spike amplitude during synaptic stimulation in both cell groups (Fig. 27, 4th row). Our data suggested that the effect of reduced spike amplitude was not caused simply by accumulation of Na^+ channel inactivation during repetitive firing.
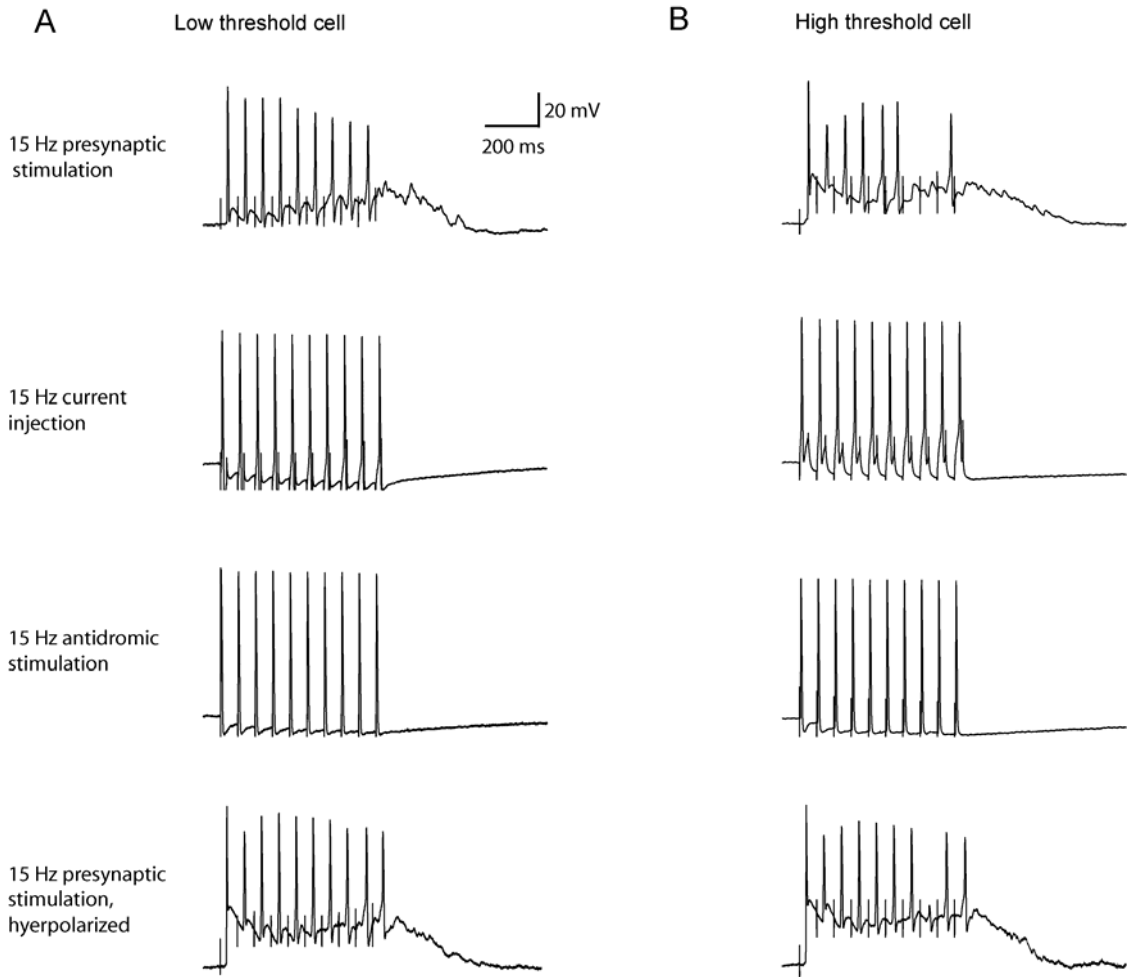
Figure 27. Trains of action potentials that were evoked in a low threshold cell (A) and high threshold cell (B) by synaptic and non-synaptic stimulation at 15 Hz stimulation

Top row, in both cell groups, presynaptic stimulation reduced action potential amplitude and sometimes led to failure of spikes (see right side). Second row, low and high threshold neurons were stimulated by injected 10 ms, 300 pA pulses at 15 Hz. Third row, full amplitude spikes were evoked by antidromic stimulation at 15 Hz. Bottom row, both cell groups were unable to fire action potentials with normal size even when hyperpolarized to -100 mV by current injection.

5.4.5 Activation of alpha 2 adrenergic receptors causes the norepinephrine modulation of synaptic transmission.

It has been demonstrated that the adrenergic receptors expressed in rat SCG neurons are mainly α2 subtype (Pieribone et al., 1994; Gold et al., 1997; Vidovic and Hill, 1997; McCallum et al., 1998; Ruiz-Velasco and Ikeda, 1998; Delmas et al., 1999; Fernandez-Fernandez et al., 2001). Previous studies also showed that α2-adrenergic receptor antagonists can attenuate the inhibition of ACh release, which suggests that the inhibition is mediated by presynaptic α-2 adrenergic receptors (Vizi, 1979; Belluzzi et al., 1987; McCallum et al., 1998; Stephens and Mochida, 2005). To confirm whether α-2 adrenergic receptors are responsible for NE modulation of synaptic transmission, we tested the effects of antagonists of all three adrenergic receptors α-1, α-2 and β respectively. α-1 and β receptor antagonists (prazosin, 1 μM and propranolol, 1 μM) did not block the modulation effects of NE (data not shown). However, in both low (n=4) and high (n=3) threshold cells (Fig. 28 and 29), pre-incubation of an α2-adrenergic receptor antagonist, yohimbine (1 μM, 20 minutes) blocked NE attenuation of reduced spike amplitude, reversed high success rate of firing and partially maintained large cumulative EPSPs.
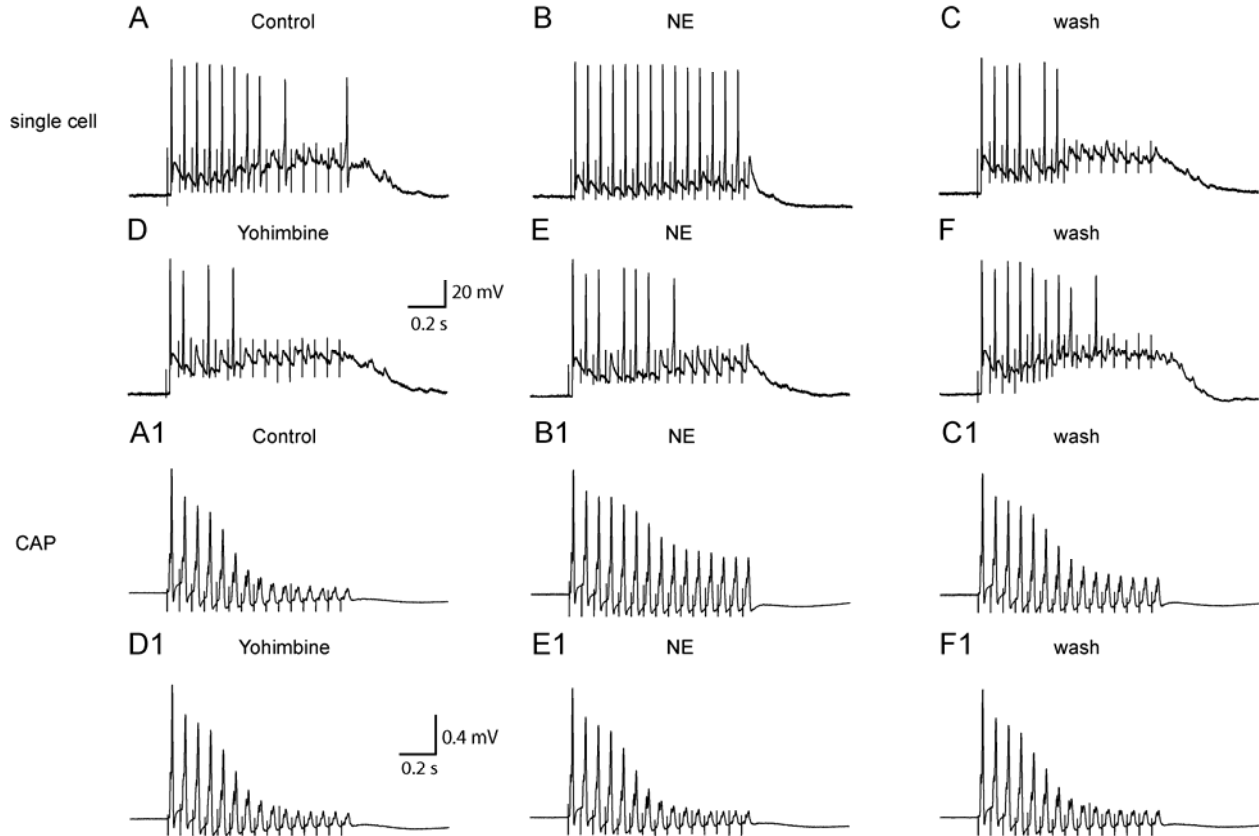
Figure 28. Effects of 1µM yohimbine, an α2- adrenergic receptor antagonist, upon a low threshold cell. Top two rows denote single cell response; bottom two rows are corresponding CAPs recorded from ECN. A and A1, Traces were taken in control Ringer. B and B1, the experiment traces of neuron responses were generated after 6 minutes exposure to 10 µM NE. C and C1, neurons were washed back to control Ringer. D and D1, neuron responses after 20 minutes incubation of yohimbine (1 µM). E and E1, the experiment of B and B1 was repeated after incubation of yohimbine. F and F1, cell response after being washed back to control Ringer again. Note the CAPs correspond nicely with single cell response.

116
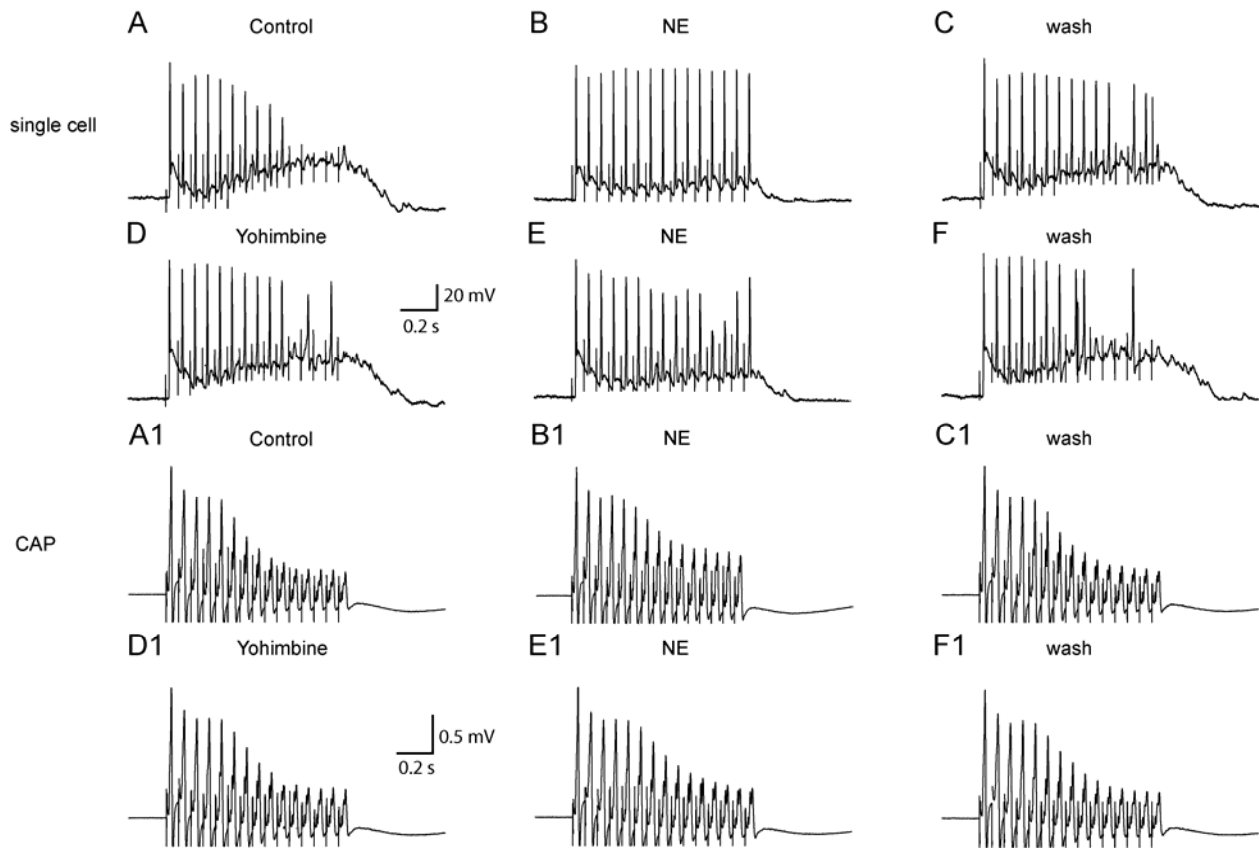
Figure 29. Effects of 1μM yohimbine, an α2- adrenergic receptor antagonist, upon a high threshold cell. The experimental protocol in this figure was the same as in Figure 28, except that the intracellular recording was from a high threshold neuron.

5.5 DISCUSSION

This chapter shows that inhibition of ACh release induced by NE affects synaptic

transmission in secretomotor, pilomotor and vasoconstrictor sympathetic neurons.

Presynaptic stimulation at 15 Hz causes spike attenuation, spike failure and cumulative

EPSPs. However, the data indicate that the magnitude of spike failure is less prominent

in low threshold secretomotor neurons than in high threshold pilomotor and

vasoconstrictor neurons. Interestingly, NE can relieve spike attenuation, reverse spike

failure and decrease cumulative EPSPs. Our results demonstrate that pilomotor and

vasoconstrictor neurons are more sensitive to NE effects upon spike failure.

5.5.1 Inhibition of presynaptic ACh release induced by NE affects synaptic

transmission in functional subsets of rat SCG neurons

Activation of presynaptic α2-adrenergic receptors by catecholamines inhibits ACh

release from preganglionic nerve terminals (Christ and Nishi, 1971; Dun and Karczmar,

1977). The direct analysis of ACh release requires collection of radio-labeled ACh

(Bulbring, 1944; Araujo and Collier, 1986). However, this method is not suitable for our

study because it is not possible to determine from which specific type of nerve terminals

ACh is released. Our method of accessing presynaptic modulatory effects of NE is

indirect and relies on previous studies. Nishi and colleagues showed that reduction of

amplitude of nicotinic EPSPs parallels with reduced ACh release induced by

catecholamines. Postsynaptic sensitivity to ACh is unaltered by catecholamines when

ACh depolarization is induced from iontophoretic ACh. In addition, catecholamines can decrease the frequency of miniature EPSPs and the quantal content of EPSPs without change in the quantal size (Christ and Nishi, 1971; Dun and Karczmar, 1977). Not only did these studies suggested that synaptic blockade of ganglionic transmission is due to α-adrenergic receptors at the presynaptic site but also provided us with a way to examine the presynaptic modulatory effects of NE upon ganglionic transmission.

This chapter focused on examining NE effects upon synaptic transmission at high (15 Hz) frequency presynaptic stimulation. Synaptic strength can rapidly increase or decrease during and after brief bursts of activities. All synapses show some form of short-term facilitation, depression or both. The extent of facilitation or depression varies at a given synapse, depending on presynaptic AP frequency, release probability (P) and neuromodulation (Thomson, 2000). Facilitation dominates when P is low, while depression is apparent when P is high. The short-term depression of cell discharge in a spike train suggested that release probability (P) is high at presynaptic terminals of all functional subtypes of neurons. The neurotransmitter, in this case ACh, in presynaptic vesicles easily gets depleted during high frequency stimulation, which causes reduction of EPSPs size. Our data showed that non-synaptic stimulation at 15 Hz stimulation allows cells to fire robustly and in full size. This suggested that the spike failure and shortened AP amplitude observed in all three functional subsets of neurons are most likely due to nicotinic shunting of postsynaptic membrane conductance.

Furthermore, our results showed that NE has presynaptic modulatory effects in all three cell types which are unlike the specificity of postsynaptic effects (Chapter 5). NE can reverse spike failure, relieve spike attenuation and reduce cumulative EPSPs in a spike train. These effects are probably because inhibition of calcium channels induced by activation of α2-adrenergic receptors at presynaptic terminals could reduce depletion of ACh during repetitive activities. In the context of different modulatory effects of NE upon secretomotor, pilomotor and vasoconstrictor neurons, our data demonstrated that spike failure was less prominent in secretomotor neurons. It suggested that the safety factor of synaptic transmission is probably higher in secretomotor neurons than that in the other two subsets of neurons, which is the analogy of difference between secretomotor B and vasoconstrictor C neurons in bullfrog sympathetic ganglia (Shen and Horn, 1995; Karila and Horn, 2000). In addition, bath-applied NE can cause pilomotor and vasoconstrictor neurons to fire as robustly as secretomotor neurons. It suggested that NE can decrease Ca^{2+} influx into presynaptic terminal and reduce ACh release to a determined value in all three cell types.

5.5.2 Implication for ganglionic integration

A key goal of this chapter was to compare NE neuromodulatory mechanism of synaptic transmission in different sympathetic phenotypes. Although previous work has examined the variation of muscarinic mechanisms that occur in secretomotor and vasomotor neurons in bullfrog sympathetic ganglia (Libet et al., 1968; Dodd and Horn, 1983a; Horn, 1992), the difference between functional subsets of neurons in

mammalian sympathetic ganglia has not been studied. In the gain theory of ganglionic

integration, it has been proposed that neuromodulatory mechanisms can regulate

synaptic gain by altering the strength of secondary nicotinic synapses and enable

sympathetic ganglia to function as synaptic amplifiers of preganglionic activity (Karila

and Horn, 2000; Wheeler et al., 2004). If one was to observe cell-specific differences in

NE modulatory mechanism, then it would suggest that gain varies in different

sympathetic modalities. When this hypothesis was tested by comparing the NE

modulatory effects upon putative secretomotor, pilomotor and vasoconstrictor neurons

(Fig. 25), our results showed clearly that these three cell types express different NE

modulatory effects upon synaptic transmission. Although spike failure was less

prominent in secretomotor neurons than in the other two sympathetic phenotypes, bath-

applied NE brought the level of successful firing of pilomotor and vasoconstrictor

neurons close to that of successful firing of secretomotor neurons. It indicated that

pilomotor and vasoconstrictor neurons might fire robustly during emergent conditions in

spite of relatively weaker synaptic strength.

CHAPTER 6

DISCUSSION

This dissertation first focused on the neuronal classification of secretomotor, pilomotor and vasoconstrictor neurons in the rat SCG (Chapter 2). Then using these classification criteria, I examined the cellular specialization of synaptic convergence and NE modulatory mechanism of synaptic transmission, each of which is determinant of gain function (Table 6). Secretomotor, pilomotor and vasoconstrictor neurons identified by our classification criteria are indistinguishable in terms of synaptic convergence (Chapter 3). Furthermore, NE acts on postsynaptic α2-adrenergic receptors to inhibit Ca^{2+}-dependent components of the spike in secretomotor and pilomotor neurons while not evident in vasoconstrictor neurons (Chapter 4). In addition, it is demonstrated in this dissertation that presynaptic α2-adrenergic receptors can modulate nicotinic transmission in all three cellular phenotypes while the effects appear stronger in pilomotor and vasoconstrictor neurons (Chapter 5). In this chapter some of the gaps that remain in our understanding of adrenergic modulation of synaptic transmission will be addressed. Finally, possible future areas of study will be raised for discussion. These include the molecular mechanism of the signaling transduction pathway between adrenergic receptors and calcium channels, cellular specialization of synaptic strength and experimental methods of studying the origin of NE.

Table 6. Summary of cellular specialization of synaptic convergence and NE modulatory mechanisms in secretomotor, pilomotor and vasoconstrictor neurons

Cell Type	Synaptic convergence	Postsynaptic modulatory effects of NE	Presynaptic modulatory effects of NE
Secretomotor neurons	8.4	+++	+
Pilomotor neurons	8.4	+++	+++
Vasoconstrictor neurons	8.6	-	+++

Each phenotype of neurons has a similar range and an average number of synaptic convergence. Bath-applied 10 µM NE inhibits calcium-dependent components (AP shoulder and AHP) in secretomotor and pilomotor, but not in vasoconstrictor neurons. In addition, Presynaptic alpha adrenergic receptors can modulate nicotinic transmission by relieving spike attenuation, spike failure and cumulative depolarization during 15 Hz presynaptic stimulation in all 3 cell types, but the effects appear stronger in high threshold pilomotor and vasoconstrictor neurons. +, denotes effects of NE;+++, marks strong effects of NE; -, no effects of NE.

6.1 FUNCTIONAL IMPLICATION OF OUR NEW CLASSIFICATION SCHEME

The first finding in this study was that presynaptic stimulus threshold and NPY immunoreactivity can serve as neuronal classification criteria of secretomotor, pilomotor and vasoconstrictor neurons. These two criteria are unambiguous and relatively easy to apply in future studies. Previous studies in the bullfrog suggested that axonal conduction velocity, soma size and NPY immunoreactivity distinguish secretomotor B and vasoconstrictor C neurons. Axonal conduction velocity serves as classification criteria of bullfrog sympathetic neurons because secretomotor B neurons have myelinated axons with conduction velocities in the B fiber range (Nishi et al., 1965; Dodd and Horn, 1983b) while vasoconstrictor C neurons have unmyelinated axon with velocity in the C fiber range (about 0.3 m/s) (Nishi et al., 1965; Dodd and Horn, 1983b; Horn et al., 1987). However, almost all presynaptic and postsynaptic nerve fibers of rat SCG neurons are unmyelinated (Gabella, 1976). In fact, our studies demonstrated that the conductional velocities of almost all pre and postsynaptic fibers are among C fiber range (Fig 8 and 9). Therefore, conductional velocity is an ambiguous criterion of neuronal classification of rat SCG neurons. Interestingly, we found that presynaptic stimulus threshold can serve as a clear-cut criterion that distinguishes secretomotor neurons from the other two cell types. This is even more useful when only pilomotor and vasoconstrictor neurons are targets of study in electrophysiological experiment. In addition, secretomotor and vasoconstrictor neurons of rat and bullfrog share similarities of other properties. For example, secretomotor neurons of rat and bullfrog are both relatively large while vasoconstrictor C neurons have small somata (Nishi et al., 1965;

Dodd and Horn, 1983b; Morris et al., 1986; Li and Horn, 2006). Secretomotor neurons of rat and bullfrog lack NPY (Horn et al., 1987; Li and Horn, 2006) and vasoconstrictor C neurons contain neuropeptide Y (NPY) (Horn et al., 1987; Morris et al., 1989; Li and Horn, 2006). The analogies between mammalian and amphibian sympathetic neurons indicate these features are evolutionarily conserved. Furthermore, the classification method we establishes can be extended by future experiments to differentiate rat SCG neurons projecting through ICN to supply the cerebral vasculature, pineal gland, skin of forehead and the eye. In addition, these classification criteria might also allow study of sympathetic neurons that control heart and visceral organs such as middle and inferior cervical ganglion and celiac ganglion.

We subsequently found that only AP shape of vasoconstrictor neurons (high threshold, NPY positive cells) do not respond to NE. Presynaptic stimulus threshold and sensitivity to NE are two electrophysiological criteria. Therefore, these two practical experimental criteria that distinguish three functional subsets of neurons can serve as very useful methods of examining cellular specialization of other physiological properties when electrophysiological experiments are undertaken.

6.2 THE MOLECULAR MECHANISM OF CELLULAR SPECIALIZATION OF ADRENERGIC MODULATION IN THE RAT SCG NEURONS

In the postsynaptic site, activation of α2-adrenergic receptors both activates GIRK

channels via direct binding of βγ dissociated from G_i/G_o (Ruiz-Velasco and Ikeda, 1998;

Fernandez-Fernandez et al., 2001) and inhibits N-type Ca^{2+} channels (Horn and

McAfee, 1980; Galvan and Adams, 1982) via βγ dimers dissociated from $G_{\alpha o}$ (Caulfield

et al., 1994; Delmas et al., 1998a; Delmas et al., 1999). The focus of my thesis

(Chapter 4) is to examine the inhibition of postsynaptic N-type calcium channel induced

by activation of α2-adrenergic receptors in different functional cell groups. It is because

AP shape is a direct manifestation of N-type calcium inhibition and easy to measure.

Previous studies found a splicing form of the main α1 subunit of the N-type calcium with

mutually exclusive exons 37a and 37b (Bell et al., 2004). N(37a) is able to allow more

Ca^{2+} influx into cells by increasing opening duration and trans-locating more channels

onto the synaptic membrane (Castiglioni et al., 2006). The work in Chapter 4

demonstrated that AP shoulder, which is a direct manifestation of calcium current

elicited by AP, remains the same in all three cellular phenotypes in control Ringer (Fig.

12, 13 and 14, Table 3). It suggested that N-type calcium channels in secretomotor,

pilomotor and vasoconstrictor neurons conduct the same amount of Ca^{2+} current in

control. Interestingly, recent study also showed that e37a allows N-type channels to be

substantially more sensitive to G-protein-mediated inhibition (Raingo et al., 2007). Our

results showed that adrenergic receptor agonist NE does not influence N-type calcium

currents in vasoconstrictor neurons. One of the possibilities is that vasoconstrictor

neurons only express e37b-containing N –type channels and thus are much less

sensitive to NE than the other two types of neurons. Another possibility is that

vasoconstrictor neurons express a different form of β subunits of N-type channels.

Calcium channels contain α1,α2-δ, β and γ subunits (Catterall, 2000). α1 subunit is organized in four repeated domains (I to IV), each of which contains six transmembrane segments (S1 to S6) and is the pore-forming subunit. α2-δ, β and γ subunits are the auxiliary subunits. It has been demonstrated that β subunits influence the level of expression and voltage dependence and gating of calcium channels (Walker and De Waard, 1998; Catterall, 2000). Furthermore, recent study showed that distinct types of auxiliary β subunits can differentially modulate the inhibition of α1 N-type calcium channels, in which β_4-containing subunit are much less sensitive to G-protein induced inhibition (Feng et al., 2001). This might be caused by the close proximity of the calcium channel β subunit interaction site and putative G-protein-binding sites within the domain I-II linker region of α1 subunit. Therefore, vasoconstrictor neurons expressing β_4-containing subunit of N-type calcium channels might be much less sensitive to NE than the other two functional subsets of neurons.

Calcium influx results in numerous subsequent events such as phosphorylation of downstream channels and kinase, protein translocation and even protein synthesis in the long term (Sjostrom and Nelson, 2002; Zucker and Regehr, 2002; Merrill et al., 2005). Our results showed that adrenergic receptors in vasoconstrictor neurons are probably not associated with N-type calcium channels. It suggests that Ca^{2+} influx is not inhibited by adrenergic receptors and could be larger in vasoconstrictor neurons than that in other functional subsets of neurons when NE is released by high frequency presynaptic activities. This might lead to more protein synthesis in the long run and

increase synaptic strength between presynaptic terminals and postsynaptic vasoconstrictor neurons.

In the presynaptic site, previous studies showed that activation of presynaptic α2-adrenergic receptors decrease ACh output in mammalian SCG (Christ and Nishi, 1971; Dun and Karczmar, 1977; Vizi, 1979; Belluzzi et al., 1987). Presynaptic inhibition of neurotransmitter release by GPCRs has been proposed variously to involve an inhibition of Ca^{2+} channels, an activation of K^+ channels, and a direct action on the exocytotic release machinery itself (Scanziani et al., 1993; Thompson et al., 1993; Wu and Saggau, 1997; Miller, 1998). Subsequent studies demonstrated that neurotransmission in sympathetic ganglion neurons is initiated exclusively by N-type Ca^{2+} channels ($Ca_v2.2$) (Mochida et al., 1995; Koh and Hille, 1997). The temporal dynamics of calcium channel responses to action potential trains at presynaptic nerve terminals influence the fidelity of synaptic transmission (Forsythe et al., 1998). With repetitive depolarization induced by action potentials, inactivation of calcium channels accumulates over time and progressively reduces calcium entry into presynaptic nerve terminals. This cumulative inactivation of calcium channels is thought to stem from closed-state inactivation which is a process that voltage-dependent calcium channels switch to inactivation status in response to depolarization that is not large enough to open the channels (Patil et al., 1998; Jones et al., 1999). Recent studies showed that $Ca_v2.2$ channels that contain e18a (a post-translational alternative splicing isoform) protect the channel from entering into closed-state inactivation (Thaler et al., 2004; Gray et al., 2007). This causes calcium influx during repetitive action potential trains to be

maintained in contrast to that through $Ca_v2.2$ channels lacking e18a. My study (Chapter 5) demonstrated that secretomotor neurons have less spike failure than pilomotor and vasoconstrictor neurons. One of the possibilities is that nerve terminals forming synapse with secretomotor neurons express e18a-containing $Ca_v2.2$ channels. Sustained calcium influx triggers sustained exocytosis of vesicles from presynaptic terminals and transmitter release, which guarantee that EPSPs are sufficient to reach threshold and lead to high safety factor of synaptic transmission in postganglionic neurons. However, this scenario does not exclude involvement of other factors that modulate susceptibility of N-type calcium channels to cumulative inactivation such as interaction with presynaptic proteins (Zhong et al., 1999).

Recent studies revealed that the adrenergic modulation of presynaptic transmitter release has close parallels with the modulation of calcium channel and $G_{\beta\gamma}$ serves as an essential presynaptic inhibitory mediator for cholinergic synaptic transmission in sympathetic ganglia (Stephens and Mochida, 2005). Inactivation of presynaptic N-type channels modulated by α2-adrenergic receptors could contribute to the fidelity of synaptic transmission by reducing probability of transmitter release during high frequency stimulation. This could slow or prevent presynaptic vesicle depletion and might promote recovery of the postsynaptic nicotinic receptors from desensitization (Borst and Sakmann, 1996; Forsythe et al., 1998). The most common type of neurotransmitter-initiated inhibition of N-type calcium channels is fast, membrane delimited, mediated by direct binding of $G_{\beta\gamma}$ and voltage-dependent. The voltage-dependent inhibition is especially effective upon Ca^{2+} influx triggered by single action

potentials but less effective during repetitive stimulation because depolarization elicited by trains of action potentials relieves it. Another form of G-protein-mediated inhibition is voltage-independent (Diverse-Pierluissi and Dunlap, 1993). This form of inhibition is not relieved by strong depolarization and may require protein kinase activation (Rane and Dunlap, 1986; Diverse-Pierluissi et al., 1997). Lipscombe and colleagues showed that N-type calcium channels consists of two exclusive splicing variants: N(37a) and N(37b) (Raingo et al., 2007). E37a (exon 37a) increases N-type channel sensitivity to G-protein-mediated inhibition by introducing an inhibitory pathway that is independent of voltage besides voltage-dependent inhibition. My work (Chapter 5) demonstrated that bath-applied NE can increase the successful firing of pilomotor and vasoconstrictor neurons and cause them to fire as robustly as secretomotor neurons in a spike train. One of the possibilities is that nerve terminals forming synapses with pilomotor and vasoconstrictor neurons express e37a-containing N-type channels. This can introduce voltage-independent inhibition of N-type calcium channels and allow presynaptic α2-adrenergic receptors for downregulating N-type currents, preventing presynaptic vesicle depletion and causing sustained neurotransmitter release even during periods of repetitive neuronal activities.

6.3 FUTURE AREAS OF STUDY

6.3.1 Synaptic convergence and synaptic strength

Computational simulation and dynamic clamp experiments (Wheeler et al., 2004) have revealed that synaptic convergence, synaptic strength, neuromodulatory mechanism and presynaptic plasticity are critical determinants of synaptic gain. My thesis has examined synaptic convergence and NE neuromodulation. The second part of my work (Chapter 3) showed that no synaptic convergence was found among different functional subsets of neurons. It suggests that synaptic convergence does not contribute to the possible difference of gain function in different cell phenotypes. However, this does not rule out the possibility that different functional subclasses of sympathetic neurons in the rostral part of SCG or other ganglia could have distinct synaptic convergence. The vasoconstrictor neurons examined in my thesis are the ones that project to cutaneous targets such as skin in the face. It is possible that vasoconstrictor neurons that innervate vascular beds in the limb muscle and cerebral vasculature might have different synaptic convergence than secretomotor and pilomotor neurons. The larger synaptic convergence of this type of vasoconstrictor neurons could result in more synaptic gain and therefore more tight control over blood pressure during posture change. Therefore, future research can focus on examining the synaptic convergence of these types of vasoconstrictor neurons and compare with that of other functional subclasses of sympathetic neurons.

Although our results showed that synaptic convergence is unrelated with phenotypic identity, it is important to note that other determinants of synaptic gain could contribute to the phenotypic specialization of synaptic integration. For instance, the simulation study in our lab showed that the peak of gain function varies as a function of

secondary synaptic strength (Wheeler et al., 2004). Therefore, synaptic strength in different cellular phenotypes could be the subsequent target of study. Purves and colleagues examined the number of axons innervating individual postganglionic neurons by counting multiple steps in EPSP sizes with gradually increasing presynaptic stimulation intensity (Purves and Hume, 1981; Purves and Lichtman, 1985). This method was very useful in counting the number of synaptic inputs. However, the amplitude of each EPSP step does not equal to the strength of each synaptic input due to the fluctuation of EPSPs from every single experimental trial to another. Consequently, the precise measurement of the synaptic strength of each input requires averaging each EPSP step with many experimental trials or measuring EPSCs and calculating synaptic conductance of each input by voltage clamp study.

6.3.2 The mechanism of the postsynaptic insensitivity to NE of vasoconstrictor neurons

The second area of study is to examine why vasoconstrictor neurons do not respond to NE. As is discussed in Chapters 4.5.1 and 6.2, this phenomenon can be caused by several mechanisms. Among all of these mechanisms, it is most likely that different isoforms of N-type calcium channels are expressed in vasoconstrictor neurons. Based on literatures and our observations, the hypothesis is that the α1 pore-forming subunit of N-type calcium channels in vasoconstrictor neurons might have a different C-terminal or the domain I-II linker region that is not well associated with α2-adrenergic receptors as channels in the other two phenotypes. In principle, they could be tested by Isoform

specific antibodies to examine the anatomical distribution of different types of N-type calcium channels in these cell groups. Another method to examine specialized cellular expression of different types of N-type calcium channels is single cell RT-PCR. Another line of future study might require genetic methods to examine the lack of coupling between adrenergic receptors and N-type calcium channels in vasoconstrictor neurons. This could be achieved by altering specific amino acid residues in the $G_{\beta\gamma}$ binding site of $\alpha 1$ subunit of N-type channels. Restoration of calcium channel sensitivity to NE in vasoconstrictor neurons by this way would suggests that the specific type of calcium channels expressed in vasoconstrictor neurons causes the insensitivity to NE. A third possibility could use isoform specific toxins, however these toxins have not been identified and require future discovery.

6.3.3 Activation of GIRK channels by postsynaptic α2-adrenergic receptors

In the 1920s, Otto Loewi's experiments with isolated frog hearts demonstrated the concept of chemical synaptic transmission (Loewi, 1921). Subsequent studies identified ACh as neurotransmitter (Dale et al., 1936), which upon binding to atrial muscarinic receptors activates a specific type of GIRK channels (Breitwieser and Szabo, 1985; Pfaffinger et al., 1985; Kofuji et al., 1995). It leads to hyperpolarization of the myocyte membrane and bradycardia. Since the initial molecular identification of the GIRK channels (Ho et al., 1993; Kubo et al., 1993a; Kubo et al., 1993b), subsequent studies showed that these channels are expressed in the heart, endocrine tissues and the central and peripheral nervous systems (DePaoli et al., 1994; Yamada et al., 1998).

They primarily produce slow postsynaptic inhibitory potentials and could contribute to

neuronal excitability (Yamada et al., 1998). As is described in Chapter 5.5.1, the small

hyperpolarization of membrane potential elicited by activation of GIRK does not seem to

affect synaptic transmission directly, at least in high frequency stimulation. Investigation

of the cellular specialization of inward rectifying current (GIRK expression) requires

voltage clamp study. However, connective tissues and glia cells make it very difficult to

perform in isolated rat SCG. Cultured SCG neurons might be useful in future studies.

6.3.4 Muscarinic neuromodulatory mechanism

In addition to NE neuromodulatory mechanism, activation of muscarinic (Brown et al.,

1980; Adams et al., 1982; Tokimasa and Akasu, 1995), angiotensin (Shapiro et al.,

1994; Zaika et al., 2006), adenosine (Henon and McAfee, 1983) and other G protein-

coupled receptors (GPCRs) either through synaptic release or the circulation can

produce slow electrophysiological events mediated by metabotropic signal transduction

pathways. The next step towards understanding other neuromodulatory mechanism

could be examining cellular specialization of muscarinic modulation of synaptic

transmission. It has already been shown that the muscarinic neuromodulatory

responses in bullfrog B and C neurons are different. Muscarine triggers an excitatory

response in B neurons but an inhibitory one in C neurons (Horn, 1992). Future study

can focus on examining whether there is an analogy in mammalian sympathetic ganglia.

In fact, I have already conducted preliminary experiments and observed slow EPSPs in

most rat SCG neurons by 20 HZ presynaptic stimulation. Interestingly, there were a few

cells that expressed slow IPSP. However, the major problem we encountered was that

nicotinic receptor blocker, hexamethonium chloride (works perfectly in rabbit, cat and

guinea pig) were unable to fully block fast transmission in rat SCG neurons even when

the concentration was increased to 1 mM. We also tried other nicotinic receptor

blockers (d-tubocurarine, 100 µM and mecamylamine, 100 µM) but none were capable

of fully blocking nicotinic EPSPs. Continuing of these studies will require identification

of nicotinic blockers that are more effective.

6.3.5 Origin of NE

Another interesting area we can explore is to examine the origin of NE. Chapter 4.5.2

laid out three possible sources: dendritic release, presynaptic nerve terminal release

and from circulation. NA released from short-term SCG neuron cultures could be

detected by amperometry (Koh and Hille, 1997). This method allows the amount of NA

released to be detected in a very precise way. Stimulating one possible route and

combined with amperometry is an ideal way to demonstrate the origin of released NE.

For example, SCG neurons in isolated ganglia can be activated by antidromic

stimulation with output nerve ECN. Amperometry can be used to detect the amount of

NA released afterwards. We may reach a conclusion that NE is released from dendrites

and soma if NE can be detected by amperometry probe.

6.3.6 Direct measurement of synaptic gain in distinct phenotypes

Last but not least, we can examine how synaptic convergence and NE or other neuromodulatory mechanisms affect synaptic gain. Although we are able to show cellular specialization of all four critical determinants of synaptic gain, we still need to conduct direct examination of the relationship between synaptic input and output to find out how these properties affect synaptic gain. Detailed experimental studies of synaptic strength, neuromodulatory mechanism and synaptic plasticity can provide comprehensive findings of how these properties influence synaptic conductance. The precisely controlled changes of synaptic conductance which mimic synaptic conductance changes induced by these properties in reality can be virtually fed into sympathetic ganglionic neurons. By recording those output spikes and comparing with inputs, we are able to examine synaptic gain in different functional subsets of neurons directly by these dynamic clamp experiments.

6.4 CONCLUDING REMARKS

The results in this thesis provided a better understanding of several important issues in ganglionic physiology. This work has shown that different sympathetic phenotypes, specifically secretomotor, pilomotor and vasoconstrictor neurons can be identified by presynaptic stimulus intensity and NPY expression. The work presented here has also characterized phenotypic specialization of synaptic convergence and both pre and postsynaptic noradrenergic modulatory effects. Our cellular identification scheme opens possibilities for examining an expanded range of new issues. Immediate future

studies should be a sharpened focus on cellular specialization of other synaptic

properties that are critical determinants of synaptic gain and detailed molecular

mechanisms of noradrenergic modulation of N-type calcium channels.

BIBLIOGRAPHY

Adams PR, Brown DA, Constanti A (1982) M-currents and other potassium currents in bullfrog sympathetic neurones. J Physiol 330:537-572.

Aguayo AJ, Terry LC, Bray GM (1973) Spontaneous loss of axons in sympathetic unmyelinated nerve fibers of the rat during development. Brain Res 54:360-364.

Andrews TJ, Thrasivoulou C, Nesbit W, Cowen T (1996) Target-specific differences in the dendritic morphology and neuropeptide content of neurons in the rat SCG during development and aging. J Comp Neurol 368:33-44.

Araujo DM, Collier B (1986) Evidence that endogenous catecholamines can regulate acetylcholine release in a sympathetic ganglion. Eur J Pharmacol 125:93-101.

Beaudet MM, Braas KM, May V (1998) Pituitary adenylate cyclase activating polypeptide (PACAP) expression in sympathetic preganglionic projection neurons to the superior cervical ganglion. J Neurobiol 36:325-336.

Beaudet MM, Parsons RL, Braas KM, May V (2000) Mechanisms mediating pituitary adenylate cyclase-activating polypeptide depolarization of rat sympathetic neurons. J Neurosci 20:7353-7361.

Bell TJ, Thaler C, Castiglioni AJ, Helton TD, Lipscombe D (2004) Cell-specific alternative splicing increases calcium channel current density in the pain pathway. Neuron 41:127-138.

Belluzzi O, Travagli RA, Bonifazzi C, Perri V (1987) Quantitative evaluation of alpha- and beta-adrenoceptor modulation of [3H]choline release in guinea pig superior cervical ganglia. Neurosci Lett 73:65-70.

Bernheim L, Mathie A, Hille B (1992) Characterization of muscarinic receptor subtypes inhibiting Ca^{2+} current and M current in rat sympathetic neurons. Proc Natl Acad Sci U S A 89:9544-9548.

Bjorklund H, Hokfelt T, Goldstein M, Terenius L, Olson L (1985) Appearance of the noradrenergic markers tyrosine hydroxylase and neuropeptide Y in cholinergic nerves of the iris following sympathectomy. J Neurosci 5:1633-1640.

Borst JG, Sakmann B (1996) Calcium influx and transmitter release in a fast CNS synapse. Nature 383:431-434.

Bowers CW, Zigmond RE (1979) Localization of neurons in the rat superior cervical ganglion that project into different postganglionic trunks. J Comp Neurol 185:381-391.

Bowers CW, Dahm LM, Zigmond RE (1984) The number and distribution of sympathetic neurons that innervate the rat pineal gland. Neuroscience 13:87-96.

Bray GM, Aguayo AJ (1974) Regeneration of peripheral unmyelinated nerves. Fate of the axonal sprouts which develop after injury. J Anat 117:517-529.

Breitwieser GE, Szabo G (1985) Uncoupling of cardiac muscarinic and beta-adrenergic receptors from ion channels by a guanine nucleotide analogue. Nature 317:538-540.

Brown DA, Caulfield MP (1979) Hyperpolarizing 'alpha 2'-adrenoceptors in rat sympathetic ganglia. Br J Pharmacol 65:435-445.

Brown DA, Fatherazi S, Garthwaite J, White RD (1980) Muscarinic receptors in rat sympathetic ganglia. Br J Pharmacol 70:577-592.

Buhler HU, da Prada M, Haefely W, Picotti GB (1978) Plasma adrenaline, noradrenaline and dopamine in man and different animal species. J Physiol 276:311-320.

Bulbring E (1944) The action of adrenaline on transmission in the superior cervical ganglion. J Physiol 103:55-67.

Castiglioni AJ, Raingo J, Lipscombe D (2006) Alternative splicing in the C-terminus of CaV2.2 controls expression and gating of N-type calcium channels. J Physiol 576:119-134.

Catterall WA (2000) Structure and regulation of voltage-gated Ca2+ channels. Annu Rev Cell Dev Biol 16:521-555.

Caulfield MP, Jones S, Vallis Y, Buckley NJ, Kim GD, Milligan G, Brown DA (1994) Muscarinic M-current inhibition via G alpha q/11 and alpha-adrenoceptor inhibition of Ca2+ current via G alpha o in rat sympathetic neurones. J Physiol 477 (Pt 3):415-422.

Christ DD, Nishi S (1971) Site of adrenaline blockade in the superior cervical ganglion of the rabbit. J Physiol 213:107-117.

Dale HH, Feldberg W, Vogt M (1936) Release of acetylcholine at voluntary motor nerve endings. J Physiol 86:353-380.

Dampney RA (1994) Functional organization of central pathways regulating the cardiovascular system. Physiol Rev 74:323-364.

De Groat WC, Volle RL (1966) The actions of the catecholamines on transmission in the superior cervical ganglion of the cat. J Pharmacol Exp Ther 154:1-13.

Delmas P, Abogadie FC, Milligan G, Buckley NJ, Brown DA (1999) betagamma dimers derived from Go and Gi proteins contribute different components of adrenergic inhibition of Ca2+ channels in rat sympathetic neurones. J Physiol 518 (Pt 1):23-36.

Delmas P, Brown DA, Dayrell M, Abogadie FC, Caulfield MP, Buckley NJ (1998a) On the role of endogenous G-protein beta gamma subunits in N-type Ca2+ current inhibition by neurotransmitters in rat sympathetic neurones. J Physiol 506 (Pt 2):319-329.

Delmas P, Abogadie FC, Dayrell M, Haley JE, Milligan G, Caulfield MP, Brown DA, Buckley NJ (1998b) G-proteins and G-protein subunits mediating cholinergic inhibition of N-type calcium currents in sympathetic neurons. Eur J Neurosci 10:1654-1666.

DePaoli AM, Bell GI, Stoffel M (1994) G protein-activated inwardly rectifying potassium channel (GIRK1/KGA) mRNA in adult rat heart and brain by in situ hybridization histochemistry. Mol Cell Neurosci 5:515-522.

Diverse-Pierluissi M, Dunlap K (1993) Distinct, convergent second messenger pathways modulate neuronal calcium currents. Neuron 10:753-760.

Diverse-Pierluissi M, Remmers AE, Neubig RR, Dunlap K (1997) Novel form of crosstalk between G protein and tyrosine kinase pathways. Proc Natl Acad Sci U S A 94:5417-5421.

Dodd J, Horn JP (1983a) Muscarinic inhibition of sympathetic C neurones in the bullfrog. J Physiol 334:271-291.

Dodd J, Horn JP (1983b) A reclassification of B and C neurones in the ninth and tenth paravertebral sympathetic ganglia of the bullfrog. J Physiol 334:255-269.

Dun N, Karczmar AG (1977) The presynaptic site of action of norepinephrine in the superior cervical ganglion of guinea pig. J Pharmacol Exp Ther 200:328-335.

Dunlap K, Fischbach GD (1978) Neurotransmitters decrease the calcium ocmponent of sensory neurone action potentials. Nature 276:837-839.

Eccles JC (1935) The action potential of the superior cervical ganglion. J Physiol 85:179-206 172.

Eccles RM (1955) Intracellular potentials recorded from a mammalian sympathetic ganglion. J Physiol 130:572-584.

Eccles RM, Libet B (1961) Origin and blockade of the synaptic responses of curarized sympathetic ganglia. J Physiol 157:484-503.

Edvinsson L, Hara H, Uddman R (1989) Retrograde tracing of nerve fibers to the rat middle cerebral artery with true blue: colocalization with different peptides. J Cereb Blood Flow Metab 9:212-218.

Erulkar SD, Woodward JK (1968) Intracellular recording from mammalian superior cervical ganglion in situ. J Physiol 199:189-203.

Feldberg W, Gaddum JH (1934) The chemical transmitter at synapses in a sympathetic ganglion. J Physiol 81:305-319.

Feldberg W, Vartiainen A (1934) Further observations on the physiology and pharmacology of a sympathetic ganglion. J Physiol 83:103-128.

Feng ZP, Arnot MI, Doering CJ, Zamponi GW (2001) Calcium channel beta subunits differentially regulate the inhibition of N-type channels by individual Gbeta isoforms. J Biol Chem 276:45051-45058.

Fernandez-Fernandez JM, Wanaverbecq N, Halley P, Caulfield MP, Brown DA (1999) Selective activation of heterologously expressed G protein-gated K+ channels by M2 muscarinic receptors in rat sympathetic neurones. J Physiol 515 (Pt 3):631-637.

Fernandez-Fernandez JM, Abogadie FC, Milligan G, Delmas P, Brown DA (2001) Multiple pertussis toxin-sensitive G-proteins can couple receptors to GIRK channels in rat sympathetic neurons when expressed heterologously, but only native G(i)-proteins do so in situ. Eur J Neurosci 14:283-292.

Flett DL, Bell C (1991) Topography of functional subpopulations of neurons in the superior cervical ganglion of the rat. J Anat 177:55-66.

Forsythe ID, Tsujimoto T, Barnes-Davies M, Cuttle MF, Takahashi T (1998) Inactivation of presynaptic calcium current contributes to synaptic depression at a fast central synapse. Neuron 20:797-807.

Gabella G (1976) Structure of the autonomic nervous system.

Galvan M, Adams PR (1982) Control of calcium current in rat sympathetic neurons by norepinephrine. Brain Res 244:135-144.

Gamper N, Reznikov V, Yamada Y, Yang J, Shapiro MS (2004) Phosphatidylinositol [correction] 4,5-bisphosphate signals underlie receptor-specific Gq/11-mediated modulation of N-type Ca2+ channels. J Neurosci 24:10980-10992.

Gibbins IL (1991) Vasomotor, pilomotor and secretomotor neurons distinguished by size and neuropeptide content in superior cervical ganglia of mice. J Auton Nerv Syst 34:171-183.

Gibbins IL (1992) Vasoconstrictor, vasodilator and pilomotor pathways in sympathetic ganglia of guinea-pigs. Neuroscience 47:657-672.

Gibbins IL (1995) Chemical neuroanatomy of sympathetic ganglia. In: Autonomic ganglia (McLachlan EM, ed).

Gibbins IL (2004) Peripheral autonomic pathways. In: The human nervous system (Paxinos G, Mai JK, eds).

Gibbins IL, Matthew SE (1996) Dendritic morphology of presumptive vasoconstrictor and pilomotor neurons and their relations with neuropeptide-containing preganglionic fibres in lumbar sympathetic ganglia of guinea-pigs. Neuroscience 70:999-1012.

Gibbins IL, Morris JL (2006) Structure of peripheral synapses: autonomic ganglia. Cell Tissue Res 326:205-220.

Gibbins IL, Matthew SE, Bridgman N, Morris JL (1996) Sympathetic vasoconstrictor neurons projecting from the guinea-pig superior cervical ganglion to cutaneous or

skeletal muscle vascular beds can be distinguished by soma size. Neurosci Lett 213:197-200.

Gold MS, Dastmalchi S, Levine JD (1997) Alpha 2-adrenergic receptor subtypes in rat dorsal root and superior cervical ganglion neurons. Pain 69:179-190.

Goldberg LI, Dacosta FM (1960) Selective depression of sympathetic transmission by intravenous administration of iproniazid and harmine. Proc Soc Exp Biol Med 105:223-227.

Gray AC, Raingo J, Lipscombe D (2007) Neuronal calcium channels: splicing for optimal performance. Cell Calcium 42:409-417.

Grkovic I, Anderson CR (1995) Calretinin-containing preganglionic nerve terminals in the rat superior cervical ganglion surround neurons projecting to the submandibular salivary gland. Brain Res 684:127-135.

Grkovic I, Anderson CR (1997) Calbindin D28K-immunoreactivity identifies distinct subpopulations of sympathetic pre- and postganglionic neurons in the rat. J Comp Neurol 386:245-259.

Grkovic I, Edwards SL, Murphy SM, Anderson CR (1999) Chemically distinct preganglionic inputs to iris-projecting postganglionic neurons in the rat: A light and electron microscopic study. J Comp Neurol 412:606-616.

Grunditz T, Hakanson R, Sundler F, Uddman R (1988) Neuronal pathways to the rat thyroid revealed by retrograde tracing and immunocytochemistry. Neuroscience 24:321-335.

Headley DB, Suhan NM, Horn JP (2005) Rostro-caudal variations in neuronal size reflect the topography of cellular phenotypes in the rat superior cervical sympathetic ganglion. Brain Res 1057:98-104.

Henon BK, McAfee DA (1983) The ionic basis of adenosine receptor actions on post-ganglionic neurones in the rat. J Physiol 336:607-620.

Hille B (1994) Modulation of ion-channel function by G-protein-coupled receptors. Trends Neurosci 17:531-536.

Hirst GD, McLachlan EM (1986) Development of dendritic calcium currents in ganglion cells of the rat lower lumbar sympathetic chain. J Physiol 377:349-368.

Ho K, Nichols CG, Lederer WJ, Lytton J, Vassilev PM, Kanazirska MV, Hebert SC (1993) Cloning and expression of an inwardly rectifying ATP-regulated potassium channel. Nature 362:31-38.

Horn JP (1992) The integrative role of synaptic cotransmission in the bullfrog vasomotor C system: evidence for a synaptic gain hypothesis. Can J Physiol Pharmacol 70 Suppl:S19-26.

Horn JP, McAfee DA (1980) Alpha-drenergic inhibition of calcium-dependent potentials in rat sympathetic neurones. J Physiol 301:191-204.

Horn JP, Stofer WD (1988) Spinal origins of preganglionic B and C neurons that innervate paravertebral sympathetic ganglia nine and ten of the bullfrog. J Comp Neurol 268:71-83.

Horn JP, Stofer WD (1989) Preganglionic and sensory origins of calcitonin gene-related peptide-like and substance P-like immunoreactivities in bullfrog sympathetic ganglia. J Neurosci 9:2543-2561.

Horn JP, Stofer WD, Fatherazi S (1987) Neuropeptide Y-like immunoreactivity in bullfrog sympathetic ganglia is restricted to C cells. J Neurosci 7:1717-1727.

Horn JP, Fatherazi S, Stofer WD (1988) Differential projections of B and C sympathetic axons in peripheral nerves of the bullfrog. J Comp Neurol 278:570-580.

Hulme EC, Birdsall NJ, Buckley NJ (1990) Muscarinic receptor subtypes. Annu Rev Pharmacol Toxicol 30:633-673.

Ivanov AY, Skok VI (1980) Slow inhibitory postsynaptic potentials and hyperpolarization evoked by noradrenaline in the neurones of mammalian sympathetic ganglion. J Auton Nerv Syst 1:255-263.

Izzo J, Black H, eds (2003) Hypertension Primer, 3rd Edition. Philadelphia: Lippincott, Williams and Wilkins.

Jan LY, Jan YN (1981) Role of an LHRH-like peptide as a neurotransmitter is sympathetic ganglia of the frog. Fed Proc 40:2560-2564.

Jan LY, Jan YN (1982) Peptidergic transmission in sympathetic ganglia of the frog. J Physiol 327:219-246.

Jan YN, Jan LY, Kuffler SW (1979) A peptide as a possible transmitter in sympathetic ganglia of the frog. Proc Natl Acad Sci U S A 76:1501-1505.

Janig W (1985) Organization of the lumbar sympathetic outflow to skeletal muscle and skin of the cat hindlimb and tail. Rev Physiol Biochem Pharmacol 102:119-213.

Janig W (1988) Pre- and postganglionic vasoconstrictor neurons: differentiation, types, and discharge properties. Annu Rev Physiol 50:525-539.

Janig W (1995) Ganglionic transmission in vivo. In: Autonomic ganglia (McLachlan EM, ed). australia;U.S.

Janig W, Szulczyk P (1981) The organization of lumbar preganglionic neurons. J Auton Nerv Syst 3:177-191.

Janig W, McLachlan EM (1992) Characteristics of function-specific pathways in the sympathetic nervous system. Trends Neurosci 15:475-481.

Janig W, Habler H (1999) organization of the autonomic nervous system: structure and function. In: The autonomic nervous system, 1st Edition (Appenzeller O, ed). Amsterdam ; New York: Elsevier.

Jarvi R, Helen P, Pelto-Huikko M, Hervonen A (1986) Neuropeptide Y (NPY)-like immunoreactivity in rat sympathetic neurons and small granule-containing cells. Neurosci Lett 67:223-227.

Jobling P, Horn JP (1996) In vitro relation between preganglionic sympathetic stimulation and activity of cutaneous glands in the bullfrog. J Physiol 494 (Pt 1):287-296.

Jobling P, Gibbins IL (1999) Electrophysiological and morphological diversity of mouse sympathetic neurons. J Neurophysiol 82:2747-2764.

Jobling P, Messenger JP, Gibbins IL (2001) Differential expression of functionally identified and immunohistochemically identified NK(1) receptors on sympathetic neurons. J Neurophysiol 85:1888-1898.

Jones LP, DeMaria CD, Yue DT (1999) N-type calcium channel inactivation probed by gating-current analysis. Biophys J 76:2530-2552.

Jones SW (1985) Muscarinic and peptidergic excitation of bull-frog sympathetic neurones. J Physiol 366:63-87.

Kafka MS, Thoa NB (1979) Alpha-adrenergic receptors in the rat superior cervical ganglion. Biochem Pharmacol 28:2485-2489.

Karila P, Horn JP (2000) Secondary nicotinic synapses on sympathetic B neurons and their putative role in ganglionic amplification of activity. J Neurosci 20:908-918.

Kawai Y, Tamai Y, Senba E (1993) Principal neurons as local circuit neurons in the rat superior cervical ganglion: the synaptology of the neuronal processes revealed by intracellular injection of biocytin. J Comp Neurol 328:562-574.

Keynes RDA, D.J. (1991) Nerve and Muscle: CAmbridge University Press,CAmbridge,1991.

Kiraly M, Favrod P, Matthews MR (1989) Neuroneuronal interconnections in the rat superior cervical ganglion; possible anatomical bases for modulatory interactions revealed by intracellular horseradish peroxidase labelling. Neuroscience 33:617-642.

Kobayashi H, Libet B (1970) Actions of noradrenaline and acetylcholine on sympathetic ganglion cells. J Physiol 208:353-372.

Kofuji P, Davidson N, Lester HA (1995) Evidence that neuronal G-protein-gated inwardly rectifying K+ channels are activated by G beta gamma subunits and function as heteromultimers. Proc Natl Acad Sci U S A 92:6542-6546.

Koh DS, Hille B (1997) Modulation by neurotransmitters of catecholamine secretion from sympathetic ganglion neurons detected by amperometry. Proc Natl Acad Sci U S A 94:1506-1511.

Kondo H, Dun NJ, Pappas GD (1980) A light and electron microscopic study of the rat superior cervical ganglion cells by intracellular HRP-labeling. Brain Res 197:193-199.

Kubo Y, Baldwin TJ, Jan YN, Jan LY (1993a) Primary structure and functional expression of a mouse inward rectifier potassium channel. Nature 362:127-133.

Kubo Y, Reuveny E, Slesinger PA, Jan YN, Jan LY (1993b) Primary structure and functional expression of a rat G-protein-coupled muscarinic potassium channel. Nature 364:802-806.

Kullmann PH, Horn JP (2006) Excitatory muscarinic modulation strengthens virtual nicotinic synapses on sympathetic neurons and thereby enhances synaptic gain. J Neurophysiol 96:3104-3113.

Langer SZ (1980) Presynaptic regulation of the release of catecholamines. Pharmacol Rev 32:337-362.

Levison WH, Barnett GO, Jackson WD (1966) Nonlinear analysis of the baroreceptor reflex system. Circ Res 18:673-682.

Lewis GP, Reit E (1965) The action of angiotensin and bradykinin on the superior cervical ganglion of the cat. J Physiol 179:538-553.

Li C, Horn JP (2006) Physiological classification of sympathetic neurons in the rat superior cervical ganglion. J Neurophysiol 95:187-195.

Libet B (1970) Generation of slow inhibitory and excitatory postsynaptic potentials. Fed Proc 29:1945-1956.

Libet B, Chichibu S, Tosaka T (1968) Slow synaptic responses and excitability in sympathetic ganglia of the bullfrog. J Neurophysiol 31:383-395.

Limberger N, Trendelenburg AU, Starke K (1992) Pharmacological characterization of presynaptic alpha 2-autoreceptors in rat submaxillary gland and heart atrium. Br J Pharmacol 107:246-255.

Lindh B, Lundberg JM, Hokfelt T (1989) NPY-, galanin-, VIP/PHI-, CGRP- and substance P-immunoreactive neuronal subpopulations in cat autonomic and sensory ganglia and their projections. Cell Tissue Res 256:259-273.

Liu L, Roberts ML, Rittenhouse AR (2004) Phospholipid metabolism is required for M1 muscarinic inhibition of N-type calcium current in sympathetic neurons. Eur Biophys J 33:255-264.

Liu L, Zhao R, Bai Y, Stanish LF, Evans JE, Sanderson MJ, Bonventre JV, Rittenhouse AR (2006) M1 muscarinic receptors inhibit L-type Ca2+ current and M-current by divergent signal transduction cascades. J Neurosci 26:11588-11598.

Loewi O (1921) On the Humoral propagation of cardiac nerve action. Pfugers Arch:239-242.

Loewy AD, Spyer KM (1990) Central regulation of autonomic functions. New York: Oxford University Press.

Luebke JI, Wright LL (1992) Characterization of superior cervical ganglion neurons that project to the submandibular glands, the eyes, and the pineal gland in rats. Brain Res 589:1-14.

Lundberg JM, Saria A, Anggard A, Hokfelt T, Terenius L (1984) Neuropeptide Y and noradrenaline interaction in peripheral cardiovascular control. Clin Exp Hypertens A 6:1961-1972.

Lundberg JM, Terenius L, Hokfelt T, Martling CR, Tatemoto K, Mutt V, Polak J, Bloom S, Goldstein M (1982) Neuropeptide Y (NPY)-like immunoreactivity in peripheral noradrenergic neurons and effects of NPY on sympathetic function. Acta Physiol Scand 116:477-480.

Marrazzi A (1939) Electrical studies on the pharmacology of autonomic synapses. II. The action of a sympathomimetic drug (epinephrine) on sympathetic ganglia. J Pharmacol ExpTher 65::395-404.

Marrion NV, Smart TG, Marsh SJ, Brown DA (1989) Muscarinic suppression of the M-current in the rat sympathetic ganglion is mediated by receptors of the M1-subtype. Br J Pharmacol 98:557-573.

Martinez AE, Adler-Graschinsky E (1980) Release of norepinephrine induced by preganglionic stimulation of the isolated superior cervical ganglion of the cat. J Pharmacol Exp Ther 212:527-532.

Mathie A, Bernheim L, Hille B (1992) Inhibition of N- and L-type calcium channels by muscarinic receptor activation in rat sympathetic neurons. Neuron 8:907-914.

McCallum JB, Boban N, Hogan Q, Schmeling WT, Kampine JP, Bosnjak ZJ (1998) The mechanism of alpha2-adrenergic inhibition of sympathetic ganglionic transmission. Anesth Analg 87:503-510.

McLachlan EM (1995) Autonomic ganglia. Australia ; U.S.: Harwood Academic Publishers.

McLachlan EM (2003) Transmission of signals through sympathetic ganglia--modulation, integration or simply distribution? Acta Physiol Scand 177:227-235.

McLachlan EM, Davies PJ, Habler HJ, Jamieson J (1997) On-going and reflex synaptic events in rat superior cervical ganglion cells. J Physiol 501 (Pt 1):165-181.

McLachlan EM, Habler HJ, Jamieson J, Davies PJ (1998) Analysis of the periodicity of synaptic events in neurones in the superior cervical ganglion of anaesthetized rats. J Physiol 511 (Pt 2):461-478.

Merrill MA, Chen Y, Strack S, Hell JW (2005) Activity-driven postsynaptic translocation of CaMKII. Trends Pharmacol Sci 26:645-653.

Miller RJ (1998) Presynaptic receptors. Annu Rev Pharmacol Toxicol 38:201-227.

Minota S, Koketsu K (1977) Effects of adrenaline on the action potential of sympathetic ganglion cells in bullfrogs. Jpn J Physiol 27:353-366.

Mintz IM, Adams ME, Bean BP (1992) P-type calcium channels in rat central and peripheral neurons. Neuron 9:85-95.

Mirgorodsky VN, Skok VI (1970) The role of different preganglionic fibres in tonic activity of the mammalian sympathetic ganglion. Brain Res 22:262-263.

Mochida S, Saisu H, Kobayashi H, Abe T (1995) Impairment of syntaxin by botulinum neurotoxin C1 or antibodies inhibits acetylcholine release but not Ca2+ channel activity. Neuroscience 65:905-915.

Morris JL, Gibbins IL (1992) Co-transmission and neuromodulation. In: Autonomic neuroeffector mechanisms (Burnstock G, Hoyle CHV, eds), pp 3-119: Harwood Academic Publishers.

Morris JL, Gibbins IL, Osborne PB (1989) Galanin-like immunoreactivity in sympathetic and parasympathetic neurons of the toad Bufo marinus. Neurosci Lett 102:142-148.

Morris JL, Gibbins IL, Campbell G, Murphy R, Furness JB, Costa M (1986) Innervation of the large arteries and heart of the toad (Bufo marinus) by adrenergic and peptide-containing neurons. Cell Tissue Res 243:171-184.

Murata Y, Shibata H, Chiba T (1982) A correlative quantitative study comparing the nerve fibers in the cervical sympathetic trunk and the locus of the somata from which they originate in the rat. J Auton Nerv Syst 6:323-333.

Nishi S, Soeda H, Koketsu K (1965) Studies on sympathetic B and C neurons and patterns of pregnaglionic innervation. J Cell Physiol 66:19-32.

Nja A, Purves D (1977) Specific innervation of guinea-pig superior cervical ganglion cells by preganglionic fibres arising from different levels of the spinal cord. J Physiol 264:565-583.

Noon JP, McAfee DA, Roth RH (1975) Norepinephrine release from nerve terminals within the rabbit superior cervical ganglion. Naunyn Schmiedebergs Arch Pharmacol 291:139-162.

Patil PG, Brody DL, Yue DT (1998) Preferential closed-state inactivation of neuronal calcium channels. Neuron 20:1027-1038.

Persson PB, Kirchheim HR (1991) Baroreceptor reflexes : integrative functions and clinical aspects. Berlin ; New York: Springer-Verlag.

Pfaffinger PJ, Martin JM, Hunter DD, Nathanson NM, Hille B (1985) GTP-binding proteins couple cardiac muscarinic receptors to a K channel. Nature 317:536-538.

Pieribone VA, Nicholas AP, Dagerlind A, Hokfelt T (1994) Distribution of alpha 1 adrenoceptors in rat brain revealed by in situ hybridization experiments utilizing subtype-specific probes. J Neurosci 14:4252-4268.

Plummer MR, Logothetis DE, Hess P (1989) Elementary properties and pharmacological sensitivities of calcium channels in mammalian peripheral neurons. Neuron 2:1453-1463.

Powley TL (1999) Central control of autonomic functions: the organization of the autonomic nervous system. In: Fundamental neuroscience (Zigmond MJ, Bloom FE, Landis SC, Roberts JL, Squire LR, eds).

Purves D, Hume RI (1981) The relation of postsynaptic geometry to the number of presynaptic axons that innervate autonomic ganglion cells. J Neurosci 1:441-452.

Purves D, Lichtman JW (1985) Geometrical differences among homologous neurons in mammals. Science 228:298-302.

Purves D, Rubin E, Snider WD, Lichtman J (1986) Relation of animal size to convergence, divergence, and neuronal number in peripheral sympathetic pathways. J Neurosci 6:158-163.

Raingo J, Castiglioni AJ, Lipscombe D (2007) Alternative splicing controls G protein-dependent inhibition of N-type calcium channels in nociceptors. Nat Neurosci 10:285-292.

Rando TA, Bowers CW, Zigmond RE (1981) Localization of neurons in the rat spinal cord which project to the superior cervical ganglion. J Comp Neurol 196:73-83.

Rane SG, Dunlap K (1986) Kinase C activator 1,2-oleoylacetylglycerol attenuates voltage-dependent calcium current in sensory neurons. Proc Natl Acad Sci U S A 83:184-188.

Regan LJ, Sah DW, Bean BP (1991) Ca2+ channels in rat central and peripheral neurons: high-threshold current resistant to dihydropyridine blockers and omega-conotoxin. Neuron 6:269-280.

Reinert H (1963) Role and origin of noradrenaline in the superior cervical ganglion. J Physiol 167:18-29.

Reuss S, Moore RY (1989) Neuropeptide Y-containing neurons in the rat superior cervical ganglion: projections to the pineal gland. J Pineal Res 6:307-316.

Romeo HE, Gonzalez Solveyra C, Vacas MI, Rosenstein RE, Barontini M, Cardinali DP (1986) Origins of the sympathetic projections to rat thyroid and parathyroid glands. J Auton Nerv Syst 17:63-70.

Ruiz-Velasco V, Ikeda SR (1998) Heterologous expression and coupling of G protein-gated inwardly rectifying K+ channels in adult rat sympathetic neurons. J Physiol 513 (Pt 3):761-773.

Sagawa K (1978) Concerning "gain". Am J Physiol 235:H117.

Scanziani M, Gahwiler BH, Thompson SM (1993) Presynaptic inhibition of excitatory synaptic transmission mediated by alpha adrenergic receptors in area CA3 of the rat hippocampus in vitro. J Neurosci 13:5393-5401.

Schobesberger H, Wheeler DW, Horn JP (2000) A model for pleiotropic muscarinic potentiation of fast synaptic transmission. J Neurophysiol 83:1912-1923.

Selyanko AA, Skok VI (1979) Activation of acetylcholine receptors in mammalian sympathetic ganglion neurones. Prog Brain Res 49:241-252.

Selyanko AA, Skok VI (1992) Synaptic transmission in rat cardiac neurones. J Auton Nerv Syst 39:191-199.

Selyanko AA, Derkach VA, Skok VI (1979) Fast excitatory postsynaptic currents in voltage-clamped mammalian sympathetic ganglion neurones. J Auton Nerv Syst 1:127-137.

Shapiro MS, Wollmuth LP, Hille B (1994) Angiotensin II inhibits calcium and M current channels in rat sympathetic neurons via G proteins. Neuron 12:1319-1329.

Shapiro MS, Gomeza J, Hamilton SE, Hille B, Loose MD, Nathanson NM, Roche JP, Wess J (2001) Identification of subtypes of muscarinic receptors that regulate Ca2+ and K+ channel activity in sympathetic neurons. Life Sci 68:2481-2487.

Shen WX, Horn JP (1995) A presynaptic mechanism accounts for the differential block of nicotinic synapses on sympathetic B and C neurons by d-tubocurarine. J Neurosci 15:5025-5035.

Shen WX, Horn JP (1996) Presynaptic muscarinic inhibition in bullfrog sympathetic ganglia. J Physiol 491 (Pt 2):413-421.

Sjostrom PJ, Nelson SB (2002) Spike timing, calcium signals and synaptic plasticity. Curr Opin Neurobiol 12:305-314.

Skok VI (1973a) General physiolgical properties of autonomic ganglia. In: Physiology of autonomic ganglia (Skok VI, ed), pp 101-104.

Skok VI (1973b) Anatomy,development and microscopic structure of autonomic ganglia. In: Physiology of autonomic ganglia (Skok VI, ed), pp 1-15.

Skok VI (1973c) Physiology of Autonomic Ganglia. Tokyo: Igaku Shoin.

Skok VI (1992) Molecular mechanisms of open-channel blockade in nicotinic acetylcholine receptors of autonomic ganglia neurons. Can J Physiol Pharmacol 70 Suppl:S78-85.

Skok VI (2002) Nicotinic acetylcholine receptors in autonomic ganglia. Auton Neurosci 97:1-11.

Skok VI, Ivanov AY (1983) What is the ongoing activity of sympathetic neurons? J Auton Nerv Syst 7:263-270.

Smith PA (1994) Amphibian sympathetic ganglia: an owner's and operator's manual. Prog Neurobiol 43:439-510.

Starke K (2001) Presynaptic autoreceptors in the third decade: focus on alpha2-adrenoceptors. J Neurochem 78:685-693.

Stephens GJ, Mochida S (2005) G protein {beta}{gamma} subunits mediate presynaptic inhibition of transmitter release from rat superior cervical ganglion neurones in culture. J Physiol 563:765-776.

Suh BC, Hille B (2005) Regulation of ion channels by phosphatidylinositol 4,5-bisphosphate. Curr Opin Neurobiol 15:370-378.

Sun MK (1995) Central neural organization and control of sympathetic nervous system in mammals. Prog Neurobiol 47:157-233.

Sundler F, Grunditz T, Hakanson R, Uddman R (1989) Innervation of the thyroid. A study of the rat using retrograde tracing and immunocytochemistry. Acta Histochem Suppl 37:191-198.

Thaler C, Gray AC, Lipscombe D (2004) Cumulative inactivation of N-type CaV2.2 calcium channels modified by alternative splicing. Proc Natl Acad Sci U S A 101:5675-5679.

Thompson SM, Capogna M, Scanziani M (1993) Presynaptic inhibition in the hippocampus. Trends Neurosci 16:222-227.

Thomson AM (2000) Facilitation, augmentation and potentiation at central synapses. Trends Neurosci 23:305-312.

Thorne R, Horn JP (1997) Role of ganglionic cotransmission in sympathetic control of the isolated bullfrog aorta. J Physiol 498 (Pt 1):201-214.

166

Thorne R, Stofer WD, Horn JP (1995) An aortic projection of lumbar paravertebral sympathetic neurons in the bullfrog. J Auton Nerv Syst 56:38-44.

Tokimasa T, Akasu T (1995) Biochemical gating for voltage-gated channels: mechanisms for slow synaptic potentials in autonomic ganglia. In: Autonomic ganglia (McLachlan EM, ed).

Tompkins JD, Ardell JL, Hoover DB, Parsons RL (2007) Neurally released pituitary adenylate cyclase-activating polypeptide enhances guinea pig intrinsic cardiac neurone excitability. J Physiol 582:87-93.

Uddman R, Edvinsson L, Hara H (1989) Axonal tracing of autonomic nerve fibers to the superficial temporal artery in the rat. Cell Tissue Res 256:559-565.

Unnerstall JR, Kopajtic TA, Kuhar MJ (1984) Distribution of alpha 2 agonist binding sites in the rat and human central nervous system: analysis of some functional, anatomic correlates of the pharmacologic effects of clonidine and related adrenergic agents. Brain Res 319:69-101.

Vidovic M, Hill CE (1997) Transient expression of alpha-1B adrenoceptor messenger ribonucleic acids in the rat superior cervical ganglion during postnatal development. Neuroscience 77:841-848.

Vizi ES (1979) Presynaptic modulation of neurochemical transmission. Prog Neurobiol 12:181-290.

Voyvodic JT (1989) Peripheral target regulation of dendritic geometry in the rat superior cervical ganglion. J Neurosci 9:1997-2010.

Walker D, De Waard M (1998) Subunit interaction sites in voltage-dependent Ca2+ channels: role in channel function. Trends Neurosci 21:148-154.

Wang HS, McKinnon D (1996) Modulation of inwardly rectifying currents in rat sympathetic neurones by muscarinic receptors. J Physiol 492 (Pt 2):467-478.

Westfall DP, Todorov LD, Mihaylova-Todorova ST (2002) ATP as a cotransmitter in sympathetic nerves and its inactivation by releasable enzymes. J Pharmacol Exp Ther 303:439-444.

Wheeler DW, Kullmann PH, Horn JP (2004) Estimating use-dependent synaptic gain in autonomic ganglia by computational simulation and dynamic-clamp analysis. J Neurophysiol 92:2659-2671.

Wright LL, Cunningham TJ, Smolen AJ (1983) Developmental neuron death in the rat superior cervical sympathetic ganglion: cell counts and ultrastructure. J Neurocytol 12:727-738.

Wu LG, Saggau P (1997) Presynaptic inhibition of elicited neurotransmitter release. Trends Neurosci 20:204-212.

Yamada M, Inanobe A, Kurachi Y (1998) G protein regulation of potassium ion channels. Pharmacol Rev 50:723-760.

Zaika O, Lara LS, Gamper N, Hilgemann DW, Jaffe DB, Shapiro MS (2006) Angiotensin II regulates neuronal excitability via phosphatidylinositol 4,5-bisphosphate-dependent modulation of Kv7 (M-type) K+ channels. J Physiol 575:49-67.

Zhang H, Craciun LC, Mirshahi T, Rohacs T, Lopes CM, Jin T, Logothetis DE (2003) PIP(2) activates KCNQ channels, and its hydrolysis underlies receptor-mediated inhibition of M currents. Neuron 37:963-975.

Zhao FY, Saito K, Yoshioka K, Guo JZ, Murakoshi T, Konishi S, Otsuka M (1995) Subtypes of tachykinin receptors on tonic and phasic neurones in coeliac ganglion of the guinea-pig. Br J Pharmacol 115:25-30.

Zhao FY, Saito K, Yoshioka K, Guo JZ, Murakoshi T, Konishi S, Otsuka M (1996) Tachykininergic synaptic transmission in the coeliac ganglion of the guinea-pig. Br J Pharmacol 118:2059-2066.

Zhong H, Yokoyama CT, Scheuer T, Catterall WA (1999) Reciprocal regulation of P/Q-type Ca2+ channels by SNAP-25, syntaxin and synaptotagmin. Nat Neurosci 2:939-941.

Zhu Y, Ikeda SR (1993) Adenosine modulates voltage-gated Ca2+ channels in adult rat sympathetic neurons. J Neurophysiol 70:610-620.

Zucker RS, Regehr WG (2002) Short-term synaptic plasticity. Annu Rev Physiol 64:355-405.